THE UNIVERSITY OF CHICAGO

MYCN AND HIF-1 DIRECTLY REGULATE *TET1* EXPRESSION TO CONTROL 5-HMC GAINS AND ENHANCE NEUROBLASTOMA CELL MIGRATION IN HYPOXIA

A DISSERTATION SUBMITTED TO

THE FACULTY OF THE DIVISION OF THE BIOLOGICAL SCIENCES

AND PRITZKER SCHOOL OF MEDICINE

IN CANDIDACY FOR THE DEGREE OF

DOCTOR OF PHILOSOPHY

DEPARTMENT OF PATHOLOGY

BY

ANASTASIA ELIZABETH HAINS

CHICAGO, ILLINOIS

DECEMBER 2021

Dedication

To my parents.

Table of Contents

List of Figures

List of Tables

List of Abbreviations

2-OG	2-oxoglutarate
3'UTR	3' Untranslated Region
5-caC	5-carboxylcytosine
5-fC	5-formylcytosine
5-hmC	5-hydroxymethylcytosine
5-mC	5-methylcytosine
5' UTR	5' Untranslated Region
BER	Base-excision repair
ChIP-seq	Chromatin-immunoprecipitation sequencing
CoIP	Co-immunoprecipitation
DNMT	DNA methyltransferase
DSBH	Double-stranded beta-helix
FPKM	Fragments per kilobase per million reads
GO	Gene ontology
gRNA	Guide RNA
HIF	Hypoxia-inducible factor
HPSC	Hematopoietic stem cell
IDH	Isocitrate dehydrogenases
IP	Immunoprecipitation
LC	Low complexity
NB	Neuroblastoma
NTC	Non-target control
PCR	Polymerase chain reaction
PHD	Prolyl hydroxylase
PTM	Post-translational modification

qPCR	Quantitative polymerase chain reaction
RNA-seq	RNA-sequencing
SAM	S-adenosyl methionine
SDS-PAGE	Sodium dodecyl sulphate-polyacrylamide gel electrophoresis
TET1	Ten-eleven-translocation 5-methylcytosine dioxygenase
TF	Transcription factor
VEGF	Vascular endothelial growth factor

Acknowledgements

I would like to thank my advisor, Dr. Lucy Godley, for the mentorship and guidance she provided during my doctoral work. She has helped me develop my approach to science, by showing me how to identify the important scientific questions and prioritize my research ideas. She has trained me to be persistent in the pursuit of scientific discovery, a skill I will always be grateful for as I move on to my postdoctoral training and beyond.

I would also like to thank my committee members, Drs. Marsha Rosner, Susan Cohn, Ben Glick, and Nanduri Prabhakar for their time, advice, and support throughout my doctoral work. My committee meetings always provided clarity as you all helped me work towards my goals. I would like to thank my Chair Dr. Rosner in particular, for her enthusiasm, expertise, and guidance. At least half of the results presented in this dissertation arose from her ideas discussed in my committee meetings. I also owe my gratitude to her post-doctoral scholar, Dr. Long Nguyen, for his invaluable help with experimental planning. I would also like to thank Dr. Mark Applebaum and members of the Cohn/Applebaum Laboratories, Helen Salwen and Kelley Moore, for their advice and expertise on all things neuroblastoma.

I have so many current and past members of the Godley Laboratory to thank. Dr. Chris Mariani, Dr. Sakshi Uppal, Dr. John Cao, Stephen Arnovitz, Dr. Lorraine Canham, Shawn Albert, Janet Lepore, Art Wolin, Maya Lewinsohn, Matthew Pozsgai, Aelin Kim, Connie Phung, Kelsey McNeely, and Dr. Michael Drazer. I have to especially thank Dr. John Cao. As he was one year ahead of me, he acted as my ‘snow plow’, clearing my way and making my life infinitely easier.

Finally, I have to thank my parents for all they have taught me and their unconditional love and support. They inspired me to seek higher education, and I can only hope I have made them proud.

Abstract

Ten-Eleven-Translocation 5-methylcytosine dioxygenases 1-3 (TET1-3) convert 5-methylcytosine to 5-hydroxymethylcytosine (5-hmC), using O_2 as a co-substrate. Prior work in the Godley Laboratory showed that contrary to expectations, hypoxia induces 5-hmC gains in *MYCN*-amplified neuroblastoma (NB) cells through *TET1* up-regulation. There were several unanswered questions from this work including why this phenotype was unique to *MYCN*-amplified NB and whether the transcription factor (TF) HIF-1 interacts with the *TET1* gene and/or the TET1 protein. Additionally, it was unclear if 5-hmC enrichment in hypoxic response genes and subsequent augmentation of gene expression mediated aggressive hypoxic phenotypes characteristic of NB cell lines. In my doctoral work, I show that MYCN directly controls *TET1* expression in normoxia via binding to two genomic sites within the first and second introns of *TET1*. Further I show that MYCN specifically drives expression of the full-length *TET1* transcript. In hypoxia, HIF-1 augments *TET1* expression through the same binding sites as those bound by MYCN. Unexpectedly, in gene-edited cells that lack the binding sites, TET1 protein still increases over normoxic levels. Subsequently, 5-hmC levels were also induced in hypoxia compared to normoxic 5-hmC levels. Using TET1 degradation assays, I demonstrate that the TET1 protein half-life is 20 hours, whereas it is extended to 40 hours in hypoxia. The increased TET1 stability in hypoxia is mediated by a binding interaction between HIF-1 and TET1. I used 5-hmC profiling to determine how 5-hmC distribution changes in hypoxic cells over 72 hours, and in combination with RNA-sequencing data across this time course, show that 5-hmC density correlates with expression of genes important for cell migration, including *CXCR4*. Treatment of *MYCN*-amplified NB cells with a CXCR4 antagonist results in slower migration in hypoxia, suggesting that inclusion of a CXCR4 antagonist into NB treatment regimens could be beneficial. When parental and gene-edited SK-N-BE(2) cells that lack the transcription factor binding sites in *TET1* were injected into athymic mice, gene-edited tumors grew slower compared to controls, indicating 5-hmC may mediate tumor growth as well.

Overall, I show how MYCN and HIF-1 regulate the *TET1* gene and TET1 protein, and subsequently, how the 5-hmC epigenetic landscape is regulated in NB. I also show that CXCR4 is an integral part of *MYCN*-amplified NB cell migration pathway in hypoxia, suggesting inclusion of a CXCR4 antagonist into NB treatment regimens could be beneficial for children with MYCN-amplified NBs.

CHAPTER I

Introduction

This chapter is adapted from a review of the TET enzymes co-authored by myself and John Z. Cao under the supervision of Dr. Lucy Godley, published as a chapter in *The DNA, RNA, and Histone Methylomes:* Cao J.Z., Hains A.E., Godley L.A. Regulation of 5-Hydroxymethylcytosine Distribution by the TET Enzymes. In: Jurga SB, Jan, editor. *The DNA, RNA, and Histone Methylomes:* Springer; 2019. p. 229-63. ISBN 978-3-030-14792-1

Epigenetic regulation of transcription in human cells

Epigenetic regulation of gene expression occurs at multiple molecular levels, including chromatin structure, non-coding RNAs, histone replacement and modifications, and covalent cytosine modifications in DNA, to regulate transcription in cells (Allis and Jenuwein, 2016). Many of these modifications and mechanisms were first described in model organisms between the 1940s and the 1970s (Avery et al., 1944; Holliday and Pugh, 1975; Riggs, 1975). The field evolved as researchers discovered their relevance and importance in human biology, particularly in the context of disease (Cheng et al., 2019). Current studies have illustrated the importance of understanding epigenetic modifications, how they contribute to cancer pathogenesis, and their potential use as therapeutic targets (Cheng et al., 2019).

Among the different classes of epigenetic mechanisms, single base modifications of cytosines within DNA were one of the first to be described and are therefore among the most well-known. However, although their presence in mammalian DNA has been known for nearly 75 years, their role in gene regulation and cancer pathogenesis is the subject of an actively evolving field (Allis and Jenuwein, 2016; Cao et al., 2019; Feinberg and Tycko, 2004; Hotchkiss, 1948)

The function and physiological roles of 5-methycytosine

In mammalian DNA, cytosine bases found within the context of a 5'-CpG-3' dinucleotide can be modified covalently to 5-methylcytosine (5-mC) by DNA methyltransferases (DNMTs). DNMT1, DNMT3A, and DNMT3B utilize S-adenosylmethionine (SAM) as a methyl group donor to add the methyl group to cytosine. DNMT1 primarily functions in methylating hemimethylated cytosines that are generated after DNA replication, thereby maintaining DNA methylation patterns post-replication (Lee et al., 2014). In contrast, DNMT3A and DNMT3B function as *de novo* methyltransferases, adding methyl groups to unmodified cytosines (Lee et al., 2014) During early embryogenesis and primordial germ cell development DNMT3A/B are

highly active and establish methylation patterns (Chen and Chan, 2014; Okano et al., 1999). Homozygous DNMT3b deleted (DNMT3b$^{-/-}$) mice are not viable at birth, whereas DNMT3a$^{-/-}$ mice appear normal at birth but die at about 4 weeks (Okano et al., 1999). This indicates that, although co-expressed at several stages during development, DNMT3A/B have distinct roles in addition to overlapping functions (Chen and Chan, 2014; Okano et al., 1999).

5-mC has an important role in regulating transcription from genes (Jjingo et al., 2012; Jones, 2012; Varley et al., 2013). When 5-mC is enriched within gene bodies, it is associated with active gene expression (Jjingo et al., 2012; Jones, 2012; Varley et al., 2013). However, when 5-mC is found clustered in gene promoters and CpG islands, expression from the corresponding gene is repressed. Both transcriptional repression and activation via aberrant deposition of 5-mC in genes is a commonly observed phenomenon in many cancers (Baylin et al., 1986; Feinberg and Tycko, 2004; Feinberg and Vogelstein, 1983; Gama-Sosa et al., 1983).

Before 1990, many scientists in the field of developmental biology debated whether the loss of a methyl group from a cytosine through DNA replication was the only mechanism by which a cytosine could lose its methyl group, or if an alternative, active demethylation pathway exists (Li, 2013). Several studies originating from multiple model systems found some genomic regions became hypomethylated despite a lack of cell division (Mayer et al., 2000; Sullivan and Grainger, 1987; Zhang et al., 2007). This indicated that an active and rapid mechanism of DNA demethylation outside of DNA replication likely exists but was yet to be identified.

5-hydroxymethylcytosine in the mammalian genome and its role in demethylation

5-hydroxymethylcytosine (5-hmC) was identified as both the first step in the active cytosine demethylation pathway (to be described in additional detail in sections below) and as a functioning part of the mammalian genome in 2009 (Kriaucionis and Heintz, 2009; Tahiliani et al., 2009). The amount of 5-hmC in the human genome varies across tissue type. Total genomic percentage of 5-hmC can be as low as 0.01% in myeloid cells, around 1% in cerebral tissue,

Table 1.1. Common available methods that specifically detect 5-hmC.

Method	Name	Description	Resolution	Limitation	References
Mass spectrometry	HPLC-MS/MS	Digested nucleoside separated by liquid chromatography and measured by tandem mass-spectrometry	Global	Cannot detect local cytosine modifications	Fernandez et al.,2018
Affinity	hMe-SEAL	Streptavidin pull-down of biotin-labeled 5-hmC in fragmented DNA	50-100 bp	Requires expensive specialized reagents	Song et al., 2011
Affinity	hMe-DIP	Immunoprecipitation of fragmented DNA with 5-hmC specific antibody	50-100 bp	Antibody specificity	Nestor and Meehan, 2014
Affinity	JBP1-seq	JPB1 affinity pull-down of glycosylated 5-hmC in fragmented DNA	50-100 bp	Requires specialized beads	Robertson et al., 2012
Redox	TAB-seq	TET-mediated oxidation of 5-mC to 5-caC, while 5-hmC is protected by glycosylation, followed by bisulfite treatment	Single-base	Expensive enzyme	Yu et al., 2012
Redox	oxBS-seq	Selective oxidation of 5-hmC to 5-fC followed by bisulfite treatment	Single-base	Requires parallel bisulfite sequencing	Booth et al., 2013
Restriction enzymes	MspJ1 family	Digest DNA near modified cytosine except glycosylated 5-hmC	Single-base	Sequence specificity of the enzyme	Cohen-Kami et al., 2011
Restriction enzymes	PvuRts1I family	5-hmC specific restriction enzyme	Single-base	Sequence specificity of the enzyme	Wang et al., 2011

and as high as 5% in undifferentiated embryonic stem cells (Field et al., 2015; Ko et al., 2010; Kriaucionis and Heintz, 2009; Madzo et al., 2014; Tahiliani et al., 2009; Wen et al., 2014). As 5-hmC was identified as a product of oxidation of 5-mC, it was postulated that this base was an intermediate in a yet to be described active cytosine demethylation pathway (Tahiliani et al., 2009). Subsequently, multiple 5-hmC specific detection assays have been developed (Table 1.1), which have facilitated the investigation of 5-hmC in the mammalian genome (Booth et al., 2013; Cohen-Karni et al., 2011; Fernandez et al., 2018; Nestor and Meehan, 2014; Robertson et al., 2012; Song et al., 2011; Wang et al., 2011; Yu et al., 2012). 5-hmC has two major functions, the first of which is the base is an intermediate of the demethylation process.

5-hmC is a part of both passive and active demethylation pathways (Figure 1.1). When DNA is replicated, a newly inserted cytosine on the daughter strand is unmodified at first. If the cytosine base within the parent 5'-CpG-3' dinucleotide is methylated, then DNMT1 methylates the cytosine within the newly synthesized strand, therefore maintaining the DNA methylation pattern. However, if the cytosine base within the parent DNA strand is hydroxymethylated, then maintenance of this base in the novel strand requires two enzymes, first a DNMT to produce 5-

Figure 1.1. Cytosine methylation and demethylation pathways. DNMTs methylate unmodified cytosine to create 5-mC using SAM as methyl donor. TETs initiate the active demethylation pathway by oxidizing 5-mC to 5-hmC, 5-fC, and 5-caC stepwise using 2-OG and O2 as co-substrates and Fe2+ as a co-factor (green arrows). 5-hmC and 5-caC can be directly converted to unmodified cytosine by removal of modifications through DNMT3A/B (purple arrows). 5-fC and 5-caC can be removed by base excision repair proteins TDG and/or NEIL1 and replaced with unmodified cytosine (blue arrows).

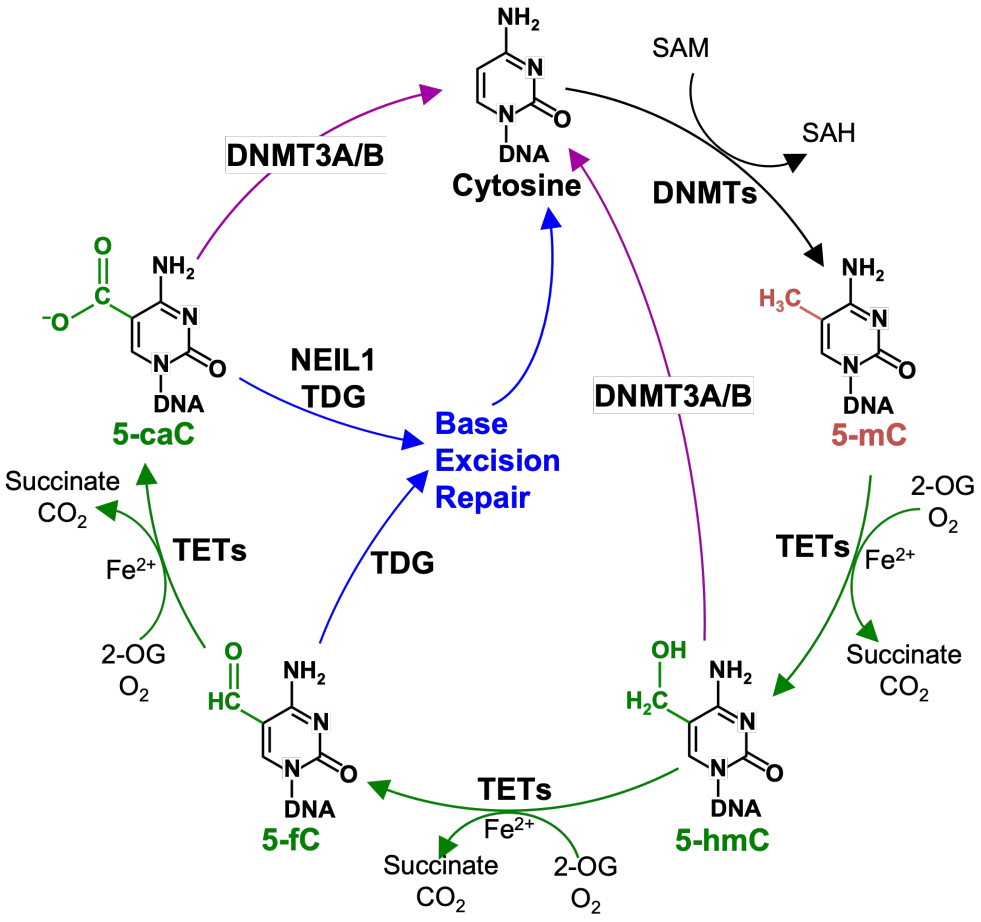

mC, and then a TET to convert that base to 5-hmC. Therefore, in this context, if a DNMT fails to recognize a 5-hmC base on the parent strand, that base will result in a cytosine in the daughter strand and the modification is lost. This process is referred to as passive demethylation (Seiler et al., 2018; Valinluck and Sowers, 2007). A more active pathway is responsible for cell-cycle independent demethylation which involves further oxidation of 5-hmC by dioxygenases to 5-formylcytosine (5-fC) and 5-carboxylcytosine (5-caC) (Ito et al., 2011), both of which can be replaced by unmodified cytosines through base-excision repair (BER) via thymine-DNA glucosylase (Figure 1.1) (He et al., 2011; Maiti and Drohat, 2011; Pidugu et al., 2016). The base

5-caC, but not 5-fC, can also undergo BER by Nei-like 1 (NEIL1) excision (Figure 1.1) (Slyvka et al., 2017). In addition to BER-mediated demethylation, some studies have also found that DNMT3A/3B have the ability to remove the 5'-modification from 5-hmC and 5-caC directly, resulting in unmodified cytosine, but not from 5-mC or 5-fC (Figure 1.1) (Chen et al., 2012; Liutkevičiūtė et al., 2014). It is within this context that 5-hmC was first recognized as a mark associated with transcriptional activation, as it represented a removal of transcriptionally repressive 5-mC. However, studies of mammalian 5-hmC and the newly discovered TET enzymes found 5-hmC functions as a stable epigenetic mark with distinct roles in chromatin structure and transcriptional regulation

The second major function of 5-hmC is as a stable epigenetic mark

Multiple studies have demonstrated that 5-hmC has a distinct role as a stable epigenetic mark associated with active transcription (Ficz et al., 2011; Lin et al., 2017; Madzo et al., 2014; Szulwach et al., 2011). 5-hmC has been found to be strongly associated with promoters, enhancers, and transcription factor (TF) binding sites (Madzo et al., 2014; Mariani et al., 2014; Vasanthakumar and Godley, 2015). In addition, 5-hmC is associated with histone modifications that are linked with open chromatin (Ficz et al., 2011; Madzo et al., 2014). As of now, the mechanism by which 5-hmC promotes gene expression is an active field of investigation, however, three proteins have been proposed to specifically bind 5-hmC as "reader" proteins: NP95/UHRF1, MeCP2, MBD3 (Arita et al., 2008; Baubec et al., 2013; Frauer et al., 2011; Iurlaro et al., 2013; Mellen et al., 2012; Sharif et al., 2007; Spruijt et al., 2013; Yildirim et al., 2011). In addition, 5-hmC may promote activation simply by baring direct protein interaction with DNA, preventing any inhibition by 5-mC binding proteins.

More recently, 5-hmC has been implicated in DNA damage repair (Kafer et al., 2016; Yamaguchi et al., 2012). In human cancer cell lines, 5-hmC foci co-localize with DNA damage foci marked by γH2AX and 53BP1 upon induced DNA damage (Kafer et al., 2016). It is

probable that 5-hmC promotes local chromatin remodeling and/or serves as an epigenetic mark to recruit additional DNA damage repair machinery (Kafer et al., 2016).

TET enzymes structure, function, substrates, and co-factors

Figure 1.2. Homo sapiens TET protein domains. The C-terminal catalytic domain, consisting of a cystein-rich domain (Cys) and two double-stranded beta-helix (DSBH) DNA binding domains, is conserved across all three TETs. A low complexity (LC) insert separates the two DSBH domains. TET1 and TET3 have an N-terminal CpG binding CXXC domain. The CXXC domain part of the gene of TET2 was evolutionarily separated and now exists as its own gene independently. Image adapted from Cao et al., 2019

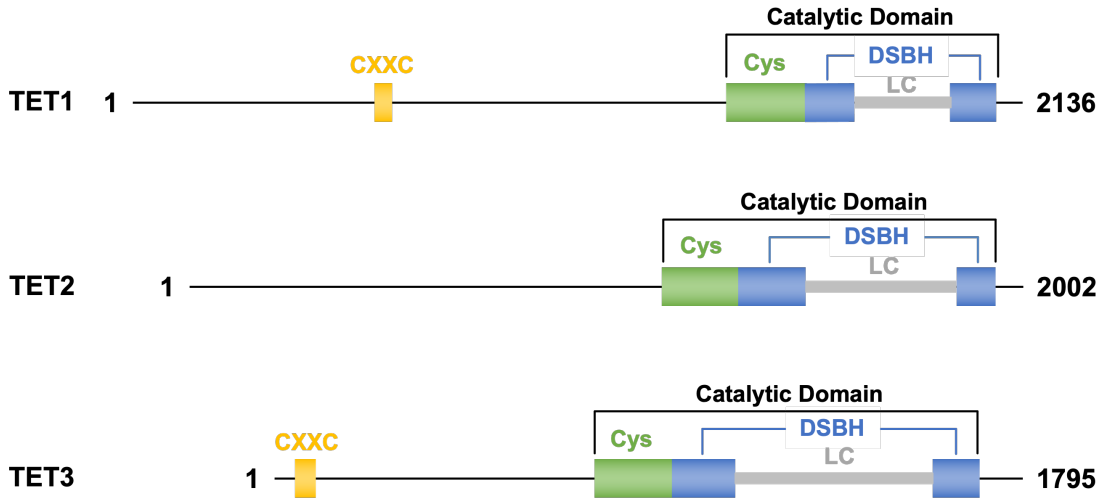

The enzymes responsible for the oxidation of 5-mC to 5-hmC are the ten-eleven-translocation 5-methylcytosine dioxygenase (TET) family consisting of TET1, TET2, and TET3 (Tahiliani et al., 2009). All three *TETs* are transcribed and translated into catalytically functional dioxygenases. All contain a C-terminal catalytic domain, which consists of a cysteine-rich domain and a double-stranded β-helix domain that binds DNA in its center (Figure 1.2) (Cao et al., 2019; Hu et al., 2013, 2015). TET catalytic domains have no preference for flanking sequences and instead specifically bind modified CpGs (Figure 1.3A) (Hu et al., 2013). To catalyze the modification of cytosine, the base is flipped into the catalytic cavity (Figure 1.3B) (Hu et al., 2013). In addition to the oxidation of 5-mC to 5-hmC, TET enzymes further oxidize 5-

Figure 1.3. Crystal structure of the catalytic domain of TET2 with DNA. A. TET2 catalytic domain forms a double-stranded beta-helix (DSBH, yellow) structure that binds the modified CpG DNA (purple). Alpha helices surround the DSBH structure and provide stabilization (red). B. Modified cytosine base (copper) is flipped out from the DNA double helix and stabilized in the pocket of the active site (green) with 2-oxogluterate and oxygen. From left to right, 5-mC, 5-hmC, and 5-fC. Protein databank (PDB) ID: 4NM6, 5DEU, 5D9Y.

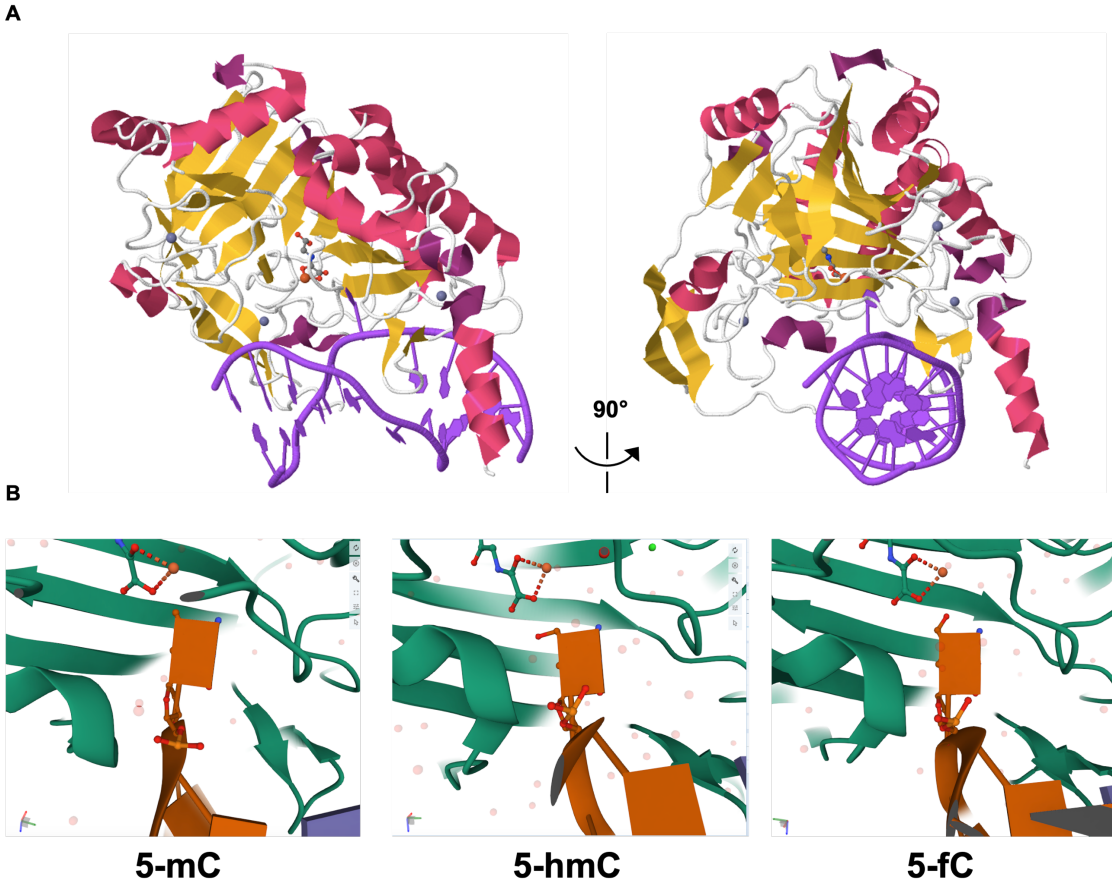

hmC to 5-fC and 5-caC progressively (Figure 1.1 and 1.3). 5-fC and 5-caC are present at very low levels in the mammalian genome, about 2-3 fold lower than those of 5-hmC (Iurlaro et al., 2013). For each oxidization step, the TET enzymes rely on 2-oxoglutarate (2-OG), iron (Fe(II)), and molecular oxygen for their activity (Tahiliani et al., 2009). The TET enzymes bind these co-substrates at 60μM, 30μM, and 4μM K_m respectively (Table 1.2) (Laukka et al., 2016). Concurrently, the TETs bind modified CpGs at a 100 nM K_m (Laukka et al., 2016). TETs have a 2-3 fold higher efficiency oxidizing 5-mC compared to oxidizing 5-hmC or 5-fC due to conformation differences in their active sites (Figure 1.3B) (Laukka et al., 2016). Therefore, 5-

hmC accumulates rather than being lost via oxidation to 5-fC. After the base is converted to 5-caC, the 5-caC is excised and an unmodified cytosine is inserted through base excision repair (Maiti and Drohat, 2011).

Table 1.2. TET1 and TET2 K_m values compared to HIF prolyl hydroxylase.

	TET1	TET2	HIF PHD
Methylated DNA K_m (nM)	75 ± 55	125 ± 85	-
Fe(II) (μM)	4.8 ± 4	3.6 ± 3	0.03 ± 0.004
2-OG (μM)	55 ± 20	60 ± 15	60
O_2 (μM)	30 ± 10	30 ± 3	250

The affinity of TETs for oxygen is much higher than that of the HIF prolyl-hydroxylases, which are also 2-OG/O_2-dependent dioxygenases like TETs, and hydroxylate hypoxia-inducible factor α (HIFα) for degradation (Laukka et al., 2016). Although both enzyme families use O_2 as a substrate, the higher affinity for O_2 in TETs (30 μM K_m) indicates that the TETs may retain activity in hypoxic environments. Later studies showed that TETs retain catalytic function under physiological hypoxia, at O_2 concentrations at which the HIF prolyl-hydroxylases no longer function (Laukka et al., 2016).

TET activity is enhanced by ascorbate (vitamin C) by maintaining the Fe co-factor in a reduced (II) state (Kuiper and Vissers, 2014). Ascorbate is essential for the function of collagen prolyl-4-hydroxylase, another 2-OG/O_2-dependent dioxygenase like the TETs. The addition of ascorbate to cultured mouse ES cells or mouse embryonic fibroblasts leads to a rapid Tet-dependent increase in 5-hmC levels (Blaschke et al., 2013; Minor et al., 2013; Yin et al., 2013). Other studies show demethylation in ascorbate treated human ES cells and mouse embryonic fibroblasts in addition to significant changes in the transcriptome (Blaschke et al., 2013; Chen et al., 2013; Chung et al., 2010).

Alternate transcripts of the *TET1* gene

Several recent papers describe alternate transcripts of *TET1* that are translated into a 'short' TET1 isoform with its own distinct role independent of full-length TET1 (Good et al., 2017; Greer et al., 2021; Yosefzon et al., 2017; Zhang et al., 2016c). To date, most of this research has been done in mouse systems. Two of these studies posit that a switch from full-length *Tet1* (*Tet1fl*) to short *Tet1* (*Tet1s*) is part of normal cell differentiation and embryonic development (Yosefzon et al., 2017; Zhang et al., 2016c). In *Tet1s,* the first two exons of *Tet1fl* are not transcribed, which means Tet1s does not have a CXXC domain, but the catalytic domain remains intact (Figure 1.4) (Zhang et al., 2016c). Tet1fl is more common in undifferentiated tissues, and Tet1s is more common in differentiated tissues, with the switch occurring after e14.5 (Yosefzon et al., 2017; Zhang et al., 2016c). Because TET1s has an intact catalytic domain, both studies questioned why the isoform switch even occurred at all, as TET1s was presumably a functional dioxygenase (Yosefzon et al., 2017; Zhang et al., 2016c). Here the findings diverged: one study claimed that TET1s was catalytically inactive, but this study had only tested its dioxygenase activity on the cytosine modifications in a single gene promoter (Yosefzon et al., 2017). In contrast, other work showed that TET1s was enzymatically active, but 5-hmC levels were not as high as those produced by TET1fl (Figure 1.5A) (Zhang et al., 2016c). Given both TET1fl and TET1s were both catalytically active in their experiments, the authors hypothesized that global chromatin binding of TET1s might be altered due to the lack of

Figure 1.4. Transcripts and isoforms of Tet1 identified in (Zhang et al., 2016). A. Transcripts of *Tet1fl* and *Tet1s.* B. Domains of Tet1fl and Tet1s isoforms.

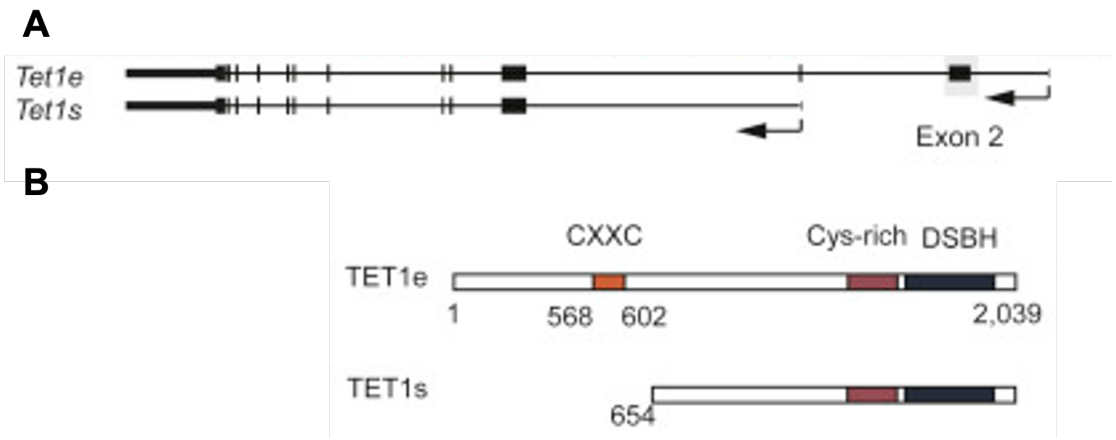

CXXC domain (Zhang et al., 2016c). When the authors separated the soluble fraction and the chromatin fraction of cells, they found far less TET1s in the chromatin fraction compared to TET1fl (Zhang et al., 2016c). From these results, the authors concluded that TET1s, although catalytically active and able to target specific sites, is a less efficient dioxygenase compared to TET1fl (Zhang et al., 2016c). They hypothesized that the efficiency of TET1fl may be required for major global demethylation, such as imprint erasure of embryonic stem cells, whereas TET1s is sufficient for normal demethylation of differentiated cells (Zhang et al., 2016c).

Figure 1.5. Downstream impacts of Tet1s on 5-hmC and gene expression. A. Dotblot of 5-hmC in cells expressing *Tet1fl* or *Tet1s* from Zhang et al., 2016. B. Number of differentially expressed genes after *Tet1fl* (pink) or *Tet1s* (blue) is overexpressed (top) or repressed (bottom). Image from Greer et al., 2021.

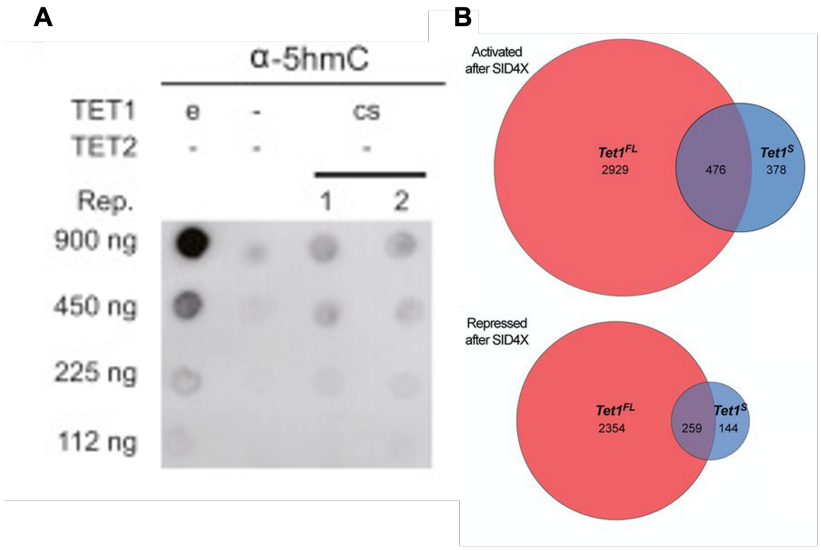

The short *Tet1* transcript has also been shown to be expressed in hippocampi neurons of mice and *Tet1fl* was found to be nearly undetectable (Greer et al., 2021). RNA-sequencing (RNA-seq) experiments with and without overexpression of each *Tet1* transcript revealed that the loss of *Tet1s* did not alter the transcriptome as much as loss of *TET1fl* (Figure 1.5B) (Greer et al., 2021). Because of its greater impact on global gene expression, the authors hypothesized *Tet1fl* is the more efficient isoform, by more proficiently modulating the 5-hmC epigenetic landscape. In addition, these results support the observations in previous studies that Tet1s seems to be the less efficient isoform of Tet1 (Greer et al., 2021; Yosefzon et al., 2017; Zhang et al., 2016c). From the RNA-sequencing experiments, the authors identified differentially

expressed genes after the loss of *Tet1fl* or *Tet1s.* They found that *Tet1fl* and *Tet1s* target distinct differentially expressed genes with some overlap (Figure 1.5), suggesting the two isoforms are not redundant and have different functional roles. In summary, studies of *Tet1* transcripts in mice have found expression of a specific transcript of *Tet1* results in altered global 5-hmC and/or gene expression and proposed a role for Tet1s that is independent of the role of Tet1fl.

Similar protein isoforms are also found in human systems: TET1fl is present in ES cells, and a smaller TET1 protein (TET1s) that lacks the CXXC domain is present in adult tissues (Figure 1.6) (Good et al. 2017). TET1s is catalytically active, but when each *TET1* was overexpressed in HEK293T cells, subsequent RNA-seq experiments showed *TET1s* overexpression did not alter the transcriptome as much as *TET1fl* overexpression (Good et al. 2017). Overall, TET1s was found to have a weaker effect on DNA methylation, indicating that TET1s was the less efficient isoform, similar to earlier observations from murine systems (Good et al., 2017). In addition, researchers showed that TET1s had targets distinct from TET1fl. The mechanism behind this is unclear, although it has been shown that the TET1s binds outside of CpG islands, a distinction from TET1fl targeting that may be due to loss of the CXXC domain (Good et al. 2017). Finally, it was determined that there was frequent overexpression of *TET1s,* but not *TET1fl,* in many cancers, including breast, uterine, and ovarian cancers (Good et al. 2017). The role of TET1s is unknown but the researchers hypothesized that this cancer-specific alternate isoform may be involved in tumorigenesis (Good et al., 2017).

Figure 1.6. Human TET1s isoforms identified in (Good et al., 2017.)

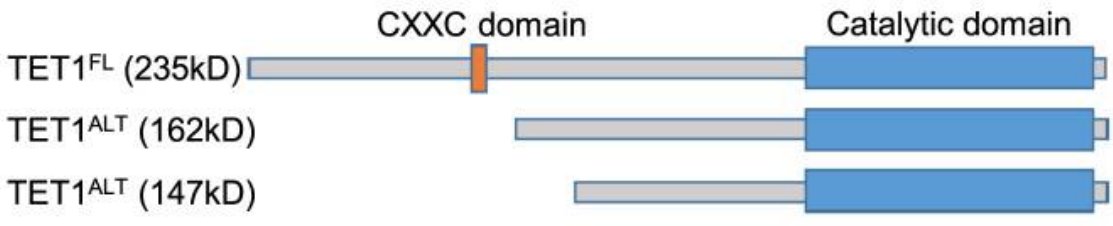

Binding partners of the TET enzymes

Since the discovery of TET proteins, multiple studies have also identified TET binding partners. A great number of binding partners and interactions involving the entire TET family has been described. Because my research focused on TET1, I will only report on known binding partners of TET1 in this chapter. Research on TET1 binding proteins suggests that the function of these binding partners can modify TET1 localization, activity, and stability (Figure 1.7). Many of the binding partners are not yet fully characterized and others may have identified functions outside of their interaction with TETs.

Regulating and directing TET1 to specific sites in the genome is the most common function of identified TET interactors. These interactors are usually classified as chromatin-binding proteins: epigenetic modifiers and TFs. A variety of proposed mechanisms of TET1 recruitment and localization have been described: from (1) promoting TET1 binding to DNA to (2) recruiting TET1 to target regions in the genome (Figure 1.7A).

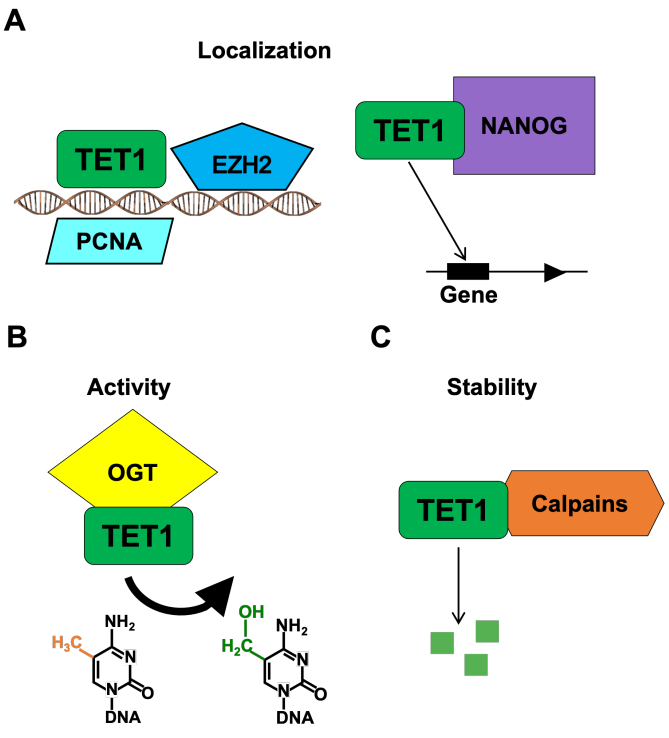

Figure 1.7. TET1 binding partners impact TET1 localization, activity, and stability. A. Two common mechanisms of TET1 localization are to assist in DNA binding (left), examples are PCNA and EZH2, and to recruit TET1 to specific genomic sites (right), such as NANOG. B. Binding of OGT increases TET1 activity when it is engaged with DNA. C. Calpains bind and degrade all three TET enzymes, reducing TET stability. Image adapted from Cao et al., 2019

Proteins that are thought to modulate TET1 binding to DNA include MeCP2, HDAC1/6/7, EZH2, mSin3A, PCNA, and LSD1 (Cartron et al., 2013). All

of these proteins: (1) promote stability of the TET1-DNA interaction, (2) were found to bind TET1 directly, (3) and form larger complexes with each other (Figure 1.7A) (Cartron et al., 2013). Further investigation revealed that TET1:EZH2 and TET1:Sin3A complexes recruit TET1 to specific genomic loci (Chandru et al., 2018). However, TET1:EZH2 and TET1:Sin3A have been only been implicated in the regulation of the genes *HOXD12* and *NES1* respectively (Cartron et al., 2013; Chandru et al., 2018; Williams et al., 2011), due to selective screening at these targets and not an unbiased approach that would include the entire genome. Loss of the complexes resulted in increased methylation at each promoter, and as a result, lowered expression from the genes. Another study in mouse ES cells examined the impact of Tet1:Sin3a complex on global genomic targets and found that Sin3a recruited Tet1 to demethylate the promoter of *Lefty1* (Zhu et al., 2018). Loss of Sin3a resulted in altered localization of Tet1 and deregulation of expression from 111 genes. The level and distribution of 5-hmC was not assessed, so it is unknown if aberrant 5-hmC was the cause of these expression changes.

The second mechanism of TET1 localization is via binding partners that act as 'recruiters' of TET1 to specific sites in the genome (Figure 1.7A). TFs that aid in the localization of TET1 include NANOG and EGR1 (Costa et al., 2013; Sun et al., 2019). In addition to binding each other, TET1 and NANOG occupy the same loci at genes (Costa et al., 2013). When NANOG was depleted, TET1:DNA binding was reduced, indicating NANOG facilitates TET1 binding of the genome. Co-expression of NANOG and TET1 together increased 5-hmC levels at specific genes involved in reprogramming to pluripotency. This study concluded that the physical association of NANOG and TET1 facilitated NANOG function in the reprogramming of mouse neural stem cells (Costa et al., 2013). In another murine system, EGR1 recruited TET1 to remove methylation marks from EGR1 gene targets, thereby activating their expression (Sun et al., 2019).

Non-TF proteins that recruit TET1 to genomic sites are the Mbd3/NuRD complex and PCNA (Cartron et al., 2013; Costa et al., 2013; Williams et al., 2011; Yildirim et al., 2011).

Sequential chromatin-immunoprecipitation (ChIP) experiments determined TET1:PCNA complexes bind *MUC2* and *RRMI* and play a role in their regulation by removing modified cytosines from the genes, thus promoting their expression (Cartron et al., 2013).

Independent of any O-GlcNAcylation activity, stable Tet-Ogt interaction promotes Tet activity and modulates Tet genomic localization (Figure 1.7B). OGT binds TET1 through a conserved C-terminal domain on TET1, and is thought to form a larger complex with SIN3A and possibly other proteins (Hrit et al., 2018; Vella et al., 2013). Ogt and Tet1 colocalized at unmethylated CpG-rich promoters (Vella et al., 2013), and other studies have found that loss of Ogt protein resulted in abnormal Tet1 localization in ES cells, indicating Ogt is important for Tet1 binding of specific genomic sites (Shi et al., 2013). Multiple groups have reported that the loss of Tet1:Ogt interaction causes reduced total 5-hmC level and reduced expression from Tet1 activated genes (Hrit et al., 2018; Shi et al., 2013). Ultimately, these experiments indicate that Tet1:Ogt binding: (1) increases Tet1 activity, and (2) recruits Tet1 to genomic sites (Figure 4B) (Hrit et al., 2018; Shi et al., 2013). TET2/3:OGT binding, alternatively, does not appear to impact the 5-hmC epigenetic landscape, and instead, TET2/3 plays a scaffolding role for OGT (Deplus et al., 2013; Ito et al., 2011).

Very few proteins have been identified that regulate TET stability in general. Proteins that aid in the degradation of TET proteins belong to a single family: the calpains. Calpains 1 and 2 regulate TET stability by binding the enzyme directly and cleaving it (Figure 1.7C) (Wang and Zhang, 2014). This mechanism of TET protein degradation predominates stages of embryonic development when TET expression is particularly high (Wang and Zhang, 2014). TET1 and TET2 are degraded by calpain1 in mouse ES cells, whereas TET3 is degraded by calpain2 during ES cell differentiation (Wang and Zhang, 2014). In ES cells, loss of calpains resulted in two-fold higher total 5-hmC levels, downregulation of genes *Cdx2* and *Eomes*, and upregulation of genes *Ngn2* and *Pax6in* (Wang and Zhang, 2014). Therefore, TET:calpain

complexes are required to maintain the 5-hmC landscape and normal gene expression in ES cells.

The role of TETs in cancer pathogenesis

In previous sections, I indicated 5-hmC and TETs contribute to certain cancers, such as through aberrant 5-hmC localization or *TET1s* expression. Availability or restrictions of TET substrates and co-factors can also promote cancerous phenotypes in cells as well. 2-OG is produced from isocitrate by the isocitrate dehydrogenases (IDH1/2) in the TCA cycle. It is usually very available in cells and is not limiting for TET activities. However, in pathological conditions, mutations in genes encoding TCA cycle enzymes can result in the accumulation of 2-OG analogs (Dang et al., 2009; Pollard et al., 2005). Commonly found in cancers, the IDH1 R100/R132 and IDH2 R140/R172 missense mutations catalyze the production of R-2-hydroxyglutarate (R-2-HG) (Dang et al., 2009; Losman and Kaelin, 2013). R-2-HG competes with 2-OG for TET binding, but cannot be used in the oxidation reaction and therefore acts as an inhibitor of TETs (Xu et al., 2011). Consistent with this finding, glioblastomas and leukemias with these *IDH* mutations exhibit global hypermethylation (Figueroa et al., 2010; Ko et al., 2010; Turcan et al., 2012). In addition, *IDH* and *TET* mutations are almost always mutually exclusive in leukemias, strongly suggesting that these pathogenic mutations have the same function in cancerous processes (Gaidzik et al., 2012; Patel et al., 2012). Two additional TCA cycle metabolites, fumarate and succinate, were found to accumulate in solid tumors with mutated fumarate hydratase or succinate dehydrogenase (Pollard et al., 2005). Fumarate and succinate are also able to inhibit TET activity by competing with 2-OG for TET binding (Laukka et al., 2016). This was shown in SK-N-BE(2) neuroblastoma cells, where 5-hmC levels decreased 10-40% upon fumarate or succinate treatment (Laukka et al., 2016). Another example of restricted resource availability is the loss of molecular oxygen in pathological hypoxia found in solid tumors, such as neuroblastoma (Thienpont et al., 2016).

The emerging role of epigenetics in pediatric cancer neuroblastoma

Neuroblastoma (NB) is the most common extracranial solid tumor of childhood and is the primary cause of death for pediatric cancer for children between the ages of one and five years (Louis and Shohet, 2015). The primary tumor can arise from a variety of tissues in the abdomen but has a predilection for the adrenal glands (Figure 1.8) (Delloye-Bourgeois and Castellani, 2019). Patients with NB have diverse clinical outcomes ranging from tumors regressing spontaneously to tumors progressing to metastatic disease (Maris et al., 2007). High risk patients receive a combination of systemic chemotherapy, surgical resection, MIBG-targeted radiation treatment, tandem autologous transplant, radiation, and immunotherapy as part of current treatment protocols (Van Arendonk and Chung, 2019).

Figure 1.8 Common sites of primary NB tumors**.** NB arises from neural crest tissue most commonly in the abdominal cavity. Although origin sites include the spine, kidneys, and paraspinal nerve tissue, NB has a predilection for the adrenal glands. Image adapted from (Delloye-Bourgeois and Castellani, 2019.)

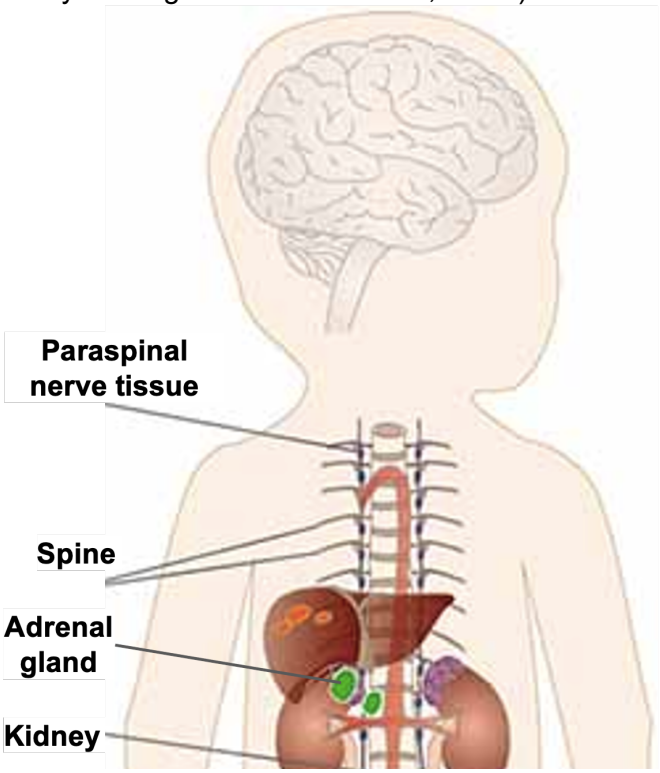

Patients with NB tumors are classified by risk based on several diagnostic criteria, including age, grade, DNA ploidy and chromosomal changes, *MYCN* status, and stage (Van Arendonk and Chung, 2019). There is an inverse relationship between the age of tumor diagnosis and prognosis in NB patients, with younger patients less than 18 months of age

generally having the best prognosis (George et al., 2005; London et al., 2005; Schmidt et al., 2005). Children who are older than 18 months are often classified as intermediate or high risk independent of other factors. NB grade is based on NB tumor histologic features and is subdivided into 3 categories: differentiating, poorly differentiated, and undifferentiated (Sokol and Desai, 2019). Although usually only indicative of risk in the context of other diagnostic criteria, patients with tumors with a 'differentiating' grade tend to be classified as low risk. 'Poorly differentiated' and 'undifferentiated' grades of tumor differentiation are usually classified as intermediate and high risk.

DNA ploidy and chromosomal changes in NB cells are analyzed and used to stratify risk. Hyperdiploid NB cells are associated with a better prognosis, specifically in patients under 24 months (George et al., 2005). In addition, there are three recurrent chromosome changes that occur in NB: 1p deletion, 11q deletion, and 17q gain (Attiyeh et al., 2005; Plantaz et al., 1997). All three chromosome changes are associated with a worse prognosis in NB (Attiyeh et al., 2005; Plantaz et al., 1997).

MYCN status refers to the presence or absence of *MYCN* amplification, which is present in about 25% of NB tumors (Otte et al., 2021). Patients with a tumor that is *MYCN* amplified are always classified as high risk. This is because the amplification of *MYCN* correlates with poorly differentiated, aggressive tumors, and poor patient outcome (Huang and Weiss, 2013; Otte et al., 2021). Multiple studies have shown that MYCN targets and promotes expression from gene targets involved in angiogenesis, self-renewal and pluripotency, and proliferation (Bell et al., 2007; Dungwa et al., 2012; Fotsis et al., 1999; Hatzi et al., 2000; Kang et al., 2008; Muth et al., 2010; Ochiai et al., 2010; Ozer et al., 2007; Tweddle et al., 2001). In addition, MYCN promotes mechanisms of evading apoptosis and immune surveillance (Slack et al., 2005; Song et al., 2007; Valsesia-Wittmann et al., 2004). Additionally, MYCN amplification is correlated with an invasive phenotype and frequency of metastatic spread in stage IV (Stage M) NB patients.

The International Neuroblastoma Risk Group Staging Systems provides a standard framework for determining a patient's stage and risk group based on imaging, physical exam, and biopsies prior to treatment initiation (Monclair et al., 2009). The INRGSS can be used in tandem with an older staging system, The International Neuroblastoma Staging System (INSS), which additionally relies on results of surgical resection (Monclair et al., 2009). Both systems stage NBs based on origin, location, and whether the tumor has spread to a distant part of the body (metastasized). Patients with tumors that have metastasized are nearly always classified as high risk, because the disease is much harder to treat at this stage (Stage M/IV). Because risk is so high for stage M/IV NB patients, NB researchers have focused on identifying oncogenic drivers of metastatic spread in NB. Several studies have identified the chemokine receptor CXCR4 as a promoter of tumor metastatic growth in NB (Klein et al., 2018; Meier et al., 2007). CXCR4 is perhaps best described in hematopoietic systems, specifically within hematopoietic stem cells (HPSCs). CXCR4 is a receptor expressed on the cell surface of HPSCs, where it binds chemoattractant stromal cell-derived factor 1 (SDF-1), playing an essential role in HPSC localization to the bone marrow (Bianchi and Mezzapelle, 2020; Nie et al., 2004). In clinical settings, CXCR4 antagonists are most commonly used to mobilize HSPCs from the bone marrow for harvest for bone marrow transplant (Bianchi and Mezzapelle, 2020; Nie et al., 2004). However, CXCR4 is also expressed on the surface of many types of cancer cells, such as breast, pancreas, melanomas, and NBs (Chatterjee et al., 2014; Russell et al., 2004), where it promotes survival, invasion, angiogenesis, and metastasis through activation of a large number of signaling pathways, including JAK/STAT, MAPK/ERK, and PI3K/AKT (Figure 1.9) (Chatterjee et al., 2014; Domanska et al., 2013; Guo et al., 2016; Xu et al., 2015). The role of CXCR4 in NBs is poorly understood but expression of CXCR4 protein in primary NB tumors correlates with poor patient outcome (Russell et al., 2004).

Large-scale sequencing projects have failed to identify many recurrent mutations in NBs (Molenaar et al., 2012a; Pugh et al., 2013), prompting investigators to study non-genetic drivers

of pathogenicity, such as altered transcription from genes (Decock et al., 2011). As epigenetic mechanisms commonly regulate gene expression, they have been singled out for study as potential drivers of pathogenicity in NBs

NB arises from the sympaticoadrenal lineage of the neural crest. This tissue is known to have high levels of 5-hmC in its genome (Globisch et al., 2010; Kriaucionis and Heintz, 2009; Szulwach et al., 2011). When neural crest cells undergo neuronal differentiation, 5-hmC increases and is enriched in the gene bodies of transcriptionally active genes, implying 5-hmC is an important epigenetic mark associated with transcription (Hahn et al., 2013; Kriaucionis and Heintz, 2009). However, it is important to consider that 5-hmC production may be reduced in NBs, because, as part of a solid tumor, NB cells are part of a heterogeneous oxygen level microenvironment.

Figure 1.9. Downstream pathways of CXCR4. CXCR4 activates downstream targets that promote migration, survival/proliferation, and transcription. Image adapted from (Xu et al., 2015).

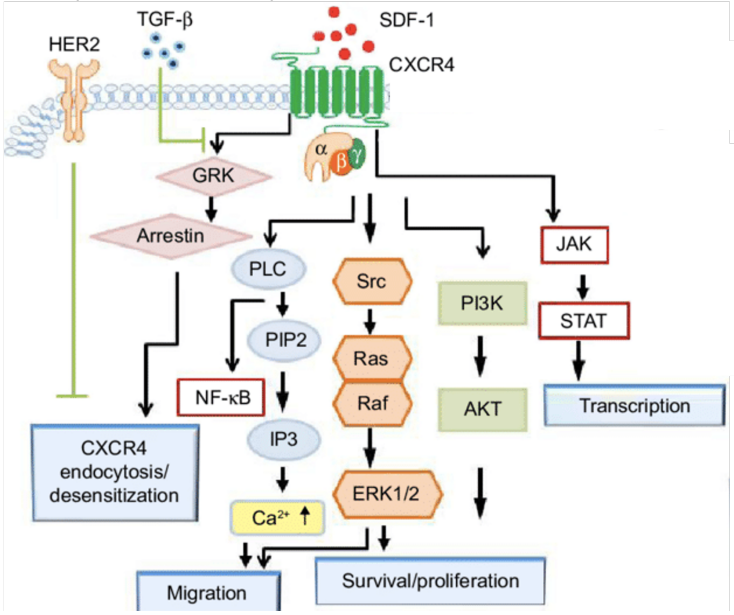

Cells in solid tumors are often subject to a hypoxic microenvironment

Although atmospheric oxygen is 21%, oxygen levels in human tissues have a median of 6.1% (Carreau et al., 2011). Tumor oxygen levels, however, are heterogeneous even within the same tumor (Vaupel et al., 2007) due to disorganized vasculature that accompanies the rapid cell proliferation characteristic of tumors (Figure 1.10) (Rankin and Giaccia, 2008; Thomas et al., 2013; Vaupel et al., 2007). As the tumor cells divide and multiply, access to available

capillaries becomes restricted, and the most isolated cells in the tumor receive less oxygen (Rankin and Giaccia, 2008).

Once a cell reaches a hypoxic state, changes occur on the molecular level to promote survival in a low oxygen environment. The mechanism by which cells survive in hypoxic environments was elucidated in the 1990s, when several groups, working in different model systems, characterized the HIF α/β-heterodimer TF family (Iliopoulos et al., 1996; Pugh et al., 1997; Wang and Semenza, 1995). HIF-1, the first member of the family to be described, consists of an α and β subunit (Wang and Semenza, 1995). The α subunit (HIF-1α), consists of four distinct domains: (1) A bHLH domain for DNA binding and dimerization; (2) A PAS domain for dimerization and target gene specificity; (3) An oxygen-dependent degradation domain (ODD); and (4) Two transactivation domains in the C-terminus of the protein(Huang et al., 1998). Among these, the ODD is the most essential part of HIF-1α for activation of the hypoxic response under low oxygen conditions, as if HIF-1α is targeted for degradation in normoxia through this domain.

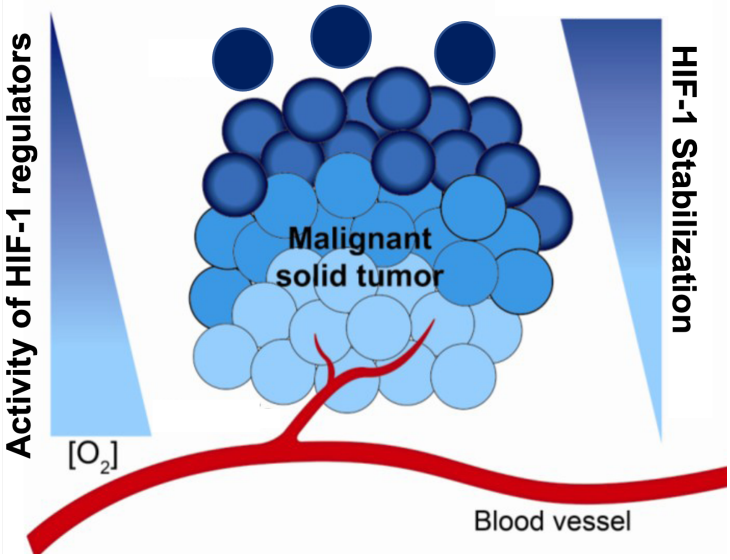

Figure 1.10. Diagram of hypoxic tumor microenvironment. Image adapted from (Thomas et al., 2013.)

Under normoxic conditions, HIF-1α is targeted for proteasomal degradation (Figure 1.11) (Ivan et al., 2001; Jaakkola et al., 2001). Both HIF-1α and HIF-1β are constitutively transcribed and translated in normoxia. In the cytoplasm, HIF-1α is bound by prolyl-4-hydroxylase domain (PHD) containing proteins. These PHDs recognize and hydroxylate two conserved proline

residues (p402 and p564) in the HIF-1α ODD (Ivan et al., 2001; Jaakkola et al., 2001). PHDs are reliant on oxygen and 2-OG to hydroxylate proline (Ivan et al., 2001; Jaakkola et al., 2001). The von Hippel Lindau tumor suppressor, pVHL, recognizes and targets the hydroxylated prolines (Ivan et al., 2001; Jaakkola et al., 2001). As pVHL is the recognition component of the E3-ubiquitin ligase complex, HIF-1α is ubiquitinated and subsequently degraded in the proteasome.

Under hypoxic conditions, PHDs lose activity, and HIF-1α accumulates and activates the hypoxic response (Figure 1.11). In a hypoxic environment, there is little free oxygen for PHDs to

Figure 1.11. HIF-1α is stabilized in hypoxic environments. A. HIF-1α is regulated through modification of two prolines. In normoxic environments, these two prolines are hydroxylated which are then recognized by VHL, which then ubiquitinates it for proteasomal degradation. In hypoxic environments, HIF-1α is not hydroxylated and therefore is allowed to accumulate. It binds HIF-1β, translocates to the nucleus, and induces expression from hypoxia target genes.

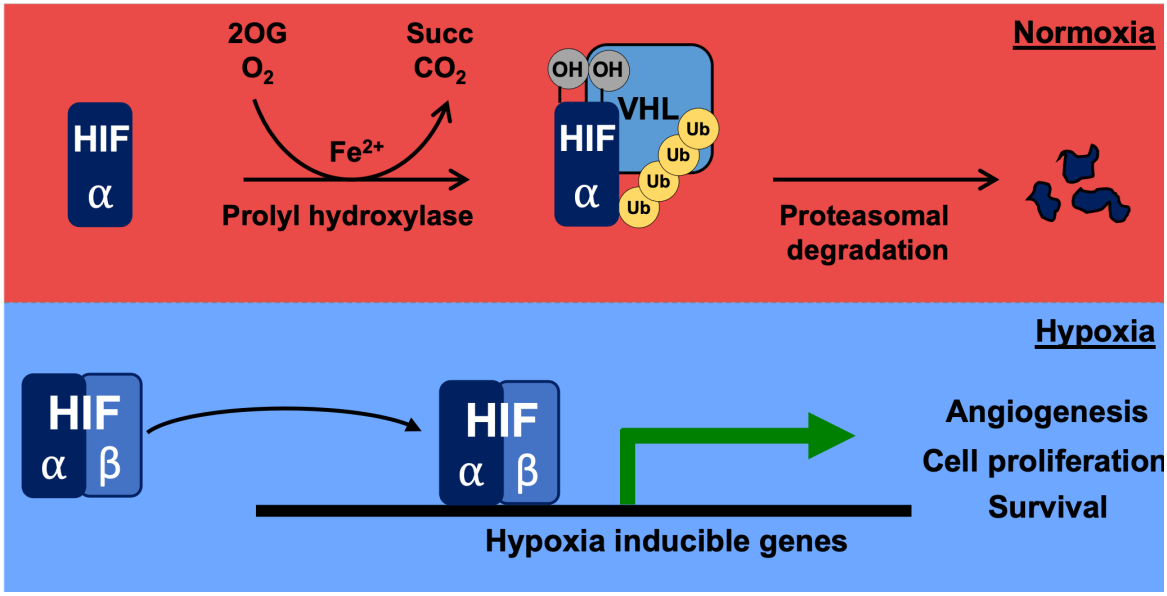

use in hydroxylation of the HIF-1α prolines. Therefore, HIF-1α is not immediately degraded in hypoxia, and it accumulates in the cytoplasm (Ivan et al., 2001; Jaakkola et al., 2001). HIF-1α binds its partner, HIF-1β, and then HIF-1 translocates into the nucleus (Wang and Semenza, 1995). Once in the nucleus, HIF-1 interacts with several binding partners and directly regulates gene expression from hypoxic response targets (Arany et al., 1996; Mahon et al., 2001). The

direct HIF-1 targets can be classified into four groups: angiogenesis, metabolism, proliferation, and invasion/metastasis (Rankin and Giaccia, 2008).

As discussed above, tumors often become hypoxic due to disorganized vasculature. Accumulation of HIF-1α is also commonly detected across many tumors (Talks et al., 2000). In many clinical cancer studies, elevated HIF-1α correlates with poor patient outcome through upregulation of pathways in angiogenesis, metabolism, proliferation, and metastasis (Figure 1.11) (Rankin and Giaccia, 2008). Researchers aim to understand how HIF-1 augments tumorigenesis specifically in each cancer in order to identify novel biomarkers and targets, including NB.

5-hmC increases in *MYCN*-amplified NB cells exposed to hypoxia

As mentioned above, NB arises from 5-hmC-rich tissue: the sympaticoadrenal lineage of the neural crest. Because of this, the Godley and Cohn laboratories thought it would be an excellent model to test the effect of hypoxia on the level of 5-hmC. They hypothesized that when NB cells were exposed to hypoxia, 5-mC levels would go up, and 5-hmC levels would decrease. Unexpectedly, when the hypoxic 5-hmC levels were measured, they found that 5-hmC increases compared to normoxic levels in *MYCN*-amplified lines (Figure 1.12) (Mariani et al., 2014). Further investigation found that the hypoxic 5-hmC was enriched along the gene bodies of canonical hypoxic response genes. To determine the mechanism behind this increase, *TET* mRNA expression was measured to determine if any of them were induced in hypoxia. They found *TET1* was upregulated in hypoxia, and when its expression was silenced, 5-hmC no longer increased. To identify the mechanism through which TET1 is regulated in hypoxia, HIF-

Figure 1.12. Model of TET1 function and 5-hmC distribution in hypoxic NB. Despite low oxygen levels, *TET1* expression is induced in *MYCN*-amplified NB. *TET1* induction subsequently increases total 5-hmC levels in hypoxia. Hypoxic 5-hmC was enriched along the gene bodies of hypoxic response genes. Image adapted from (Thomas et al., 2013.)

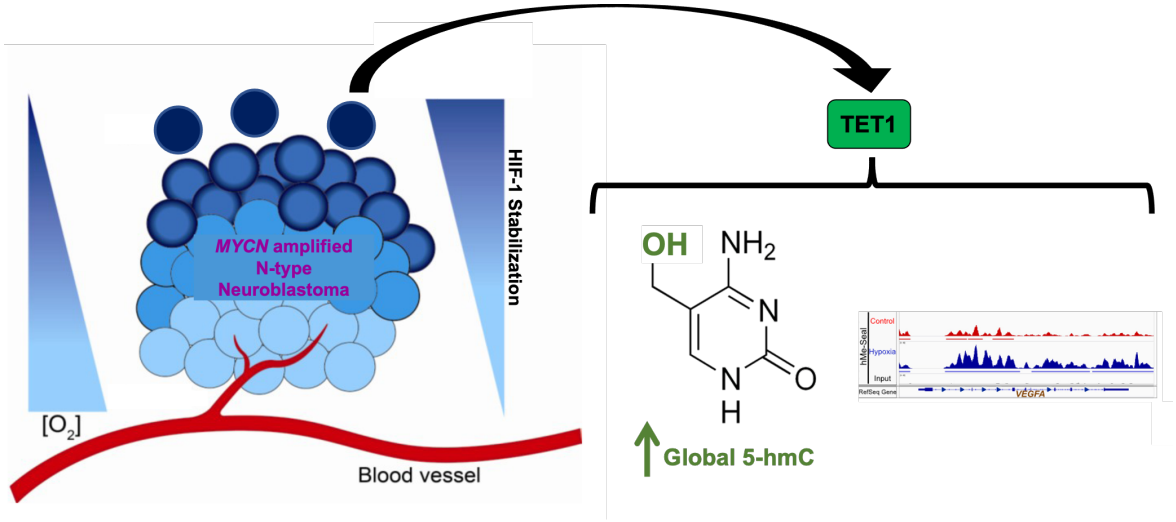

1α expression was silenced. Under these conditions *TET1* expression was no longer induced and 5-hmC level did not increase (Mariani et al., 2014).

Hypothesis and specific aims

The mechanism by which *TET1* regulates hypoxic changes of 5-hmC in NB was not elucidated fully (Mariani et al., 2014). Unanswered questions include why this phenotype was unique to *MYCN*-amplified NB and whether the TF HIF-1 directly regulates the *TET1* gene and/or TET1 protein. Additionally, it was unclear if 5-hmC enrichment in hypoxic response genes and subsequent augmentation of gene expression mediated the aggressive hypoxic phenotype characteristic of NB cell lines.

I hypothesize that TFs control and direct the 5-hmC epigenetic landscape and migratory phenotype via regulation of the *TET1* gene and TET1 protein in NB. This will address unanswered questions about why this phenotype occurred exclusively in *MYCN*-amplified NB

cells, how HIF-1 regulates *TET1,* and whether 5-hmC mediates aggressive hypoxic tumor phenotype.

My thesis work tested this hypothesis via three Specific Aims:

Aim 1: To determine if MYCN regulates normoxic *TET1* transcription in neuroblastoma. Since hypoxic *TET1* induction and 5-hmC increases were limited to NB cells that were *MYCN*-amplified (Mariani et al., 2014), I hypothesized that MYCN binds and controls transcription from *TET1* directly. I tested this hypothesis by identifying potential MYCN binding site(s) in *TET1,* then confirming MYCN binds these site(s) with ChIP. I also determined whether MYCN controls *TET1* transcription from these site(s) with gene editing.

Aim 2: Determine the molecular mechanism by which HIF-1 regulates *TET1* gene and TET1 protein in hypoxia. Previously, Godley laboratory members identified two HIF-1α binding sites in the *TET1* gene under hypoxic conditions. I hypothesized that HIF-1 controls *TET1* transcription from one or both binding sites. I determined that HIF-1 regulates transcription from these sites in hypoxia via the use of gene editing. I also determined how loss of these regulatory sites impacts 5-hmC level in hypoxic compared to normoxia. Previously, TET1 protein levels in normoxia and hypoxia were not described in Mariani et al (Mariani et al., 2014). With Western blotting I confirmed TET1 protein increases in hypoxia, reflective of *TET1* mRNA in SK-N-BE(2) cells. I also determined TET1 protein stability and compared normoxic and hypoxic conditions**.** Additionally, I hypothesized that HIF-1 or HIF-1 associated proteins bind TET1 and augment its activity.

Aim 3: To identify how 5-hmC enrichment changes in response to a hypoxic environment contribute to an aggressive tumor phenotype in NB. Although Mariani et al. described blunted expression from hypoxic response genes in *TET1* knockdown cells, any subsequent

impact altered gene expression had on NB cell hypoxic phenotype was not addressed. I hypothesized that 5-hmC enrichment in hypoxia target genes augments aggressive migration and invasion phenotype observed in hypoxic NB cells. I performed functional assays to evaluate NB cell response to hypoxia, including migration and invasion assays, and compared wild type NB cells to those that lack *TET1.*

CHAPTER II

Methods

Cell culture

NB cell lines were provided by the Cohn Laboratory and were authenticated with STR profiling analysis and tested negative for *Mycoplasma*. SK-N-BE(2), NBL-WN, LA1-55n, NBL-S, SH-SY5Y, LA1-5S, NBL-WS, and SHEP cells were cultured in RPMI with 10% fetal bovine serum (FBS). Tet-21/N cells (Lutz et al., 1996) were cultured in RPMI with 10% Tet system FBS (Clontech 631106). Normoxic culture was done at 37°C under 21% O_2 and 5% CO_2 in a humidified incubator. For hypoxic exposure, cells were incubated under 1% O_2 and 5% CO_2 in a humidified chamber. Tet-21/N cells were maintained with 1 μg/mL doxycycline, and *MYCN* induction was induced by the removal of doxycycline from the media.

CRISPR-Cas9 genome editing

A CRISPR-Cas9 system was used to perform genome editing in SK-N-BE(2) and NBL-WN cells. Guide RNAs (gRNAs) were designed and evaluated with the program CRISPOR (Concordet and Haeussler, 2018) and were ligated into plasmid Lenticrispr v2 (Addgene plasmid #52961) following the Zhang lab protocol (Sanjana et al., 2014). The plasmid with the gRNA of interest was co-transfected with psPAX2 (Addgene plasmid #12260) and pMD2.G **(**Addgene plasmid #12259) into HEK293T cells to produce lentiviral particles (Moffat et al., 2006). After 48 hours, lentiviral containing media was collected and filtered. Polybrene was added to a concentration of 4 μg/mL, and then lentiviral media was added to SK-N-BE(2) or NBL-WN cells. Lentivirus-containing media was removed after 6-12 hours, and the cells were incubated in 10% FBS RPMI for 48 hours. Puromycin was added to the cells at 2.5 μg/mL for SK-N-BE(2) cells and 0.25 μg/mL for NBL-WN cells for 72 hours. Post-puromycin selection, a

portion of the mixed clone population was cryopreserved; and another portion was diluted into 96-well plates for single clone expansion. To screen each clone, DNA was extracted using phenol:chloroform, and PCR using GoTaq (Promega PRM3005) was performed with primers targeting the region of the edited site (Table 2.1). The mutation within each single cell clone was defined using Sanger sequencing of the PCR amplicon spanning the gene edited site.

RNA isolation and sequencing

Total RNA was isolated with RNAzol (Sigma-Aldrich, R4355) following the RNAzol manufacturer's protocol. RNA was converted to cDNA with Life Technologies High-Capacity cDNA Reverse Transcription Kit (4368814). Quantitative PCR was done with Power SYBR Green PCR Master Mix (Life Technologies 4368706). Primers for qPCR can be found in Table 2.1.

RNA was sequenced on Illumina HiSeq 4000, at a single end for a length of 50 bp. Reads from RNA-seq in fastq format were aligned to the hg19 reference genome with Tophat2 (Kim et al., 2013). Gene expression was quantified and compared with tools in the Cufflinks package (Trapnell et al., 2012). Data from my RNA-seq experiments can be accessed under GSE167476.

Table 2.1. Oligos utilized in my work

Primer name	Sequence (5'->3')
TET1_qPCR_F	GAGAATAGGTATGGTCAAAA
TET1_qPCR_R	CTTCATCACTGCTTCTTCTT
MYCN_qPCR_F	CAGACCAGCGGCGGCGA
MYCN_qPCR_R	AACGCCGCTTCTCCACAGT
CXCR4_qPCR_F	CCCTCCTGCTGACTATTCCC
CXCR4_qPCR_R	TAAGGCCAACCATGATGTGC
TET3_qPCR_F	CGTCGAACAAATAGTGGAGA
TET3_qPCR_R	CTTTCCCCTTCTCTCCATAC
DNA2_qPCR_F	TGTCCCAAATGACCTGC
DNA2_qPCR_R	ATTCCCAGTCCTAAGCAAG
LARP1_ChIP_F	TGACACCCAGCCTAAAGA
LARP1_ChIP_R	GGAGGTATCTTAAAGGGCC
DNA2_ChIP_F	ACAGAAAAGACAGCGGAAC
DNA2_ChIP_R	GACACGGGTTGGAGTGT
TET1_S1_ChIP_F	GGGTGCTGGGGCTGGTC
TET1_S1_ChIP_R	CTGGGGGCGGTAGGTTGTG
TET1_S2_ChIP_F	TCTT TGT GGG GCT GTT TTT
TET1_S2_ChIP_R	GAGGTAGCCATCTTGCTTG
TET1_negcon_ChIP_F	CACTTGAGTCTAGGAGTTTAAGG
TET1_negcon_ChIP_R	GTTTCTCAATATCAGGTTTGTTTTG
guideRNA	**Sequence (5'->3')**
g1_TET1_S2_F	GCCAGCACTGTAGACGTGCT
g1_TET1_S2_R	AGCACGTCTACAGTGCTGGC
g2_TET1_S2_F	GCCCAGCACGTCTACAGTGC
g2_TET1_S2_R	GCACTGTAGACGTGCTGGGC
g3_TET1_S2_F	GCCATTGGCTGCACTCTTTG
g3_TET1_S2_R	CAAAGAGTGCAGCCAATGGC
g1_TET1_S1_F	GCTGGTCGTGCAGCACGTGA
g1_TET1_S1_R	TCACGTGCTGCACGACCAGC
g_DNA2_F	GCGTTCCACGTGGGGCCCCT
g_DNA2_R	AGGGGCCCCACGTGGAACGC

cDNA conversion and quantitative PCR

RNA was converted to cDNA with Life Technologies High-Capacity cDNA Reverse Transcription Kit. Quantitative PCR was done with Power SYBR Green PCR Master (Life Technologies) on Applied Biosystems Fast 7500 machines.

DNA isolation

DNA was extracted with phenol:chloroform**.** Following the removal of the aqueous layer, the DNA was precipitated with 100% ethanol and washed with 70% ethanol. The pellet was resuspended in 10 mM tris pH 7.8.

Detection of 5-hmC and 5-mC by UHPLC-MS/MS

UHPLC-MS was performed as described in (Song et al., 2005). Briefly,1-2 μg of genomic DNA was denatured at 100ºC for 3 minutes, followed by incubation with five units of nuclease P1 (Sigma) at 37°C for 2 hours, followed by addition of 2.5 μL of 1M ammonium bicarbonate and 0.002 units of phosphodiesterase I (Sigma-Aldrich) and incubation for 2 hours at 37°C. The sample was then incubated with 0.5 units of alkaline phosphatase (Invitrogen) for 1 hour at 37°C. The samples were diluted and filtered through 0.22 μm PVDF filters (Millipore) to remove any large particulates. Hydrolyzed DNA was run on an Acquity UPLC Oligonucleotide BEH C18 Column (Waters 186003950). After moving through the column, the sample was injected into an Agilent 6460 Triple Quad MS-MS with 1290 ultra high-performance liquid chromatography (UHPLC) for multiple reaction monitoring (MRM) quantitation.

5-hmC selective chemical labeling

5-hmC selective chemical labeling (hMe-Seal) was performed according to reported methods (Mariani et al., 2014; Song et al., 2011). 20 µg of sonicated genomic DNA was labeled with UDP-6-N3-glucose and biotinylated using DMCO-S-S-PEG3-Biotin Conjugate (Click Chemistry Tools). The biotinylated DNA was affinity purified and prepared as DNA libraries for sequencing**.** DNA libraries were sequenced on Illumina HiSeq 4000, at a single end for a length of 50 bp.

hMe-SEAL peak calling and FPKM quantification analysis

First, quality of the reads and the fastq files were checked by running FastQC. Sequenced reads were aligned to the hg19 genome with Burrows-Wheeler Aligner (Li and Durbin, 2009). Peaks were called with MACS2 (Zhang et al., 2008). Peak files from all time points were merged. To determine how the peaks were growing or shrinking over time, the bed files from every timepoint were combined with bedtools merge into a single file, which was then converted into gtf format so it could be used as an input for HTSeq-count analysis (Anders et al., 2015). Using this input and the original bam file for each timepoint, HTSeq-count calculated the number of reads present at each site per timepoint, which was converted to FPKM (number of fragments/number of kilobases/1x10^6). Selective filtering for regions that underwent ~1.3-fold changes in FPKM was done in R (R Core Team, 2020).

Following reported methods, I conducted genomic element analyses by intersecting 5-hmC peaks that underwent significant changes over time with files containing the location and annotation of genomic elements (Cao et al., 2019; Mariani et al., 2014). Defined genomic regions included 3'UTR, 5'UTR, coding domain sequences, CpG islands, CpG shores, exons, genes, intergenic regions, introns, predicted enhancer sites, HIF-1 binding regions, and MYCN binding regions. All genomic regions were previously described in (Mariani et al., 2014), with the exception of predicted enhancers and HIF-1 and MYCN binding sites. Predicted enhancers

were generated from data collected by enhanceratlas (Gao et al., 2016). Enhanceratlas identifies enhancer regions in several cell lines that are available for download. Enhancer regions from NB cell line SK-N-SH were downloaded and converted to bed files for genomic enrichment analysis (Gao et al., 2016). HIF-1 and MYCN binding regions were generated from ChIP-sequencing files (Durbin et al., 2018; Thienpont et al., 2016; Zeid et al., 2018a) for each TF respectively. The HIF-1α binding sites bedfile was generated from HIF-1α ChIP-sequencing peak files called with MACS2 (Quinlan and Hall, 2010). To identify the enrichment of 5-hmC in each genomic element, bedtools intersect was used to find peaks from the hME-SEAL file in each genomic element. To establish how many peaks were expected in each genomic region based on random chance, bedtools shuffle was utilized. Bedtools shuffle used an input of peaks found in a 5-hmC bed file and placed them randomly throughout the genome. For accuracy, the shuffle was repeated 1000 times and the sum of the peaks per genomic element was recorded each time, then averaged after shuffling was completed. Enrichment was calculated by 'sum of observed peaks in genomic element'/'expected sum based on random distribution'.

Pathway analysis was performed with PANTHER pathway analysis, using adjusted P-values (Thomas et al., 2003). Data from hMe-Seal sequencing have been deposited in GEO under the accession number GSE167475.

Chromatin-Immunoprecipitation (ChIP)

ChIP was performed as published (Shang et al., 2000) with minor modifications. Briefly, cells were crosslinked with 1% formaldehyde for 10 minutes at room temperature and quenched with 175 mM Tris pH 7. Extracted nuclei were sonicated with a Covaris S220 Sonolab 7.2 1.0. Sonicated DNA was immunocleared with 2 μg/mL sheared salmon sperm DNA (Thermo Fisher Scientific AM9680), 6 μg/mL normal mouse IgG (Santa Cruz Biotechnology sc-2025), and 30 μL Protein G Dynabeads (50% vol/vol) (Fisher Scientific 10-004-D). Antibody pulldown was

performed with 5 μg α-MYCN IgG (Santa Cruz, B8.4.B) or 5 μg α-HIF-1 (overnight at 4 °C. As an antibody control, 5 μg of normal mouse IgG was used. After immunoprecipitation, 30 μL Protein G Dynabeads and 2 μg/mL sheared salmon sperm DNA were added for an additional 2 hours. Captured protein-DNA complexes were washed, eluted, and reverse-crosslinked (Shang et al., 2000). DNA was purified for qPCR or sequencing with Genelute PCR Clean Up Kit (Sigma-Aldrich). If samples were to be used for ChIP-qPCR, the purified DNA was amplified in ChIP-qPCR with Power SYBR Green PCR Master. Serially diluted input DNA was used for the standard curve. ChIP-qPCR data were normalized using the percent input method (% input = 100*2^(adjusted input – Ct). Primers for target regions are presented in Table 2.1.

ChIP-sequencing read mapping and peak calling analysis

The quality of fastq files was checked with FastQC before files were processed. Once they passed the quality check, files were aligned to the hg19 genome with Burrows-Wheeler Aligner. Finally, peaks from the ChIP sequencing files were called using the MACS2 peak calling function. If starting with public accession data, files were downloaded in their original bigwig format, then converted to a bedgraph format with the UCSC genome tool. Peaks were called with the MACS2 bdgpeakcall function.

Protein extraction

Protein extraction was performed via high salt fractionation (Camenisch et al., 2002). Cells were resuspended by mechanical shearing in Buffer A (10 mM Tris pH 7.8, 1.5 mM $MgCl_2$, 10 mM KCl). After incubation on ice for 10 minutes and centrifugation, the supernatant containing the cytosolic proteins was removed. The nuclei pellet was resuspended in Buffer C (20 mM Tris 7.8, 1.5 mM $MgCl_2$, 420 mM KCl, 20% glycerol). After shaking for 30 minutes, the lysates were spun and nucleic proteins in the supernatant were collected.

Western blotting

Nuclear proteins were separated via SDS-PAGE on 6% acrylamide gels. Membranes were probed with primary antibody: α-TET1 (Genetex GT1462) overnight at 4ºC; α-TOP1 (abcam ab109374) for one hour at room temperature; or α-MYCN (abcam ab16898) at 1:1000 dilution for one hour at room temperature. After primary antibody incubation, the membranes were incubated with 1:5000 dilution secondary antibodies against appropriate species: α-Rabbit IgG (Millipore 401393-2ML); or α-Mouse IgG (Cell Signaling Technology 70765) for one hour at room temperature. Western blots were then incubated with Western-lightning Plus-ECL, enhanced chemiluminescence (PerkinElmer) and exposed to film.

Wound healing and transwell assays

Cells were grown in a 96-well plate until confluent. Wells were scratched with an Essen Woundmaker and then placed in IncuCyte and photographed every 4 hours. Alternatively, the wound was created with the abcam Wound Healing Assay kit (ab242285), and cells were photographed at 0, 6, 12, 24, and 48 hours on an Evos FL Auto 2 microscope. To achieve pseudo-hypoxia, cells were treated with FG-4592 at 30 μM for 24 hours and with plerixafor (Sanofi) at a concentration of 10 μg/mL at hour 0, and subsequently at every 12 hours. Transwell assays were performed by incubating cells in serum free media on Falcon cell culture insert in a 24-well plate**,** with PBS control and 10 μg/mL plerixafor in the media (Justus et al., 2014). After 6 hours, cells were fixed with methanol for four min followed by 10% formalin for 20 min and stained with crystal violet or Giemsa stain. The transwell membrane was photographed under an Evos FL Auto 2 microscope at 10x magnification, and cells were counted and averaged per field. Numbers were compared between experimental lines and the parental control line.

Tumor xenograft experiments

Athymic mice were procured from The Jackson Laboratory (stock no: 002019). Cells were injected subcutaneously into the flank at a concentration of 25 X 10^6 cells/mL. Tumor length and width were measured every other day using calipers. Tumor volume (V) was calculated using the formula V=(length*width^2)/2. Mice were followed for 90 days unless tumor reached a terminal size of 3 cm3.

Data availability

Datasets generated by this work can be found at the Gene Expression Omnibus under the SuperSeries accession number GSE167478.

GEO accession numbers for publicly available ChIP-seq datasets used in this work are GSE94822, GSE80151, GSE138315, and GSE71399 (Durbin et al., 2018; Thienpont et al., 2016; Upton et al., 2020; Zeid et al., 2018). RNA-sequencing data for NB cell lines can be found on GEO databank (GSE89413) and sequencing for NB tumors can be accessed through R2: Genomics Analysis and Visualization Platform (https://r2.amc.nl/) (Gartlgruber et al., 2021; Harenza et al., 2017).

CHAPTER III

MYCN regulates TET1 transcription in normoxic neuroblastoma cells

The data in this chapter are adapted from a manuscript currently under review at *Scientific Reports:* Hains AE, Uppal S, Cao JZ, Salwen HR, Applebaum MA, Cohn SL, Godley LA. MYCN and HIF-1 directly regulate *TET1* expression to control 5-hmC gains and enhance neuroblastoma cell migration in hypoxia.

In this chapter, I designed and performed the experiments, analyzed the data, and wrote the manuscript. S.U. performed experiments. J.Z.C. analyzed data and helped perform experiments. M.A.A. analyzed and contributed sequencing data. H.R.S. helped design experiments. L.A.G. and S.L.C. conceived the study, analyzed the data, and edited the manuscript.

Introduction

Commonly diagnosed in children 5 years and younger, NB tumors originate from the developing sympathetic nervous system, commonly located in the adrenal gland. NBs exhibit a broad range of clinical behaviors, with some tumors resolving spontaneously and others requiring intensive treatment (Van Arendonk and Chung, 2019). Patients with NB are classified by risk based on several diagnostic criteria, including *MYCN* status, age, stage, and grade (Van Arendonk and Chung, 2019). Broadly, low risk patients are young and have tumors restricted to the primary site, whereas high risk patients are older and have tumors that have spread beyond the primary site. Other factors that increase risk are the presence of undifferentiated cells and the presence of *MYCN* amplification in the tumor DNA. Over time, treatment protocols have evolved to include a combination of systemic chemotherapy, surgical resection, tandem autologous transplants, radiation, MIBG, and/or immunotherapy for high risk patients (Park et al., 2019; Van Arendonk and Chung, 2019). Although improved outcomes have been observed with these intensive multi-modal approaches, 5-year survival of high risk patients remains at less than 60% (Moreno et al., 2020), indicating that more effective therapies are still needed.

Next-generation sequencing has allowed researchers to process and analyze datasets of NB genomes and transcriptomes, with the goal of identifying additional genetic biomarkers and novel therapeutic targets (Bellini et al., 2015; Pinto et al., 2016). However, results from multiple sequencing studies show that NBs have a relatively low mutational burden compared to other cancers (Maleki Vareki, 2018; Pugh et al., 2013), and there are only a few recurrent mutations (Pugh et al., 2013). Aside from *MYCN* amplification and chromosomal aberrations, (11q-deletion, 1p-deletion, and 17q gain), the only consistently identified recurrent mutations are variants found in *ALK* (5-10% of cases) and TIAM1 (~3%) (Molenaar et al., 2012b; Pugh et al., 2013). In 1983, *MYCN* amplification was identified as the first genetic alteration associated with NB (Kohl et al., 1983; Schwab et al., 1983). Very soon after its discovery, it was shown to correlate with poor prognosis (Brodeur et al., 1984; Seeger et al., 1985). All three chromosomal

aberrations, described in greater detail in Chapter I, correlate with poor outcome as well (Attiyeh et al., 2005; Plantaz et al., 1997). Mutations in *AKT* are often activating in nature and are correlated with poor outcome (Opel et al., 2007). Alternatively, *TIAM1* variants are associated with a better outcome, particularly when the variant is located in one of the domains that interact with RAS pathway members (Pugh et al., 2013; Sanmartín et al., 2017). The paucity of recurrent somatic genetic alterations has driven a search for another source of NB pathogenesis: epigenetic modifications (Applebaum et al., 2020; Maleki Vareki, 2018; Schulte et al., 2010).

NBs originate from neural crest tissue, which contains high levels of 5-hmC epigenomic marks (Kriaucionis and Heintz, 2009). When neural crest cells differentiate into neurons, 5-hmC increases and is enriched in the gene bodies of activated genes, suggesting that 5-hmC is an important epigenetic mark associated with transcription (Hahn et al., 2013; Kriaucionis and Heintz, 2009). The 5-hmC base is associated with open chromatin and active gene transcription (Ficz et al., 2011; Madzo et al., 2014; Mariani et al., 2014) and is an intermediate in the demethylation pathway (He et al., 2011; Ito et al., 2010).

Previously the Godley and Cohn Laboratories described how increases of global 5-hmC levels are essential for induction of the hypoxic transcriptional response specifically in *MYCN*-amplified NB cell lines, and not in NB cells with low MYCN protein levels (Chlenski et al., 2019; Mariani et al., 2014). This implies that MYCN directly or indirectly regulates *TET1,* but this remained untested in prior work (Mariani et al., 2014). In this chapter, I show that MYCN directly upregulates *TET1* expression in normoxia and specifically targets transcription from the full-length *TET1* gene.

Results

MYCN binds three potential regulatory regions of TET1

Figure 3.1. *TET1 and MYCN* expression correlation in NB cell lines and tumors. A. *TET1* expression data from RNA-seq of 38 NB cell lines (Harenza et al., 2017) graphed by *MYCN*-amplified and non-amplified designations. GEO accession numbers can be found in the methods. B. *TET1* and *MYCN* expression data from RNA-seq of 38 NB cell lines. Cell lines are plotted in order of increasing *TET1* expression. *TET1* expression data are plotted in squares and on the left Y-axis. *MYCN* expression data are plotted in red circles on the right Y-axis. C. *TET1* and *MYCN* expression data from RNA-seq of 579 NB tumors (Gartlgruber et al., 2021). Tumors are plotted in order of increasing *TET1* expression. *TET1* is plotted in black squares on the left and MYCN is plotted in red circles on the right.

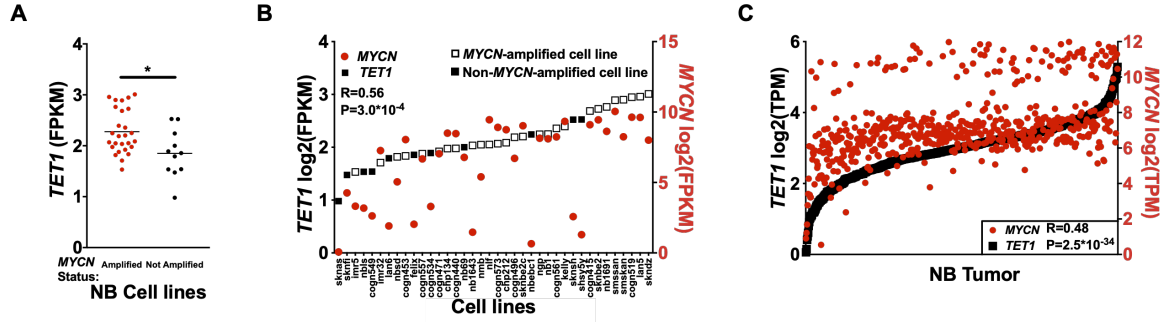

To determine if there is a link between *MYCN* and *TET1* expression, I examined the relationship between *MYCN* and *TET1* expression using publicly available RNA-sequencing (RNA-seq) data from NB cell lines and tumors (Gartlgruber et al., 2021; Harenza et al., 2017). Overall, *MYCN*-amplified NB cell lines have higher baseline *TET1* expression compared to non-*MYCN* amplified NB cell lines (Figure 3.1), and there is a positive correlation between *MYCN* and *TET1* expression levels (R=0.58, P=7.7e-5, Figure 3.1B). This positive correlation between *TET1* and *MYCN* expression is also observed in RNA-seq data from primary NB tumors (Gartlgruber et al., 2021) (R= 0.48, P=2.54e-34, Figure 3.1C). To test if this observation is specific for *TET1* or all members of the *TET* family, I performed the same correlation analysis with *TET2* and *TET3* (Gartlgruber et al., 2021; Harenza et al., 2017), and found no correlation between *MYCN* expression and that of *TET2* or *TET3* in NB cell lines (Figure 3.2A and C). In NB tumors, however, there is a modest correlation between *MYCN* and *TET3* (R=0.31, P=9.9e-15, Figure 3.2D), but not between *MYCN* and *TET2* (Figure 3.2B and D).

Next, I asked if the *TET1* gene is bound directly by MYCN. MYCN is a TF that recognizes and binds an E-box element that consists of a canonical 5'-CANNTG-3' (where N is any nucleotide) sequence (Zeid et al., 2018). Using HOMER (Heinz et al., 2010), I identified

Figure 3.2 Correlations between *MYCN* and *TET2* or *TET3* in NB cell lines. A. *TET2* and *MYCN* expression data from RNA-seq of 38 NB cell lines. Cell lines are plotted in order of increasing *TET2* expression with *TET2* on the left Y-axis (black squares) and *MYCN* on the right Y-axis (red). B. *TET2* expression data from 579 tumors are plotted in order of increasing *TET2* expression. *TET2* is represented by black squares. C. *TET3* and *MYCN* expression data from RNA-seq of 38 NB cell lines. Cell lines are plotted in order of increasing *TET3* expression with *TET3* on the left Y-axis (black squares) and *MYCN* on the right Y-axis (red). D. *TET3* expression data from 579 tumors are plotted in order of increasing *TET3* expression. *TET3* is represented by black squares.

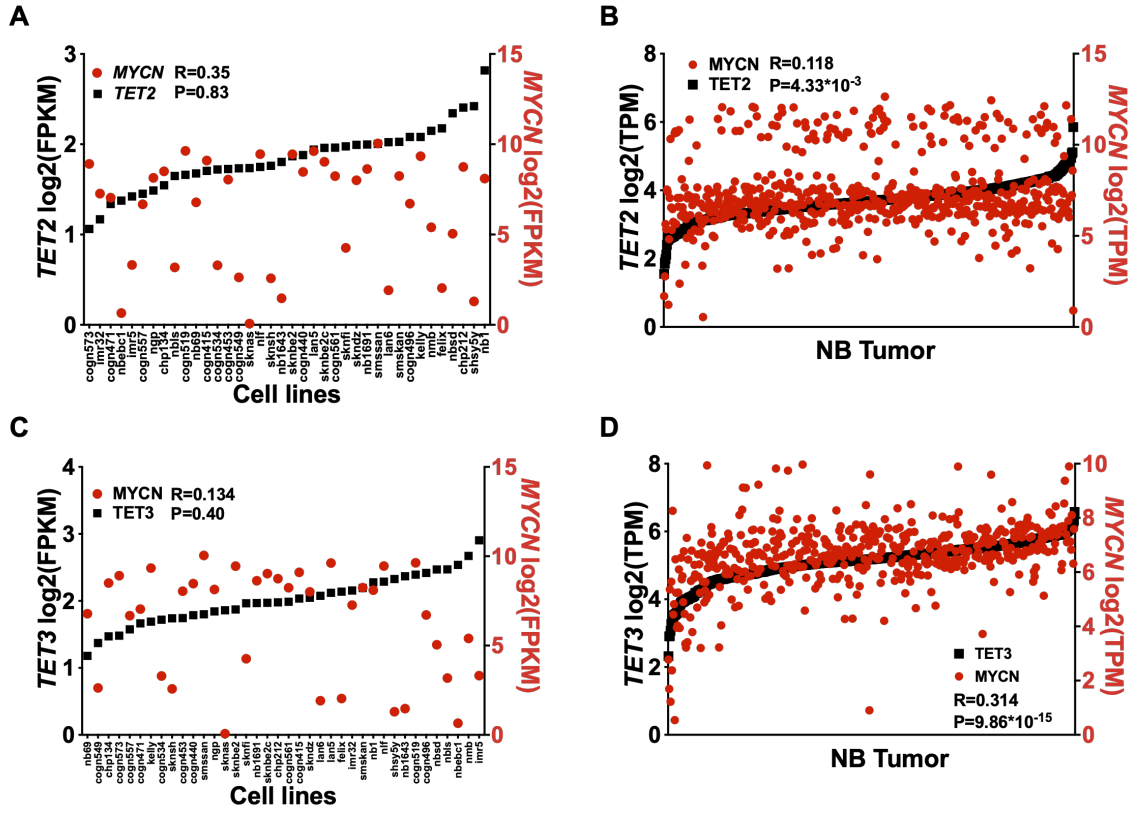

numerous 5'-CANNTG-3' motifs within and around *TET1* (Figure 3.3A), suggesting that MYCN could bind *TET1* directly and regulate transcription from several possible sites. To determine which sites are the most probable, I used EnhancerAtlas (Gao et al., 2016), an enhancer annotation tool based on compiled Chromatin-immunoprecipitation-sequencing (ChIP-seq) and chromatin accessibility data, to visualize enhancer sites where MYCN could bind and regulate *TET1* expression (Figure 3.3A). EnhancerAtlas provides a database of annotated enhancers from a variety of cell lines, and the most useful for my analysis was the only available NB cell line: non-*MYCN* amplified SK-N-SH (Gao et al., 2016). Using data from this cell line,

Figure 3.3 MYCN ChIP of *TET1*. A. MYCN ChIP sequencing data from SK-N-BE(2)-C, Kelly, NGP, NB1643, COGN415, and LAN5 cells. at locus 10q21 visualized with IGVtools. The shaded region corresponding to the first peak, from left to right, is *DNA2.* The second peak is *TET1*-intron 1 (*S1*), and the last peak is *TET1*-intron 2 (*S2*), both shaded in *TET1*. The 'Enhancer prediction' track is generated from 'EnhancerAtlas.org'. The 'Enhancer' track was generated with the UCSC LiftOver tool which remapped the mouse *TET1* superenhancer to the hg19 human genome. 'MYCN Motif' track is generated with HOMER. The Gene Ref track represents the gene positions in hg19 build of the human genome. Arrows represent the direction of gene transcription. B. Real time qPCR validation of MYCN ChIP-sequencing performed in SK-N-BE(2). From left to right, positive control (*LARP1*), *DNA2*, *S1, S2,* and negative control (neg *TET1*) binding sites are plotted on the x-axis. The y-axis corresponds to the amount of DNA pulled down normalized to the amount of input DNA. * represents p-value of $p<0.05$.

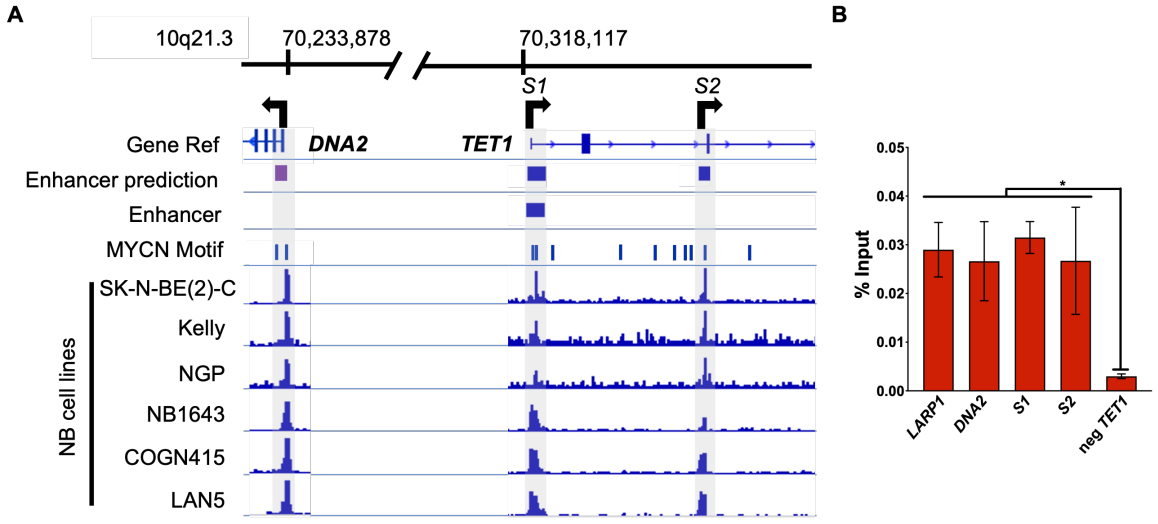

EnhancerAtlas identified two enhancers in *TET1*, in the first and second introns (Gao et al., 2016) (Figure 3.3A). In addition, data from murine systems identified a superenhancer that encompasses the enhancer located in the first intron (Whyte et al., 2013) (Figure 3.3A). Next, I examined publicly available MYCN ChIP-seq data (Durbin et al., 2018; Robinson et al., 2011; Upton et al., 2020; Zeid et al., 2018) at the *TET1* locus from as many *MYCN*-amplified NB cell lines as were available to determine experimentally validated MYCN binding sites (Figure 3.3A). In ChIP-seq data from the six available *MYCN*-amplified lines, I found evidence for direct MYCN binding to two sites in the first and second introns of *TET1,* which I will refer to hereafter as *Site 1* (*S1*) and *Site 2* (*S2*) (Figure 3.3A). *S1* is located centrally within an established

superenhancer described in the first intron, and *S2* is located in the enhancer in the second intron of *TET1* (Figure 3.3A). Since *TET1* could also be regulated by a distal enhancer, I used EnhancerAtlas to identify distal enhancer sites and found a potential *TET1*-regulatory enhancer located ~88 kb upstream in the first intron of the gene *DNA2* (Figure 3.3A). Analysis of publicly available MYCN ChIP-seq data also revealed MYCN binding to this predicted distal enhancer (Figure 3.3A). To validate the results of my analysis of the publicly available ChIP-seq data, I tested the binding of MYCN to each of these three sites with MYCN ChIP-quantitative PCR (qPCR) and found all three sites are enriched with MYCN binding in SK-N-BE(2) cells (Figure 3.3B). This suggests MYCN has the potential to regulate baseline *TET1* through any or all of these three sites.

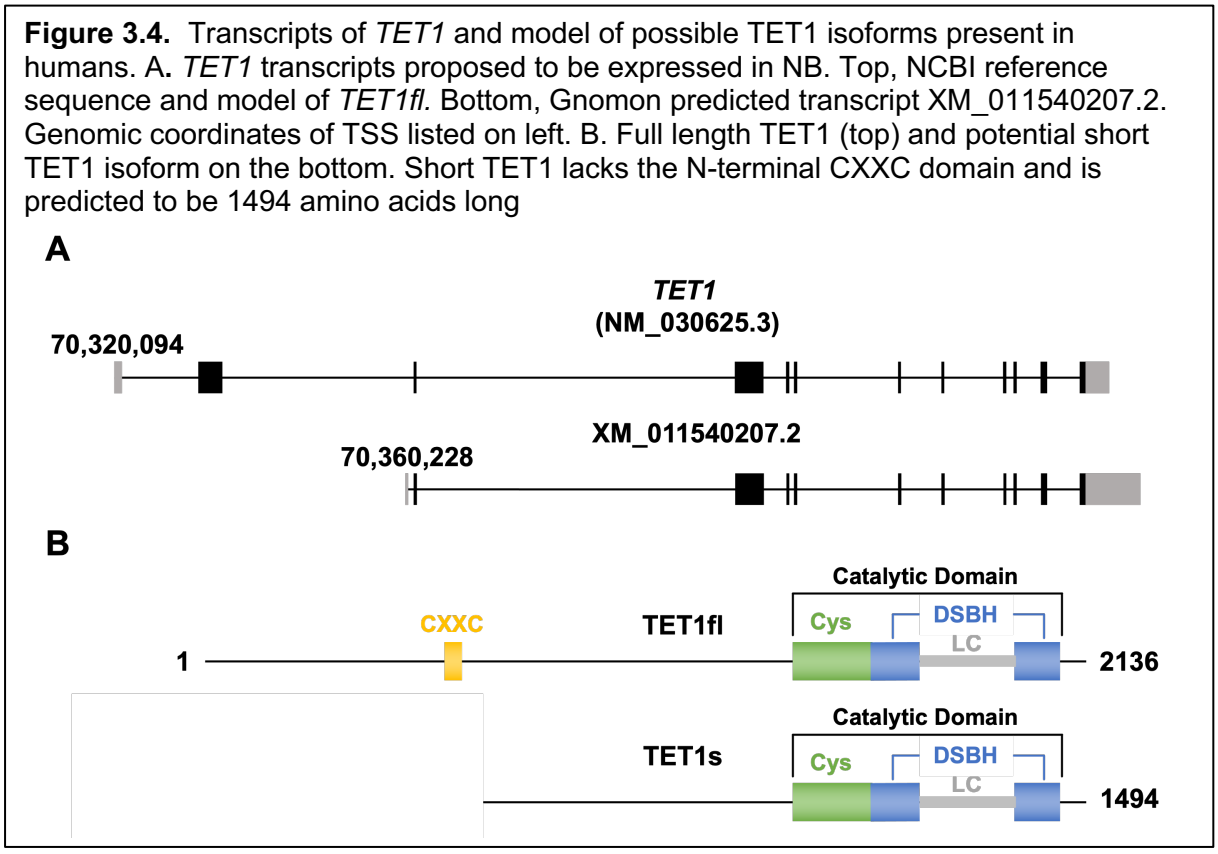

Figure 3.4. Transcripts of *TET1* and model of possible TET1 isoforms present in humans. A. *TET1* transcripts proposed to be expressed in NB. Top, NCBI reference sequence and model of *TET1fl.* Bottom, Gnomon predicted transcript XM_011540207.2. Genomic coordinates of TSS listed on left. B. Full length TET1 (top) and potential short TET1 isoform on the bottom. Short TET1 lacks the N-terminal CXXC domain and is predicted to be 1494 amino acids long

MYCN specifically drives expression of the full-length TET1 *transcript specifically*

Recent studies have determined that: (1) expression of the full-length *TET1* transcript is exclusively expressed in embryonic cells; and (2) identified the existence of an alternate 'short' *TET1* isoform that is present in differentiated tissues (Good et al., 2017; Greer et al., 2021; Yosefzon et al., 2017; Zhang et al., 2016c). Given the embryonic origins of NB tumors, I tested which *TET1* transcripts are expressed in NB cell lines. Both full-length *TET1* (*TET1fl*) and a *TET1* transcript predicted to exist by Gnomon, XM_011540207.2, were identified by Cufflinks analysis of RNA-seq data (Figure 3.4A) (Souvorov et al., 2010). Transcript XM_011540207.2, which I will refer to hereafter as *TET1s,* lacks the first two exons of *TET1fl* and has a novel exon 1 about 0.5 kb 5' of *TET1fl* exon 3 (Figure 3.4A). Because *S2* appears to be encompassed by this novel *TET1* exon, I tested whether MYCN drives *TET1s* expression specifically in *MYCN*-amplified NB cells. Analysis of *TET1* transcript expression in *MYCN*-amplified versus non-*MYCN*-amplified cells revealed that MYCN preferentially induces *TET1fl* expression (Figure 3.5A). In *MYCN*-amplified cells, *TET1fl* makes up 66% percent of all *TET1,* whereas *TET1fl* constitutes only 62% of total *TET1* transcripts in non-*MYCN*-amplified cells (Figure 3.5B). I performed correlation analysis between *MYCN* and *TET1fl,* and then between *MYCN* and

Figure 3.5. Expression of *TET1fl* and *TET1s* in common NB cell lines. A**.** *TET1fl* and *TET1s* FPKM in *MYCN*-amplified and non-*MYCN*-amplified NB*.* B. Circle represents 100% of all *TET1* expression, *TET1fl* is represented in orange, *TET1s* is represented in blue. P-value is Student's t-test comparison of *MYCN*-amplified *TET1fl* (66%) vs non-*MYCN*-amplified *TET1fl* (62%)*.*

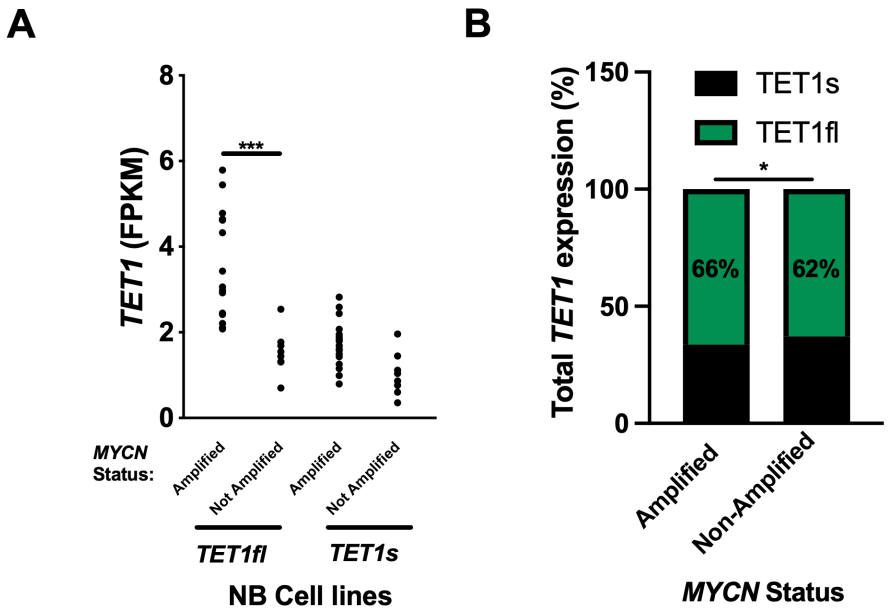

TET1s. MYCN correlated with *TET1fl* (R=0.34) better than *TET1s* (R=0.21), demonstrating that *MYCN* expression is associated with expression of *TET1fl* and suggesting that MYCN targets expression from *TET1fl* preferentially (Figure 3.6).

To determine if the presence of MYCN induces baseline *TET1* and/or *TET1fl* expression, I used the inducible-*MYCN* NB line Tet-21/N cells (Lutz et al., 1996), which overexpresses *MYCN* through a tetracycline-off system. In order to induce *MYCN* expression, I incubated the cells with doxycycline for 24 hours and then washed out the drug (Figure 3.7A). *MYCN* expression levels reached maximal expression three days after induction (Figure 3.7A), followed by induction of *TET1* expression on day 4 (Figure 3.6B and C). RNA-seq data showed that Day 4-induced expression is centered around exons 1 and 2, showing that MYCN induction targets expression from *TET1fl* (Figure 3.8). Overall, this indicates that MYCN drives *TET1* expression, preferentially expressing *TET1fl.* In addition, qPCR from Day 4 samples showed *TET3* is induced and Western blotting of TET1 protein showed TET1fl protein is also elevated (Figure

Figure 3.6. MYCN expression correlation with *TET1* isoforms. Log2(FPKM) values of *TET1fl* expression (y-axis) by *MYCN* expression (x-axis) (top). Bottom, log2(FPKM) values of *TET1s* expression (y-axis) by *MYCN* expression (x-axis).

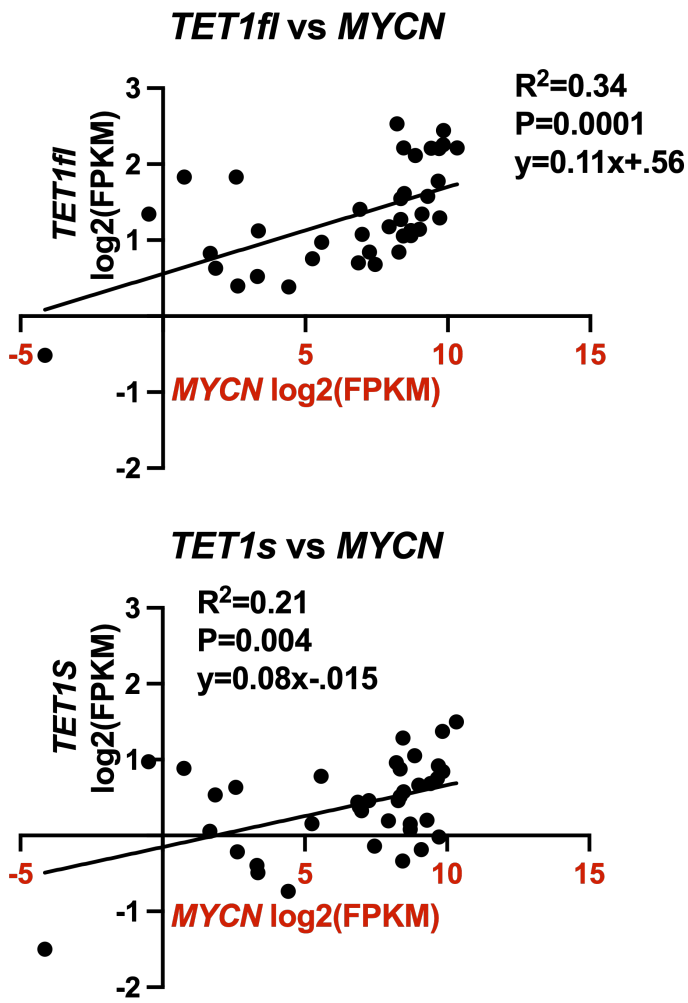

3.6B, C, D, and E). Despite induction of *TET1/3* on day 4, I observed no increase in total 5-hmC levels (Figure 3.6F), likely because the parent line of Tet-21/N cells has very low *TET1* expression in comparison to *MYCN*-amplified lines (van Groningen et al., 2017).

Figure 3.7. MYCN is sufficient to induce *TET1* and *TET3* expression but not 5-hmC levels. A. Real time qPCR quantification of *MYCN* in Tet-21/N cells (Lutz et al., 1996) over a 5 day time course. Tet-21/N cells were maintained with 1 mg/mL doxycycline, and *MYCN* induction was induced by the removal of doxycycline from the media. MYCN-induced Tet-21/N cells are plotted in green. *MYCN*-uninduced Tet-21/N cells are plotted in black. *MYCN* expression in *MYCN*-induced Tet-21/N cells (green) is normalized to *MYCN*-uninduced Tet-21/N cells (black) on respective days. P values were determined with one-tailed t-tests (n=3). B. *TET* expression analyzed from RNA-seq data from both *MYCN*-induced (green) and *MYCN*-uninduced (black) Tet-21/N cells 4 days post induction. *TET1*, *TET2*, and *TET3* are plotted along the x-axis. FPKM is plotted on the y-axis. C. Real time qPCR data for *TET1* expression 5 days post *MYCN* induction from *MYCN*-induced and *MYCN*-uninduced Tet-21/N cells. Relative *TET1* expression (y-axis) in *MYCN*-induced cells (green) is normalized to respective *TET1* expression in *MYCN*-uninduced cells (black). Each day is plotted on the x-axis. P values were determined with one-tailed t-tests (n=3). D. *TET3* expression determined by real time qPCR 5 days post *MYCN* induction from *MYCN*-induced and *MYCN*-uninduced Tet-21/N cells. Relative *TET3* expression (y-axis) in *MYCN*-induced cells (green) is normalized to respective *TET3* expression in *MYCN*-uninduced cells (black). Each day is plotted on the x-axis. P values were determined with one-tailed t-tests (n=3). ***, **, * represent p-values of p<0.05, p<0.01, and p<0.001 respectively. E. TET1, MYCN, and TOP1 protein levels 4, 5, and 6 days post *MYCN* induction assayed by Western blot. F. Quantitation of 5-hmC level with UHPLC-MS/MS performed on days 4 through 7 days post *MYCN* induction.

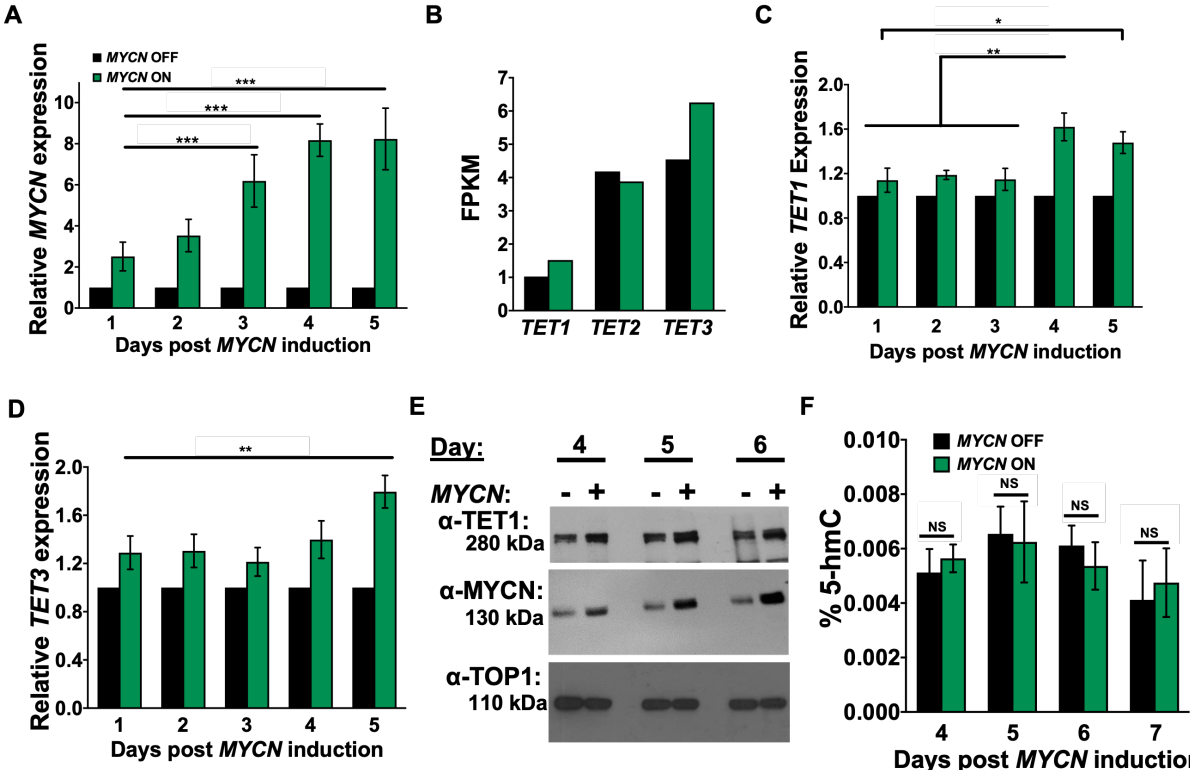

Figure 3.8. Bam files from uninduced (MYCN OFF) and induced (MYCN ON) RNA-seq data. IGVtools (Robinson et al., 2011) visualizes the first 20 kb of *TET1*.

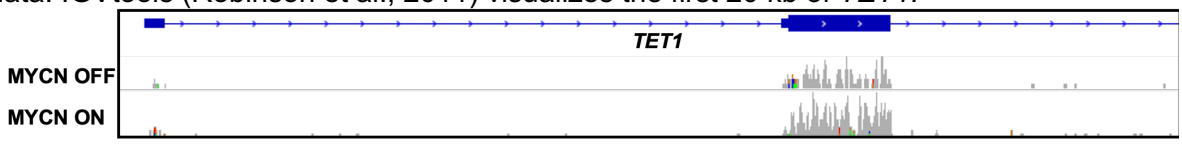

MYCN controls TET1 *expression directly in normoxia through two binding sites*

I hypothesized that one or more of the MYCN binding sites in/near *TET1* (Figure 3.3A and Figure 3.9A) directly controls *TET1* transcription. To test the functional role of each site, I used CRISPR-Cas9 gene editing in SK-N-BE(2) cells to create double strand breaks at the E-box motif and delete each potential binding site. As expected, deletions were commonly located on both alleles (Figure 3.9B). From the resulting mixed population of cells, I generated single cell clones and used PCR amplification and Sanger sequencing to confirm that the binding site of interest was eliminated (Figure 3.9B). Deletions generated by this process were often unique to each clone in their placement and length, but all lacked the core of the E-box motif (Figure

Figure 3.9. CRISPR gene editing generated deletions of *S1* and *S2*. A. Model of MYCN binding around 10q21.3. The two sites are (1) *S1*, in a superenhancer (orange) in the first intron of *TET1*, and (2) *S2* in the second intron of *TET1*. B. Sanger Sequencing of the deletions generated by gRNAs targeting the MYCN binding motifs in the *S1* site in *TET1* (Δ*S1*), and the *S2* site in TET1 (Δ*S2*) in SK-N-BE(2) cells. All clones utilized in my work lacked the CpG that makes up the core of the E-box motif. C. Sanger sequencing of the deletions generated by gRNAs targeting both MYCN binding motifs at *S1* and *S2* in TET1 (Δ*S1/2*).

A

B

Ref	CTGGTCGTGCAGCACGTGAGGGGCCTGGTCCT
Δ*TET1*-S1.1	CTGGTCGTGCAGCA--TGAGGGGCCTGGTCCT
Δ*TET1*-S1.2	C----------CTGGTCCT

Ref	TCTTTG//CAGCACGTCTACAGTGCT
Δ*TET1*-S2.1	TCTT--//----------GCT
Δ*TET1*-S2.2	TCT---//----------GCT

C

Ref	CTGGTCGTGCAGCACGTGAGGGGCCTGGTCCT	TCTT//GGCATGCCCAGCACGTCTACAGTGCT
Δ*TET1*-S1/2.1	CTGGTCGTGCAGCA--TGAGGGGCCTGGTCCT	TCT-//-GCAT----------GCT
Δ*TET1*-S1/2.2	CTGGTCGTGCAGCA--TGAGGGGCCTGGTCCT	TCTT//----------GCT

3.9B). To control for unintentional batch effects introduced by the single cell cloning process, two gene-edited single-cell clones per binding site were used in further experiments. Additionally, I generated SK-N-BE(2) lines lacking both *S1* and *S2* sites (Figure 3.C) through CRISPR-Cas9 gRNA targeting of the *S2* site in one of the Δ*S1* cell lines. Clones were named after their binding site deletion (Δ*DNA2*, Δ*S1*, Δ*S2,* and Δ*S1/2*) followed by "1" or "2" to distinguish individual clones targeting the same region (Figure 3.9A, B, C and Figure 3.10A, B). I also generated a clone that did not feature any genetic alterations at the binding sites to use as a non-targeting control in experiments (NTC).

Figure 3.10. *TET1* expression after deletion of MYCN binding site in *DNA2*. A. Model of MYCN binding near 10q21.3. Shown, a predicted enhancer site in gene *DNA2* upstream of *TET1* B. Sequences of the deletions generated by a gRNA targeting the MYCN binding motifs in the *DNA2* gene (Δ*DNA2*). C. Real time qPCR of *TET1* mRNA across Δ*DNA2* CRISPR-edited SK-N-BE(2) cell lines (n=3).

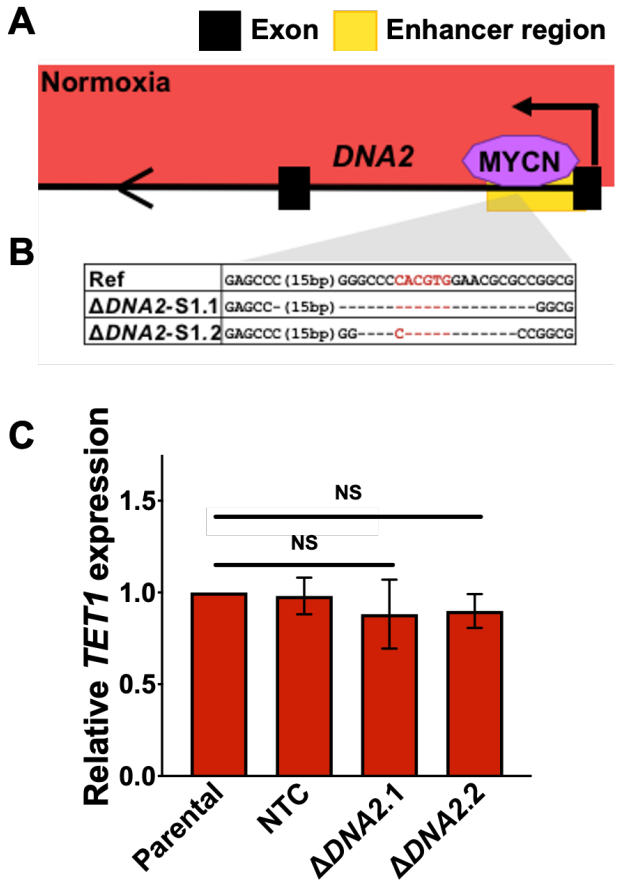

After generation of these clones, my first aim was to establish baseline *TET1* expression. It is important to note, my quantitative PCR (qPCR) primers are unable to differentiate between *TET1* transcripts, so going forward *TET1* expression refers to expression from all *TET1* transcripts. First, qPCR showed no change in *TET1* expression in SK-N-BE(2) cells when either the potential binding site near *DNA2* or *S2* was deleted, suggesting that MYCN binding at these sites is not essential for maintaining baseline *TET1* (Figure 3.10C and Figure 3.11A).

Figure 3.11. *TET1* mRNA expression after deletion of *S1*, *S2*, and *S1/2*. A. Real time qPCR of TET1 mRNA across Δ*S1*, Δ*S2*, and Δ*S1/2* CRISPR-edited SK-N-BE(2) cell lines (n=3). P-values were determined with one-tailed t-tests between the value of interest and the parental value. ***, **, * represent p-values of p<0.05, p<0.01, and p<0.001 respectively. B. Western blot for TET1 protein (top panel, cropped at ~280 kDa) in Δ*S1*, Δ*S2*, and Δ*S1/2*. In normoxia, all TET1 at 280 kDa detected and quantified. TOP1 from the same blot is visualized below (bottom panel, cropped at ~110 kDa).

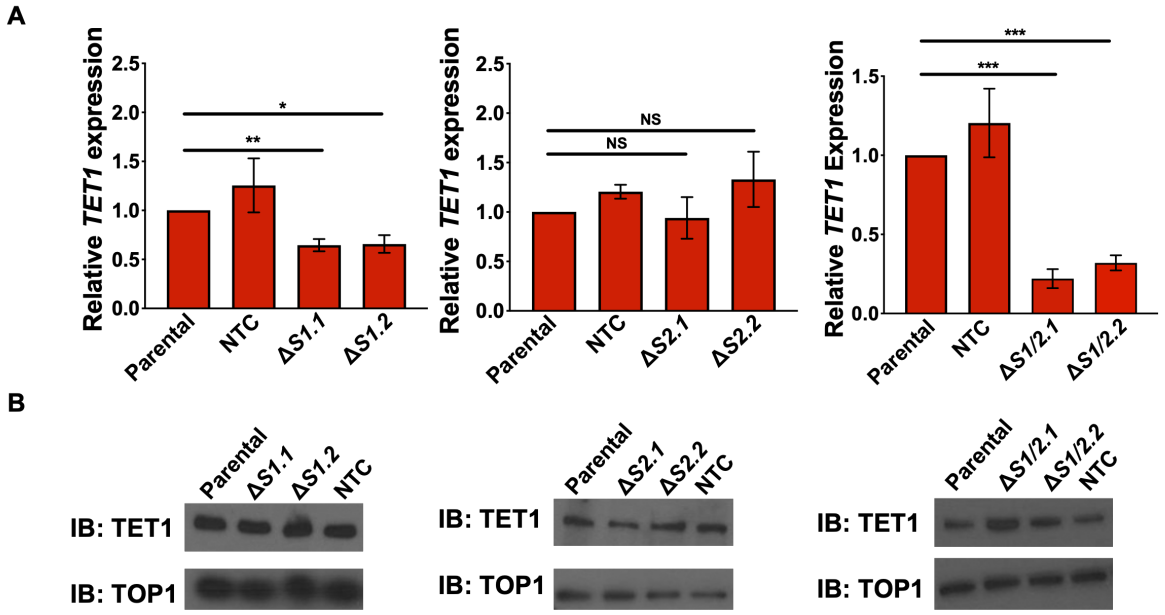

In contrast, Δ*S1* and Δ*S1/2* cells exhibit decreases in *TET1* expression, of 0.7 fold and 0.25 fold respectively, compared to parental cells (Figure 3.10A). This indicates that *S1* partially controls baseline *TET1*, but both sites together are required to maintain high baseline *TET1* expression. However, I also obtained an antibody that was able to detect the TET1fl protein reliably. I found TET1fl protein levels in Δ*S1* and Δ*S1/2* cells remain comparable to parental cell line and NTC controls (Figure 3.11B), indicating TET1 protein levels compensate for decreased *TET1* mRNA and suggests that TET1 is relatively stable in these cells. This also indicates that transcription of *TET1fl* is not exclusively controlled by *S1* as previously considered. Regulation of *TET1* isoform transcript expression appears to be more nuanced than *S1* regulating *TET1fl* and *S2* regulating *TET1s.* It is likely that *S2* at least partially compensates for the loss of *S1* and promotes expression of *TET1fl* as well as *TET1s.*

Discussion

In this chapter, I have shown that MYCN induces expression from *TET1* directly, with a preference for the *TET1fl* transcript, in normoxic *MYCN*-amplified NB cell lines. In normoxia, *TET1* is bound by MYCN at two sites in introns 1 and 2, *S1* and *S2*. Single deletions of either *S1* or *S2* lower transcription by 30%, but upon loss of both sites, *TET1* expression is severely reduced by 80%, suggesting that *S1* and *S2* compensate for each other if just one binding site is lost. This implies that preserving *TET1* expression is important in *MYCN*-amplified NB cell lines.

My data analysis of publicly available RNA-seq experiments revealed that there are at least two different *TET1* transcripts expressed in NB cell lines (Figure 3.5). The first is the original full-length transcript, the second is a 'short' transcript that lacks exons 1 and 2 of the 'full-length' transcript. Instead, the novel transcript, *TET1s* has a novel exon 1 located just before canonical exon 3. When translated, the TET1s isoform would lack the CXXC domain present in TET1fl (Figure 3.4B).

In my work above, it is important to note I detected TET1fl protein, but not TET1s, via Western blot in NB cell lines. Although I attempted to detect the short TET1 isoform, TET1s, I was never able to do so definitively via Western blot. As a positive control, I transiently transfected HEK293T cells with a *TET1s* expression vector that was expected to express TET1s with both GFP and FLAG tags (Good et al., 2017). I could not detect TET1s with α-TET1, α-GFP, or α-FLAG antibodies. Likewise, I was unable to obtain reliable qPCR results when I attempted using alternate-transcript *TET1* specific primers (Good et al., 2017). This is because the melt curve of *TET1s* primers indicated multiple products, even though a single band was present when the PCR reaction was run on a gel. For future study, devising a way to efficiently and reliably differentiate between *TET1fl* and *TET1s* in NB cells is imperative.

The implications of the presence two different TET1 isoforms and their impact on 5-hmC epigenetic landscape in NB cells are unclear. When *TET1s* was discovered in humans, the authors of that study also determined the abundance of each *TET1* transcript in several cancers (Good et al., 2017) Overall, they found *TET1s* was more frequently overexpressed than *TET1fl* in multiple different cancers than *TET1fl,* and suggested that *TET1s* was more the more pathogenic transcript of the two (Good et al., 2017). Here, I observed the opposite paradigm: *TET1fl* was always preferentially expressed over *TET1s,* and *TET1fl* correlated better with *MYCN*-amplification (Figure 3.5 and Figure 3.6). Questions remain about whether TET1fl and TET1s have different roles in NB and whether one transcript is more 'pathogenic' than the other. To answer these, I would first establish *TET1fl* and *TET1s* expression in NB tumor RNA-seq data. If I confirm *TET1fl* is also preferentially expressed in *MYCN*-amplified tumors, I would next stratify tumor samples by *TET1* transcript expression, then perform hierarchical clustering or association analysis with a number of variables to determine if one transcript has a higher association with prognosis. This would determine if one transcript is more 'pathogenic' than the other. These results have the potential to determine if *TET1* transcript quantification can be used as a clinical biomarker for NB. I would also query whether tumors that express high levels of *TET1fl* have distinct 5-hmC profiles from tumors that express lower levels of *TET1fl*. Further discussion of the role of different TET1 isoforms in the broader context of cancer can be found in Chapter VI.

CHAPTER IV

HIF-1 regulates TET1 gene and TET1 protein in hypoxia

The data presented in this chapter are adapted from a manuscript currently under review at *Scientific Reports:* Hains AE, Uppal S, Cao JZ, Salwen HR, Applebaum MA, Cohn SL, Godley LA. MYCN and HIF-1 directly regulate *TET1* expression to control 5-hmC gains and enhance neuroblastoma cell migration in hypoxia.

In this chapter, I designed and performed the experiments and analyzed the data. S.U. performed ChIP experiments.

Introduction

NB falls into the category of solid tumors that are often characterized by poor vasculature which results in various hypoxic pockets in the tumor (Rankin and Giaccia, 2008). When NB cell lines are exposed to hypoxia, they dedifferentiate, indicating they are genetically, epigenetically, and phenotypically responsive to hypoxic environments (Edsjö et al., 2007; Huertas-Castaño et al., 2019). In addition, NB cell lines become more aggressive, displaying a phenotype of enhanced proliferation, migration, and invasion. All of these phenotypes are the result of activation of hypoxic gene expression profiles by the HIF family. The HIF family consists of three members: HIF-1/2/3, all of which are α/β heterodimeric TFs. *HIF1A* mRNA is expressed at higher levels than *HIF2A* and *HIF3A* in NB cell lines (Figure 4.1) and predominates the regulation of the hypoxic response (Mariani et al., 2014).

The Godley and Cohn Laboratories used RNA silencing in *MYCN*-amplified NB cells to knock down expression of *HIF1A* (Mariani et al., 2014). When these cells were exposed to hypoxia, *TET1* expression was no longer induced and 5-hmC levels did not increase (Mariani et al., 2014). This showed that HIF-1α regulates *TET1* expression by an unknown mechanism. In addition, how TET1 protein levels change in response to hypoxia was not previously described (Mariani et al., 2014). In this chapter, I show that HIF-1 directly upregulates *TET1* in hypoxia and describe a novel interaction between HIF-1α and TET1 proteins.

Figure 4.1. Expression Log2(FPKM) data of *HIF1A, EPAS1(HIF2A),* and *HIF3A* in NB cell lines (Harenza et al., 2017).

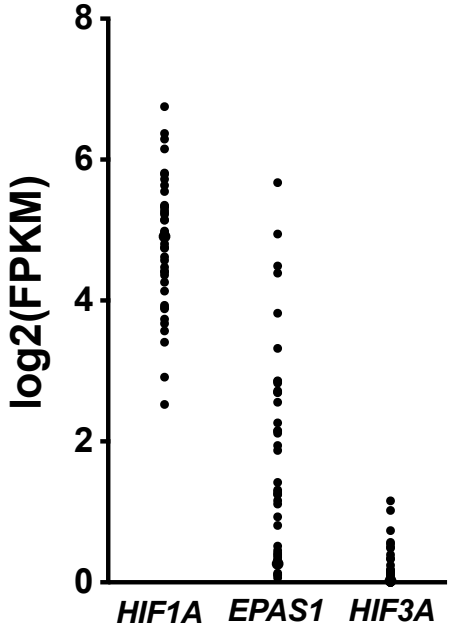

Results

S1 *and* S2 *modulate* TET1 *expression together in hypoxia*

The Godley Laboratory previously reported hypoxic *TET1* induction was dependent on the presence of HIF-1α (Mariani et al., 2014), but had not determined the mechanism through which HIF-1 regulates *TET1*. I again used HOMER (Heinz et al., 2010) to search for potential HIF-1α binding sites. HOMER finds sites that match the HIF-1 consensus motif (Figure 4.2) in a provided sequence. Because HIF-1, like MYCN, is an E-box TF both HIF-1 and MYCN have very similar consensus motifs. In addition, HIF-1 and MYCN recognize a core CpG that must be unmethylated for binding (Mariani et al., 2014). Because of these similarities, many of the MYCN binding motifs previously identified in Chapter III (Figures 3.3 and 3.8) were also identified as HIF-1 binding motifs. There are numerous HIF-1 binding motifs in

Figure 4.2. HIF-1α and MYCN consensus sequences as defined by HOMER (Heinz et al., 2010).

Figure 4.3. HIF-1 ChIP-seq at *S1* and *S2*. A. Real time qPCR of TET1 mRNA across Δ*S1*, Δ*S2*, and Δ*S1/2* CRISPR-edited SK-N-BE(2) cell lines (n=3). P-values were determined with one-tailed t-tests between the value of interest and the parental value. ***, **, * represent p-values of p<0.05, p<0.01, and p<0.001 respectively. B. Western blot for TET1 protein (top panel, cropped at ~280 kDa) in Δ*S1*, Δ*S2*, and Δ*S1/2*. In normoxia, all TET1 at 280 kDa detected and quantified. TOP1 from the same blot is visualized below (bottom panel, cropped at ~110 kDa).

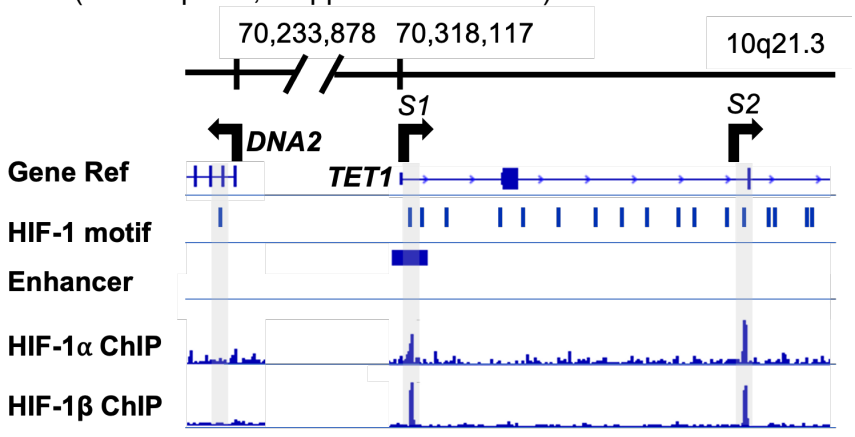

both *DNA2* and *TET1.* To determine if HIF-1 binds at any of these sites, Dr. Sakshi Uppal performed HIF-1α ChIP, and I analyzed the raw reads. I confirmed that HIF-1α binds *TET1* at the *S1* and *S2* binding sites in hypoxia. I also compared our HIF-1α results with publicly available HIF-1β ChIP-seq (Thienpont et al., 2016). HIF-1β also binds *S1* and *S2* in TET1. However, neither HIF-1α nor HIF-1β bind the E-box element present in *DNA2* that is bound by MYCN in normoxia (Figure 4.3). This suggests HIF-1 controls expression from *TET1* directly in hypoxia.

Figure 4.4. Hypoxic *TET1* expression in *TET1* gene edited clones. Real time qPCR quantification of *TET1* transcription in hypoxia across Δ*S1*, Δ*S2,* and *S1/2* clones, normalized to parental SK-N-BE(2) *TET1* expression. P-values were determined with one-tailed t-tests between the parental cell line and the cell line of interest (n=3).

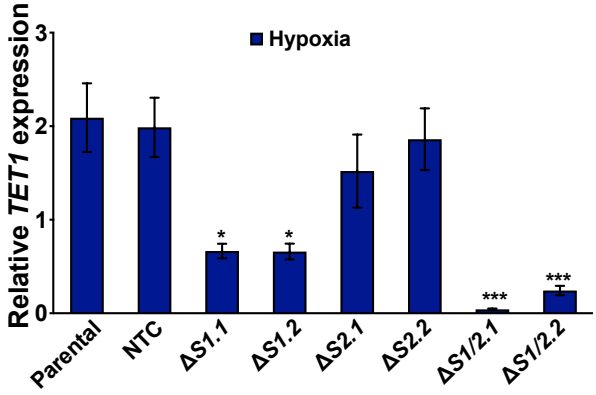

To assess the function of HIF-1 binding at *S1* and *S2* on *TET1* expression, I measured *TET1* in Δ*S1*, Δ*S2*, and Δ*S1/2* cells that were exposed to hypoxia for 48 hours with qPCR (Figure 4.4). *TET1* expression was reduced by about 60% fold in hypoxia in Δ*S1* cells compared to parental cells (Figure 4.4). Regardless, TET1 protein levels in Δ*S1* cells remained elevated in hypoxia over normoxia (Figure 4.5A). In fact, hypoxic TET1 protein levels in Δ*S1* cells were comparable to hypoxic parental levels, suggesting TET1 protein turnover is low enough to compensate for decreased *TET1* mRNA. Expression of *TET1* in Δ*S2* cells was no different from control cells. This indicates that *S2* alone does not control *TET1* expression. As expected, TET1 protein levels were also induced in hypoxia (Figure 4.4 and 4.5A). However, hypoxic Δ*S1/2* cells had very low *TET1* compared to hypoxic control lines and even Δ*S1* and Δ*S2* lines (Figure 4.4), indicating that hypoxic *TET1* expression is mediated by both *S1* and *S2*. I expected TET1 protein levels in Δ*S1/2* would be reflective of the very low *TET1* mRNA levels. Unexpectedly,

when TET1 protein was measured in hypoxic Δ*S1*/2 cells, it was detected at about the same levels as control cell TET1 (Figure 4.5A). This suggests that the TET1 protein has very low turnover and is able to compensate for low mRNA levels. Because TET1 protein is induced across all gene-edited cell lines in hypoxia, I investigated whether global 5-hmC levels are induced in hypoxia as well. Using mass spectrometry, and DNA samples from normoxic and

Figure 4.5. TET1 protein and 5-hmC levels in hypoxia. A. Western blots for TET1 protein in Δ*S1,* Δ*S2,* and Δ*S1/2* SK-N-BE(2) cells in normoxia and hypoxia, cropped at ~280 kDa. TOP1 loading control bottom, cropped at ~110 kDa. B. Fold change of hypoxic 5-hmC levels over normoxic 5-hmC levels in parental, NTC, Δ*S1*, Δ*S2*, and Δ*S1/2* cells. Percent 5-hmC measured via UHPLC-MS/MS and is calculated relative to guanine. ***, **, * represent p-values of p<0.05, p<0.01, and p<0.001 respectively.

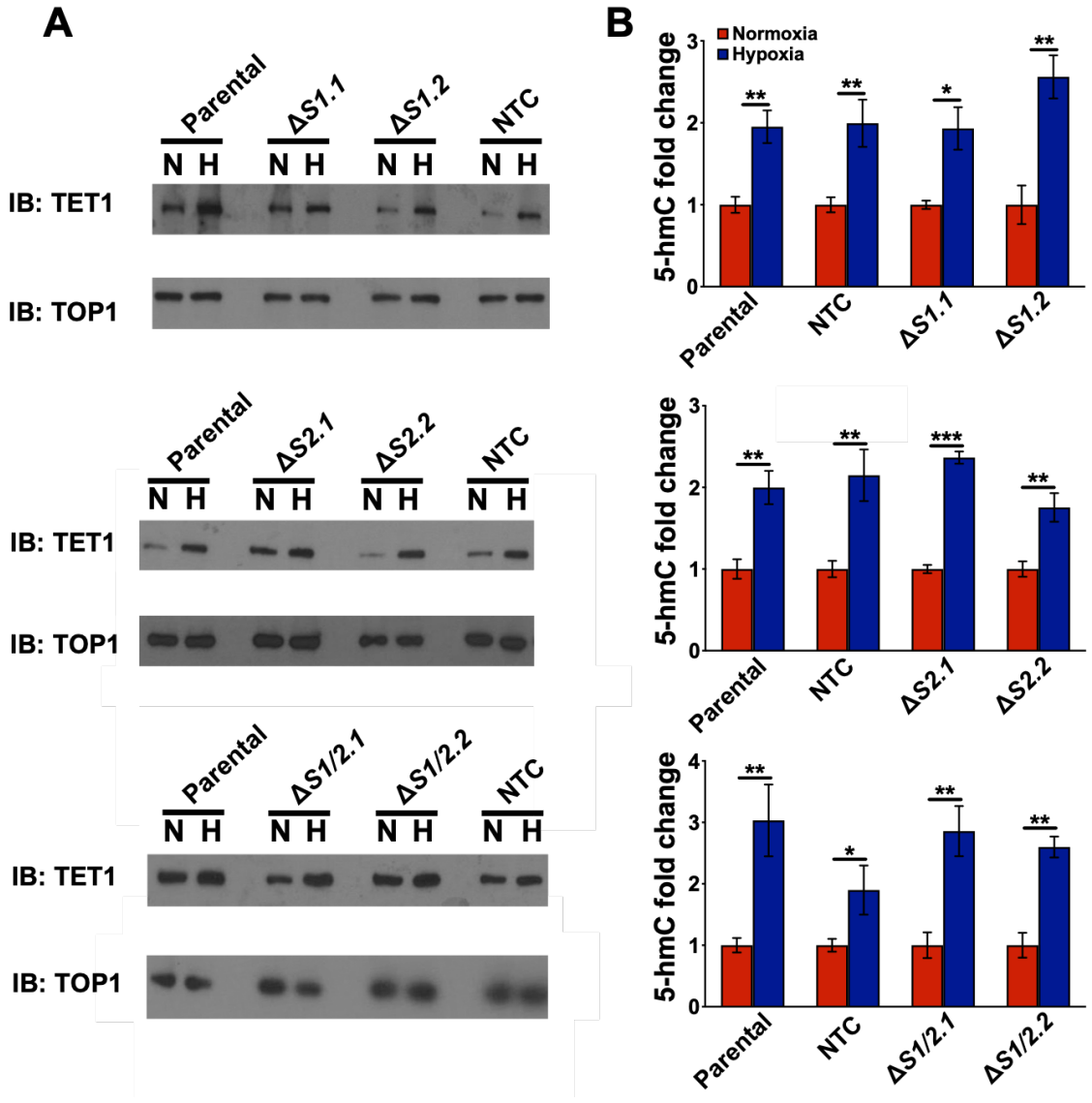

hypoxic gene-edited cells, I confirmed hypoxic 5-hmC levels are induced compared to normoxic 5-hmC levels in Δ*S1*, Δ*S2,* and Δ*S1/2* cells (Figure 4.5B).

Up until this point, all gene-editing experiments had been performed in a single NB cell line. To validate my results in a second cell line, I also generated NBL-WN Δ*S1/2* (Figure 4.6A). I selected this cell line because NBL-WN cells are also *MYCN* amplified, and have a similar N-type morphology to SK-N-BE(2) cells (Fotsis et al., 1999). After Δ*S1*/2 cells were generated, I

Figure 4.6. *S1*- and *S2*-deleted NBL-WN cells in normoxia and hypoxia. A. Model of MYCN and HIF-1a binding around 10q21.3 B. Sequences of the deletions generated by gRNAs targeting the MYCN binding motifs in the *S1* site in *TET1* (Δ*S1*), and the *S2* site in *TET1* (Δ*S2*) NBL-WN cells. C. Real time qPCR quantification of *TET1* transcription in hypoxia across clones that lack the MYCN/HIF-1 binding site in the superenhancer (Δ*S1* clones), clones that lack the MYCN/HIF-1 binding site in the second *TET1* intron (Δ*S2* clones), and clones that lack both (Δ*S1/2* clones), compared to parental NBL-WN *TET1* expression. P-values were determined with one-tailed t-tests between the parental cell line and the cell line of interest (n=3). D. Western blots for TET1 protein in Δ*S1*, Δ*S2*, and Δ*S1/2* NBL-WN cells in normoxia and hypoxia. TOP1 loading control in bottom panel. E. Fold change of hypoxic 5-hmC levels over normoxic 5-hmC levels in parental, NTC, and Δ*S1/2* cells. Percent 5-hmC measured via UHPLC-MS/MS and is calculated relative to guanine. ***, **, * represent p-values of p<0.05, p<0.01, and p<0.001 respectively.

A

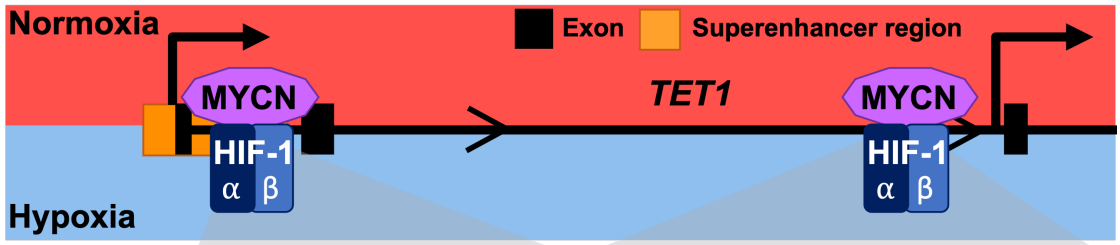

B

Ref	CTGGTCGTGCAGCACGTGA//GCTCTCG	TGCACTCTTTG//CAGCACGTCTACAGTGCT (15bp) CCTT
Δ*TET1*-S1/2.1	CTGGTCGTGCAGCAC----//-CTCTCG	TGCACTCTT--//----------GCT (15bp) CCTT
Δ*TET1*-S1/2.2	CTGGTCGTGCAGCAC----//-CTCTCG	TGC--------//----------(15bp) -CTT TGCACTCTT--//----------GCT (15bp) CCTT

C

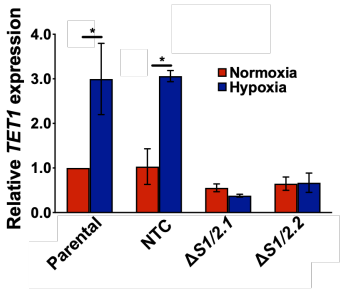

D

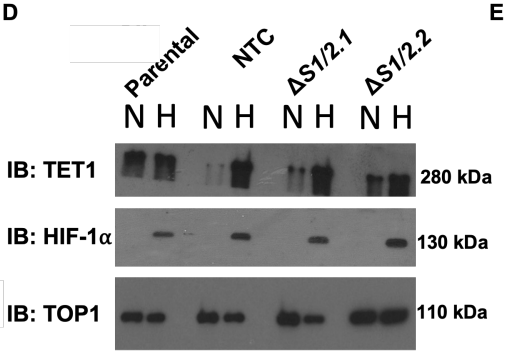

E

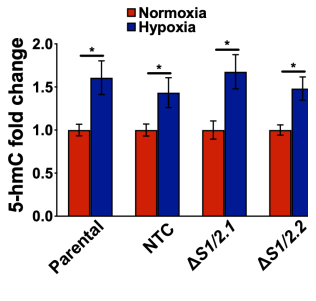

measured *TET1* expression in normoxia and hypoxia with qPCR and found *TET1* expression is low in both conditions, similar to what I reported earlier in SK-N-BE(2) cells (Figure 4.6B). I also found that TET1 protein levels were induced in hypoxia, again independent of the *TET1* mRNA status, confirming hypoxic TET1 protein levels were similar across NBL-WN and SK-N-BE(2) Δ*S1/2* cells (Figure 4.6C). Similarly, global hypoxic 5-hmC levels were elevated over normoxic levels in Δ*S1/2* NBL-WN cells as well (Figure 4.6D). These results indicate that regulation of *TET1* through *S1/2* in normoxia and hypoxia is not unique to SK-N-BE(2) cells, and the same mechanism is most likely present in other NB cell lines as well. Additionally, these results show that NB cells are able to maintain TET1 protein levels even when *TET1* mRNA is low.

HIF-1α promotes TET1 stability in hypoxia

To determine if induced TET1 protein levels in hypoxia are a consequence of low protein turnover, I performed protein degradation assays with cycloheximide in normoxic and hypoxic parental SK-N-BE(2) cells. These degradation assays demonstrated that TET1 levels, already very stable in normoxia (22 hours), persist even longer in hypoxic conditions (42 hours) (Figure 4.7A). As a control, HIF-1α degradation, which has a reported half-life ~3 hours (Huang et al., 1998), was also measured and is largely degraded by 6 hours as expected (Figure 4.7A). To determine if the presence of HIF-1α is necessary for the increased stability or lower turnover of TET1 in hypoxia, I performed the same protein degradation assays in normoxia and hypoxia in cells in which *HIF1A* had been deleted via gene editing (Δ*HIF1A*) (Figure 4.7B). Unlike the parental line, TET1 in hypoxia has similar turnover to TET1 in normoxia. Half-life calculations in both parental and Δ*HIF1A* cells in both conditions revealed that TET1 protein in normoxic

parental SK-N-BE(2) cells has a half-life of 20 hours, whereas the protein in hypoxic parental SK-N-BE(2) cells has a much longer half-life of 40 hours (Figure 4.7C). However, TET1 protein half-life returns to about 20 hours in both normoxic and hypoxic Δ*HIF1A* cells, implying that HIF-1α itself, not just enzymes activated in the hypoxia, is necessary to stabilize TET1 protein in hypoxia (Figure 4.8).

Next, I aimed to determine how HIF-1α promotes TET1 stability. Because other studies have determined TFs bind TET1 directly, I hypothesized HIF-1 binds TET1 in hypoxic NB, and this interaction promotes TET1 stability (Costa et al., 2013; Lio et al.). To determine if HIF-1 and TET1 form part of a complex, I performed TET1 co-immunoprecipitation (CoIP) experiments in normoxic and hypoxic SK-N-BE(2) cells. I found HIF-1α was precipitated with TET1, indicating HIF-1α and TET1 are part of the same protein complex (Figure 4.9A). In hypoxic

Figure 4.7. TET1 degradation assays and half-life. A. Western blot of TET1 degradation assay in parental SK-N-BE(2) cells with detection of HIF-1α and TOP1 (cropped at ~280 kDa, ~130 kDa, and ~110 kDa, respectively). Samples from normoxia and hypoxia were collected at 0, 3, 6, 12, 24, and 30 hours post treatment with cycloheximide. B. Western blot of TET1 degradation assay in gene edited Δ*HIF1A* SK-N-BE(2) cells with detection of HIF-1α and TOP1. Samples from normoxia and hypoxia were collected at 0, 3, 6, 12, 24, and 30 hours post treatment with cycloheximide. C. Half-life calculations of TET1 protein in normoxia and hypoxia in both parental and Δ*HIF1A* SK-N-BE(2) cells.

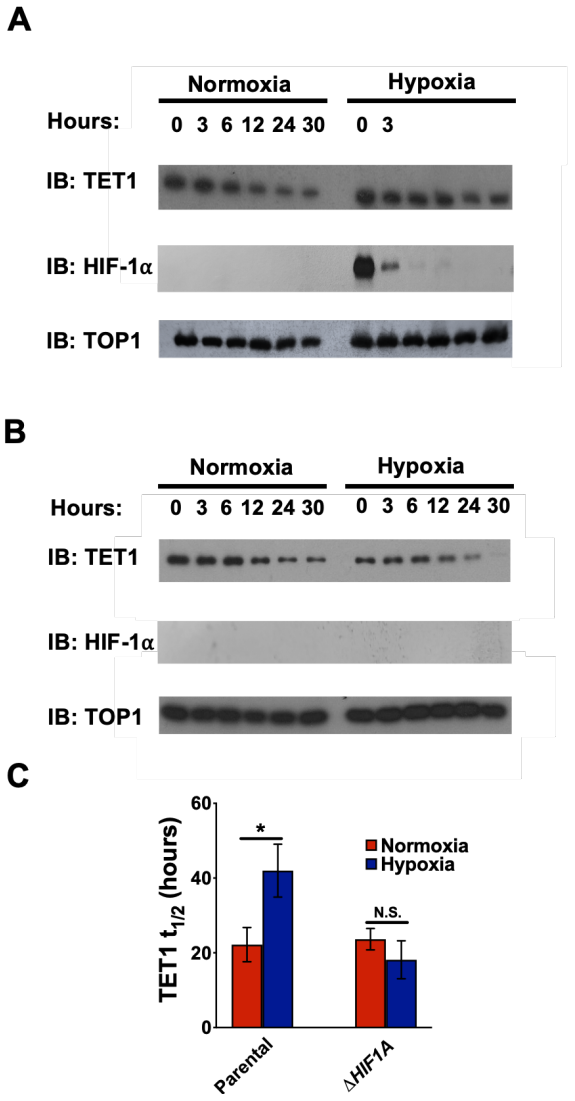

Δ*S1/2* cells it appears 5-hmC levels were induced by TET1 protein with very low turnover, therefore I wanted to measure TET1 protein activity over time to determine if it retains its activity independent of new translation. To determine if TET1 protein activity, independent of *TET1* mRNA regulation, is sufficient to induce 5-hmC levels in hypoxia, I measured global hypoxic 5-hmC after inhibition of protein synthesis in both parental and Δ*HIF1A* SK-N-BE(2) cells. After treatment with cycloheximide, hypoxic 5-hmC levels continued to increase, but hypoxic 5-hmC levels in Δ*HIF1A* cells were significantly lower than parental

Figure 4.8. Model of TET1 half life in normoxia and hypoxia. (Top) TET1 degradation in normoxic/hypoxic parental SK-N-BE(2) cells. (Bottom) TET1 degradation in normoxic/hypoxic Δ*HIF1A* SK-N-BE(2) cells.

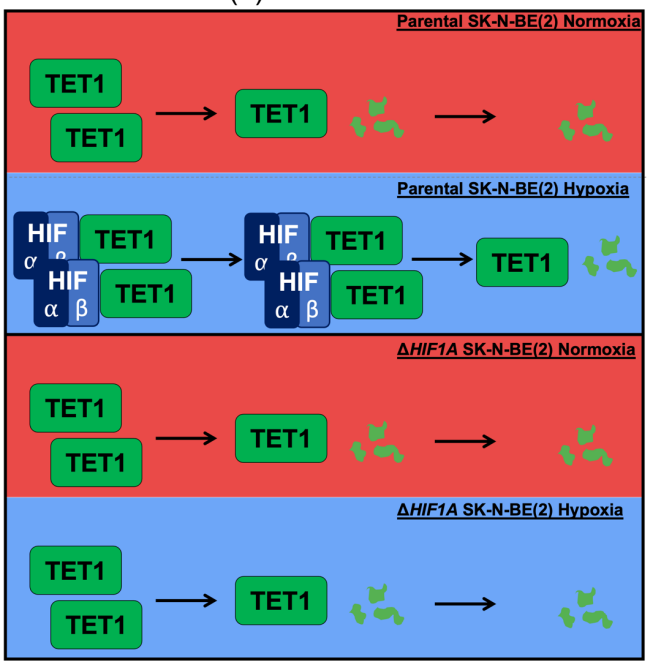

Figure 4.9. IP of TET1 and fold change of 5-hmC levels after protein translation inhibition. A. Immunoprecipitation of TET1 protein with detection of HIF-1α. B. Fold change of hypoxic 5-hmC levels over normoxic 5-hmC levels in parental and Δ*HIF1A* SK-N-BE(2) cells 0 to 36 hours after treatment with cycloheximide. Percent 5-hmC measured via UHPLC-MS/MS and is calculated relative to guanine. ***, **, * represent p-values of p<0.05, p<0.01, and p<0.001 respectively.

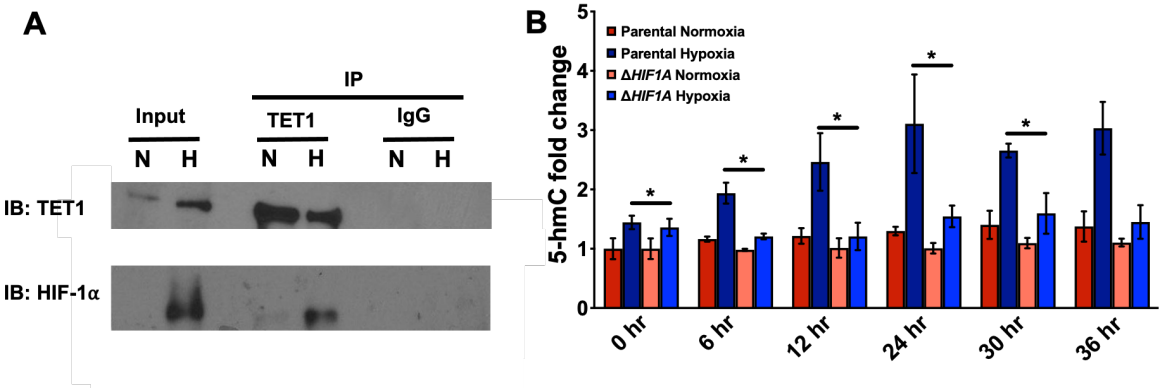

hypoxic 5-hmC levels (Figure 4.9B). This shows that HIF-1α protein is integral for hypoxic 5-hmC gains post-protein synthesis inhibition, possibly by augmenting TET1 stability or activity.

Previous work has described an antagonistic relationship between HIF-1 and MYC in hypoxia (Gordan et al., 2007). Because of this, I tested if *S1* and *S2* are bound exclusively in hypoxia by HIF-1 or if MYCN is also present at these sites in hypoxia. To test this, I performed MYCN ChIP-qPCR in hypoxia to determine if it still binds *S1* and/or *S2*. MYCN was present at both *S1* and *S2* in hypoxia, demonstrating that binding still occurred when HIF-1 was present in the cell (Figure 4.10).

Discussion

In this chapter, I describe the mechanism by which HIF-1 regulates *TET1* gene transcription and TET1 protein stability in hypoxic NB cell lines. In hypoxia, *S1* and *S2* are bound by HIF-1 and *TET1* expression is induced. However, it is interesting to note that *S1* and *S2* are not entirely functionally redundant. When *S1* was deleted, *TET1* transcription was no longer induced in hypoxia. This suggests that *S1* is more important for hypoxic expression than *S2.* However, hypoxic *TET1* transcription was not completely lost until *S2* was also deleted, demonstrating that *S2* was able to partially compensate for the loss of *S1.* Future studies will investigate why *S1* is more important

Figure 4.10. ChIP of MYCN in hypoxia. Real time qPCR of MYCN ChIP in hypoxic SK-N-BE(2) cells. Targets include Δ*S1*, Δ*S2*, and negative control (neg *TET1*) (n=3).

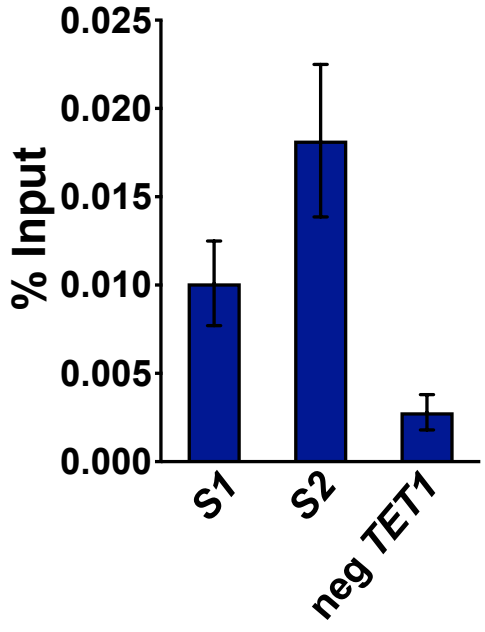

for hypoxic *TET1* transcription. It may be because *S1* and *S2* preferentially express different *TET1* isoforms, but more experiments are needed to determine this.

I also determined that HIF-1α binds TET1 protein. Past studies have described TF:TET binding and its role in their respective biological systems NANOG:TET1 and EGR1:TET1 complexes work synergistically to promote TET activity and enhance gene expression (Costa et al., 2013; Lio et al.). In NB, HIF-1α binding of TET1 appears to have a stabilizing effect. Although hypoxic *TET1* transcription was attenuated in Δ*S1/2* cells compared to controls, TET1 protein still accumulated in hypoxia. These results show that HIF-1 not only regulates *TET1* at the transcriptional level, but at the post-translational level as well. In addition, this interaction promotes TET1 activity in hypoxia through deposition of 5-hmC. This implies that, in addition to stability, HIF-1α may be directing TET1 activity. Previously, the Godley Laboratory found that TET1 modifies DNA at HIF-1 binding sites and canonical HIF-1 targets. This suggests that this HIF-1:TET1 binding interaction may be required to recruit TET1 to specific genomic sites (Figure 4.11) (Mariani et al., 2014)

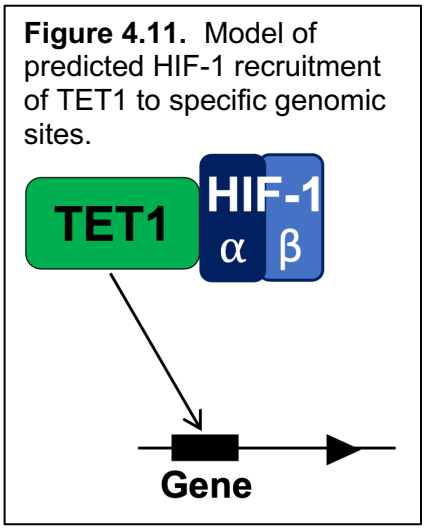

Figure 4.11. Model of predicted HIF-1 recruitment of TET1 to specific genomic sites.

Future experiments could determine how loss of this interaction changes the 5-hmC epigenetic landscape and whether other proteins participate in the HIF-1α/TET1 complex. Other possible mechanisms of TET1 post-translational regulation could also be the subject of future work, including identifying any post-translational modifications (PTMs) that increase stability and/or activity of TET1, especially in hypoxia. Currently, there are more than 40 PTMs predicted to occur on TET1 (Hornbeck et al., 2015), implying the mechanism of TET1 PTM may be complex and nuanced. In addition, although multiple PTMs of TETs and TET1 have been

described (Bauer et al., 2015; Jeong et al., 2019a), their functional roles are poorly understood. Future work will determine if TET1 PTMs regulate protein level and activity.

In this chapter, I also determined that MYCN still binds *S1* and *S2* in hypoxia despite these sites also being occupied by HIF-1 under the same conditions. This implies that *TET1* expression from *S1* and *S2* is not exclusively mediated by HIF-1. Although different genes in the same family, *MYC* overexpression will also take the same role as *MYCN* amplification in NB (Westermann et al., 2008). Because both MYCN and HIF-1 promote expression from *TET1*, my results deviate from the paradigm that HIF-1 and MYC are 'rivals' and promote opposing oncogenic pathways (Gordan et al., 2007). Future experiments could define the relationship between MYCN and HIF-1 further to determine whether they assist each other functionally. Specifically, experiments could test whether HIF-1 and MYCN are present together on the *TET1* gene or even bind each other independently of *TET1.* Further, additional investigation should determine if the relationship is synergistic for global gene regulation in NB.

CHAPTER V

5-hmC enrichment changes in response to a hypoxic environment contribute to an aggressive tumor phenotype in NB

The data presented in this chapter are adapted from a manuscript currently under review at *Scientific Reports:* Hains AE, Uppal S, Cao JZ, Salwen HR, Applebaum MA, Cohn SL, Godley LA. MYCN and HIF-1 directly regulate *TET1* expression to control 5-hmC gains and enhance neuroblastoma cell migration in hypoxia.

In this chapter, I designed and performed the experiments and analyzed the data. J.Z.C. assisted with data analysis. M.A.A. analyzed and provided RNA-seq data from NB cell lines. Michael W. Drazer assisted in data collection of mouse xenograft experiments.

Introduction

The cell surface receptor CXCR4 was originally identified as the co-receptor for HIV-1 infection of CD4+ lymphocytes (Bleul et al., 1996; Oberlin et al., 1996). Since then, it has been implicated in a myriad of cellular processes, including in hematopoietic systems where CXCR4 retains HSPCs in the bone marrow (Domanska et al., 2013). CXCR4 also promotes differentiation of human embryonic stem cells into neural stem cells and functions in chemotactic guidance in neural progenitor cells (Domanska et al., 2013; Zhang et al., 2016a). In the context of many solid tumors (Chatterjee et al., 2014; Domanska et al., 2013), CXCR4 and its ligand, SDF-1, have roles in tumor growth and metastasis, where they are thought to mediate interactions between cancer cells and the tumor microenvironment (Domanska et al., 2013). In several solid tumor cell lines, CXCR4 promotes or activates MAPK/ERK, JAK/STAT, and PI3K/AKT pathways, resulting in cell migration and survival (Fernandis et al., 2002; Pfeiffer et al., 2009; Xue et al., 2013). Few studies have examined the mechanism of CXCR4 in the pathology of neuroblastoma, although it is believed to promote tumor growth and therapeutic resistance (Klein et al., 2018). Additionally, no studies have identified a link between hypoxia and CXCR4.

When NB cells are exposed to hypoxia, they lose their primitive neuronal appearance and gain more a stem-like morphology (Jögi et al., 2004). In addition, they undergo specific phenotypic changes that promote proliferation, survival, and migration and invasion (Chen et al., 2015; Jögi et al., 2004). The Godley Laboratory previously recognized that genes involved in these processes, such as VEGF, are targeted by 5-hmC and which augments their hypoxic expression (Mariani et al., 2014). However, the extent 5-hmC-augmented gene expression profiles impact hypoxic NB cell phenotype was unknown. In this chapter, I describe how 5-hmC enrichment in NB cells changes over time in hypoxia, and I identify 5-hmC enriched *CXCR4* as a mediator of the increased migratory phenotype characteristic of hypoxic NB cells. I also observe reduced tumor growth in Δ*S1*/2 cells, possibly resulting from altered 5-hmC enrichment.

Results

Hypoxic 5-hmC gains are enriched in and around genes that are important for neuronal morphology, hypoxia adaptation, and cell migration

The Godley Laboratory described the 5-hmC landscape at 0 and 48 hours in parental SK-N-BE(2) cells, but not at intervals between these two points (Mariani et al., 2014). To characterize 5-hmC enrichment over time, I measured 5-hmC distribution changes in hypoxic *MYCN*-amplified cells with hMe-SEAL at different times (Song et al., 2011). Parental SK-N-BE(2) cells were incubated in hypoxia for 0, 6, 12, 24, 48, or 72 hours. After this, Dr. Sakshi Uppal extracted DNA and processed it for hMe-SEAL. As expected, the mean FPKM at each time point increases over time, confirming prior observations that 5-hmC peaks increase over time in hypoxia (Figure 5.1A) (Mariani et al., 2014).

I aimed to determine where the earliest 5-hmC gains occurred in the genome, so I decided to focus my analysis exclusively on 5-hmC gains in hypoxia. I filtered out all FPKM values that did not increase in hypoxia over time and found there are two distinct major increases in 5-hmC (Figure 5.1B). The first major increase consisted of the 'early' peaks that gained 5-hmC density in the first 6 hours (Figure 5.1B). The second major increase consisted of the 'late' peaks that gained 5-hmC density after 24 hours (Figure 5.1B). Genomic element

Figure 5.1. Hypoxic 5-hmC levels over time. A. FPKM values of all 5-hmC peaks plotted over time exposed to hypoxia. Timepoints consist of 0, 6, 12 24, 48, and 72 hours of hypoxia. (n= 415,416) *** represents P value of less than 2.2e-16. B. A subset of peaks from A that featured a positive log fold change from 0 to 72 hours. Shaded regions indicate high fold-change between two timepoints. Peaks are plotted the same as A, 5-hmC FPKM over time. (n= 189,949). *** represents P value of less than 2.2e-16. P-values are calculated compared to hour 0

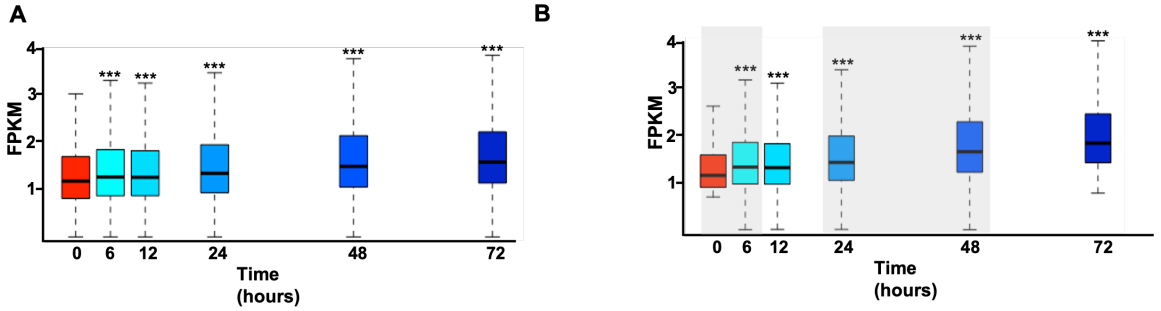

analysis of the early gains showed that they are enriched in enhancer and HIF-1α binding regions (Figure 5.2A). Next, I extracted the enriched enhancer locations and used EnhancerAtlas (Gao et al., 2016) to predict what gene targets would be regulated via those enhancers. Then I performed GO overrepresentation analysis of those gene targets (Thomas et

Figure 5.2. 5-hmC enriched genomic elements and biological pathways. A. Log2 enrichment (y-axis) of peaks that increase from 0 to 6 hours plotted by genomic element. Peaks that were classified as 'early' have a FPKM increase greater than 1.2-fold from 0 to 6 hours and remain stable throughout the rest of the time course. Genomic elements (x-axis) consist of promoters, 5' untranslated region (5' UTR), coding domain sequences (CDS), 3' untranslated region (3' UTR), introns, enhancers, HIF-1α binding regions (generated from our HIF-1α ChIP-sequencing data), CpG islands, CpG shores, and intergenic regions. (n= 26,061). *** represents P value of less than 2.2e-16. B. Genes associated with the enriched enhancers from A run through PANTHER biological process statistical overrepresentation analysis. Biological process is shown on the y-axis and enrichment score is shown on the x-axis. C. Enrichment of peaks that increase from 24 to 48 hours by genomic element. Peaks that were classified as 'late' were stable from 0 to 24 hours and increased greater than 1.1-fold between 24 and 48 hours. (n= 56,190). *** represents P value of less than 2.2e-16. D. Genes associated with enriched CDS in C run through PANTHER biological process statistical overrepresentation analysis. Biological process is shown on the y-axis and enrichment score is shown on the x-axis.

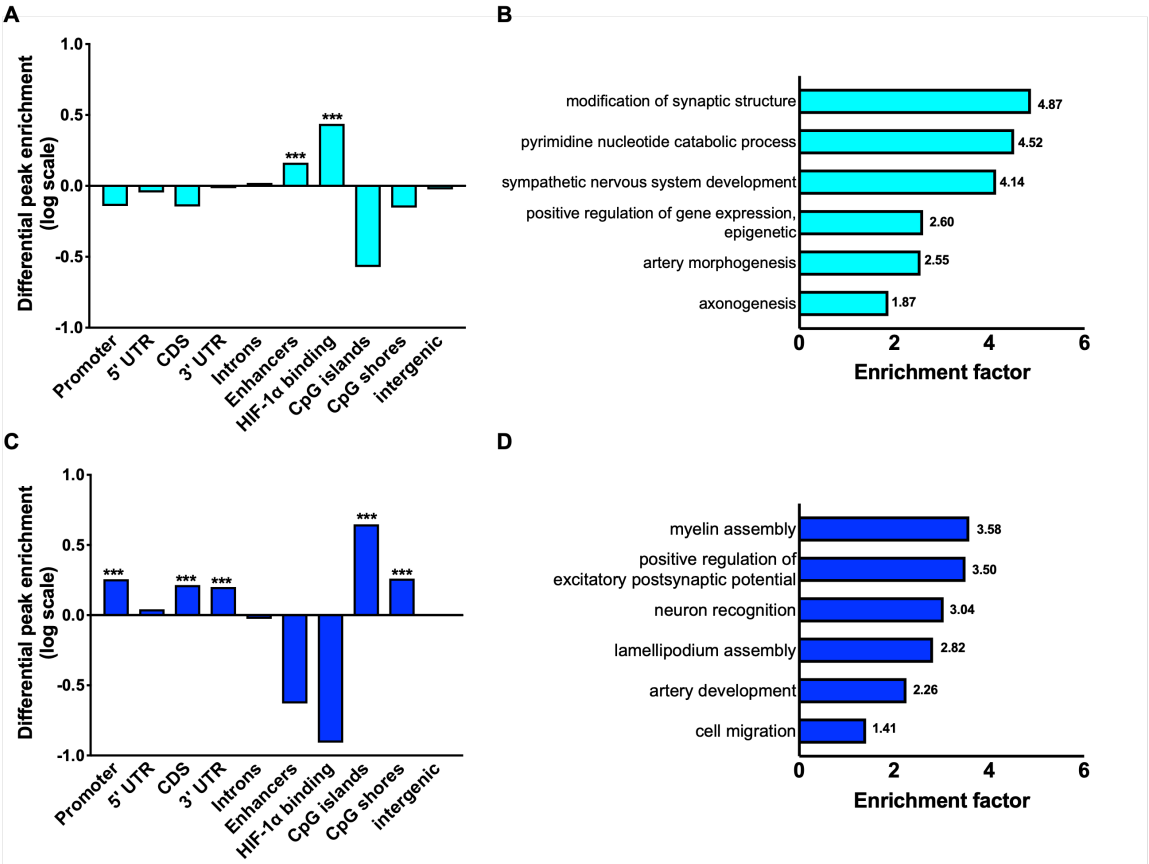

al., 2003), which showed that many of the biological processes overrepresented in my data set are related to neuronal morphology and development (Figure 5.2B), consistent with the observation that NB cells dedifferentiate and undergo morphological changes in hypoxia (Bhaskara et al., 2012). Also overrepresented were processes related to the hypoxic response, such as artery morphogenesis, which validated our earlier findings of 5-hmC enrichment in hypoxia (Figure 5.2B). A similar analysis of the late gains showed that they are enriched in distinct genomic regions compared to the early gains. The late gains occupy more genomic elements and are enriched in promoters, 5' untranslated regions (5' UTRs), coding domain sequences (CDSs), 3' untranslated regions (3' UTRs), CpG islands, and CpG shores (Figure 5.2C). Among the late gains in CDS, I found that many of the genes were overrepresented in pathways of neuronal development processes, hypoxia biological processes, and cell migration (Figure 5.2D).

CXCR4 is critical for hypoxic migration of NB cells

To identify candidate genes involved in cell migration from my earlier analysis, I extracted a list of hypoxic 5-hmC enriched genes from the pathway analysis and compared this list to RNA-seq data from normoxic and hypoxic parental SK-N-BE(2) cells, looking for those that had induced expression in hypoxia. There were two targets that increased expression in hypoxia: *CXCR4* and *CRKL* (Figure 5.3). The gene with hypoxic 5-hmC gain and the highest fold change (3.8 fold) in expression is *CXCR4* (Figure 5.3 and 5.4A). Particular to NB, *CXCR4* expression is correlated with metastatic spread and worse outcome (Russell et al., 2004). *CXCR4* is 5-hmC enriched in the gene body and the promoter, suggesting that 5-hmC augments expression from *CXCR4* in hypoxia, similar to canonical hypoxic response targets.

Given *CXCR4* is induced in hypoxia and a 5-hmC target, I aimed to determine if *CXCR4* is regulated by MYCN and/or HIF-1. I found *CXCR4* is a direct target of MYCN and HIF-1 in normoxia and hypoxia respectively (Figure 5.4A and B) (Durbin et al., 2018; Upton et al., 2020; Zeid et al., 2018). I extended my analysis of *CXCR4* expression to include RNA-seq data from several NB cell lines with varying *MYCN*-amplification statuses and MYCN protein levels to determine if *CXCR4* is a hypoxia target on other NB cell lines. Indeed, *CXCR4* is induced in hypoxia in NB cell lines that are *MYCN*-amplified and one with abundant c-MYC protein (SH-SY5Y) (Figure 5.5) (Chlenski et al., 2019). NBL-S cells are not *MYCN*-amplified, but do have high levels of MYCN protein, which probably drives high baseline *CXCR4* expression even if it is not induced in hypoxia (Cohn et al., 1990). Next, I measured *CXCR4* expression in Δ*S1/2* cells and observed hypoxic *CXCR4* is decreased in both SK-N-BE(2) and NBL-WN Δ*S1/2* cell lines (Figure 5.6A and B), possibly because the 5-hmC enrichment along the promoter or gene body of *CXCR4* is altered, and therefore, *CXCR4* expression is no longer augmented by 5-hmC in these cells.

Figure 5.3. Expression of 5-hmC targets *CXCR4* and *CRKL* in hypoxia. *CXCR4* and *CRKL* expression analyzed from RNA-seq data from both normoxic (red) and hypoxic (blue) samples. *CXCR4* and *CRKL* are plotted along the x-axis. FPKM is plotted on the y-axis.

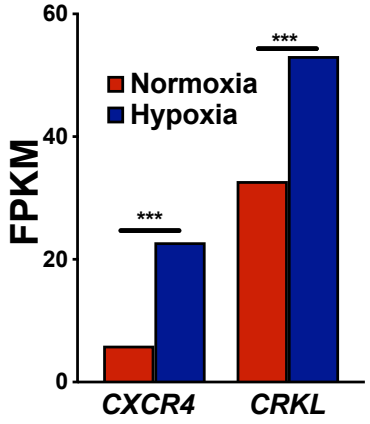

To determine whether *CXCR4* affects NB cell migration, I performed transwell assays with hypoxic SK-N-BE(2) Δ*S1/2* cells. I observed that hypoxic Δ*S1/2* cells migrate slower compared to controls (Figure 5.7A). Moreover, Δ*S1* cells, which similarly do not exhibit hypoxic induction of *TET1,* also migrate slower in hypoxia (Figure 5.7A). Wound healing assays, a complementary approach that measures cell migration, were performed under pseudo-hypoxic conditions and confirmed the migration phenotype in the Δ*S1* cells (Figure 5.7B and C). To test

Figure 5.4. TF binding and 5-hmC enrichment *CXCR4* in normoxia and hypoxia. A. Sequencing data along the *CXCR4* gene at locus 2q22.1 visualized with IGVtools. Arrows represent the direction of gene transcription. In the top two tracks, hMe-SEAL data obtained at 0 and 48 hours hypoxia are visualized. The bottom two tracks display ChIP-seq data. MYCN ChIP-seq from SK-N-BE(2)-C cells was obtained under normoxic conditions and HIF-1α ChIP-seq from SK-N-BE(2) cells was done at 48 hours hypoxia. B. MYCN ChIP-sequencing data at *CXCR4* at locus 2q22.1. In the top track, the Gene Ref track of the *CXCR4* gene. MYCN ChIP sequencing data from Kelly, NGP, NB1643, COGN415, and LAN5 cells are below the Gene Ref track. MYCN ChIP-seq files generated from publicly available data (Durbin et al., 2018, Upton et al., 2020; Zeid et al., 2018).

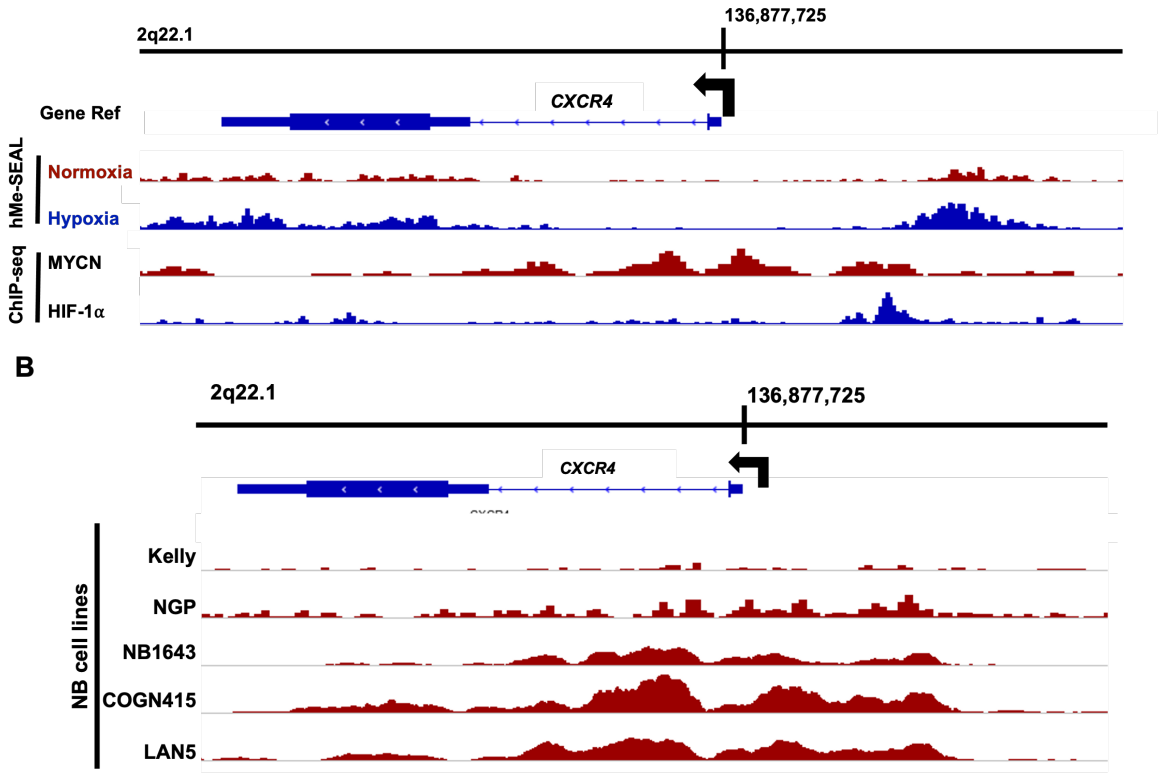

if CXCR4 promotes NB cell migration, I treated hypoxic SK-N-BE(2) and NBL-WN cells with plerixafor, a CXCR4 antagonist (Chatterjee et al., 2014). In both hypoxic transwell and pseudohypoxic wound healing assays, I found that plerixafor-treated cells migrate slower than their control counterparts (Figure 5.8), indicating CXCR4 directs *MYCN*-amplified NB tumor migration.

The mechanism of CXCR4 in hypoxic NB cell migration

In 2018, another laboratory proposed a mechanism by which CXCR4 contributes to overall NB tumor pathogenesis (Klein et al., 2018). Here I will describe their findings, why their results could not be replicated in our research, and propose a potential mechanism of CXCR4 action in hypoxic NB. The Peled Laboratory found that overexpression of *CXCR4* supports NB tumorigenesis. Treatment of NB tumor growth *in vivo* with the CXCR4 antagonist BL-8040 slowed tumor growth. Treatment of cell lines with the same antagonist resulted in the upregulation of miR-15a/16-1 and consequently, *BCL-2* and *CCND1* mRNAs were reduced, inducing cell death in these lines. These data indicated that CXCR4 promoted tumor cell survival via down regulation of miR-15a/16-1 and upregulation of BCL-2. Ultimately, the authors did not indicate any role for CXCR4 in hypoxia. Given their findings, however, I decided to compare their data to ours obtained from SK-N-BE(2) cells, one of the cell lines featured in their published paper. Comparison of their data with ours revealed an important difference: the 2018 paper found that CXCR4 could not be detected on the cell surface and only seemed to be expressed internally, whereas I had no trouble measuring CXCR4 on the surface of SK-N-BE(2) cells (Figure 5.9A) Although it was not as big effect as a lymphocyte control cell line, plerixafor bound CXCR4 on the surface of SK-N-

Figure 5.5. *CXCR4* expression in hypoxia from RNA-seq data from multiple NB cell lines. NBL-WN, SK-N-BE(2), and LA1-55n are classified as *MYCN*-amplified and have abundant MYCN protein. SH-SY5Y is a cell line that is not *MYCN*-amplified but does have elevated expression and protein levels of c-MYC. Two (5S and NBL-WS) are *MYCN*-amplified but have little to no MYCN protein. NBL-S cells are not *MYCN*-amplified but do have detectable levels of MYCN protein (Cohn et al., 1990). SHEP cells are neither *MYCN*-amplified nor have detectable MYCN protein levels. Expression (log2) measured in normoxia (red) and 48 hours hypoxia (blue). *** represents p-value of less than 0.001.

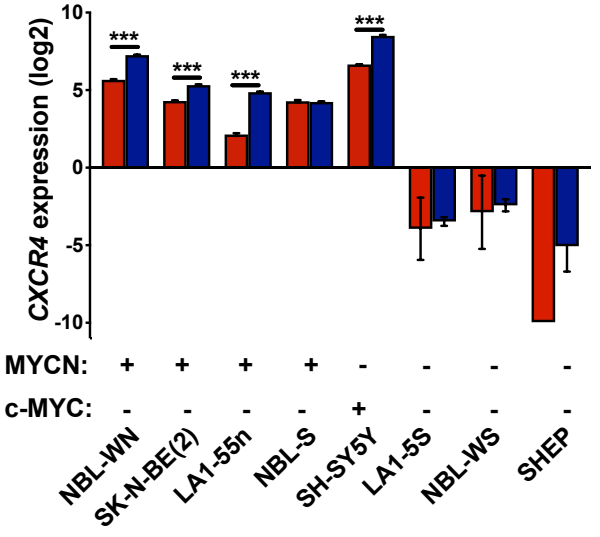

BE(2) cells (Figure 5.9). Nonetheless, I examined RNA-seq data from SK-N-BE(2) cells to see if upregulation of *CXCR4* in hypoxia had an effect on *MIR15A, CCND1,* or *BCL2.* Although the targets were expressed in normoxia, none were induced in hypoxia (Figure 5.10).

Figure 5.6. *CXCR4* hypoxic expression in hypoxia in SK-N-BE(2) and NBL-WN cells. A. Real time qPCR of *CXCR4* expression in hypoxic SK-N-BE(2) cells (Parental, NTC, Δ*S1* and Δ*S1/2*) in hypoxia at 48 hours (n=3). P values were determined with one-tailed t-tests, *, **, *** represent p-values of less than 0.05, 0.01, and 0.001 respectively. B. Real time qPCR of *CXCR4* expression in NBL-WN cells lacking *S1/2* in normoxia and hypoxia at 48 hours (n=3).

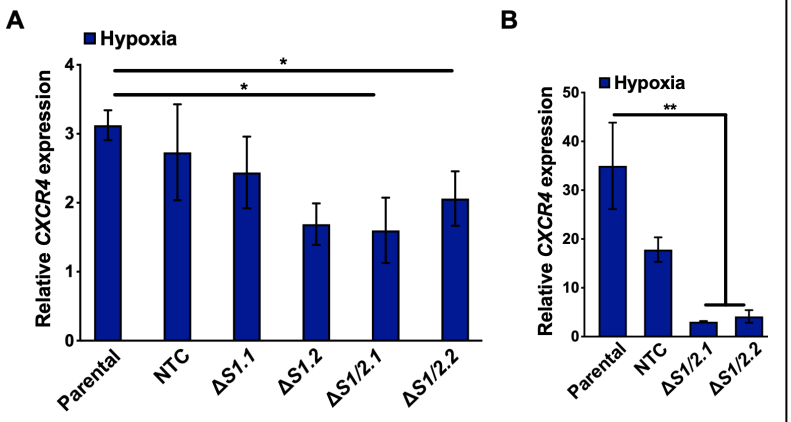

Given the results from the 2018 paper were only obtained under normoxic conditions (Klein et al., 2018), I investigated alternative genes and/or proteins that CXCR4 may target, specifically in hypoxia. Because of the 2020 pandemic, my research was limited to data that I could access via computer. I reviewed possible candidate CXCR4 targets and consulted our

Figure 5.7. Cell migration assays with cells lacking *S1* and *S1/2.* A. Transwell migration assays were performed with SK-N-BE(2) Δ*S1* and Δ*S1/2* clones in hypoxia. P values were determined with one-tailed t-tests (n=3). Percentages were calculated with respect to average number of parental SK-N-BE(2) cells B. and C. Wound healing assays with SK-N-BE(2) cells that lack the MYCN/HIF-1 binding site in the *TET1* superenhancer (Δ*S1* clones) observed in the presence of (B) DMSO or (C) FG-4592 (30 mM).

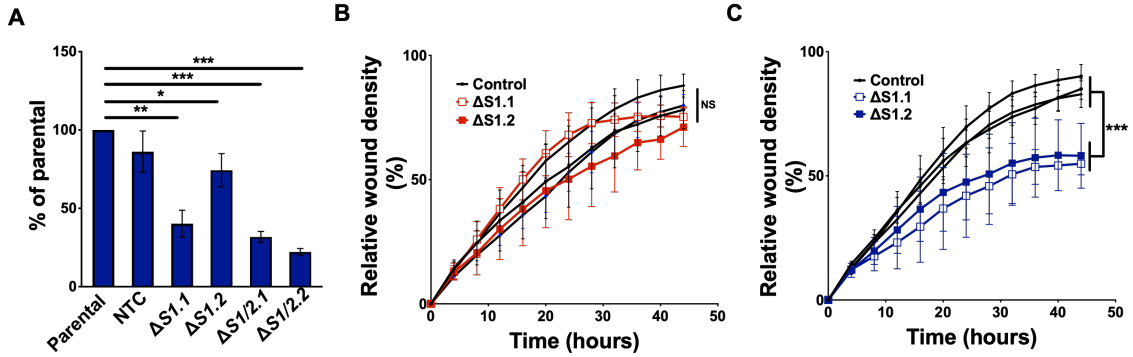

Figure 5.8. Cell migration assays with SK-N-BE(2) and NBL-WN cells with/without plerixafor. A. Transwell assays performed with parental SK-N-BE(2) and NBL-WN cells and treated with 10 ug/ml plerixafor or DPBS in hypoxia (n=4). P-values were determined with one-tailed t-tests, * represents p-value of less than 0.05. B. Wound healing migration assays performed with parental SK-N-BE(2) and NBL-WN cells and treated with 10 ug/ml plerixafor or DPBS. Both control and experimental cells treated with 30 mM FG-4592. P values were determined with one-tailed t-tests, *, **, *** represent p-values of less than 0.05, 0.01, and 0.001 respectively.

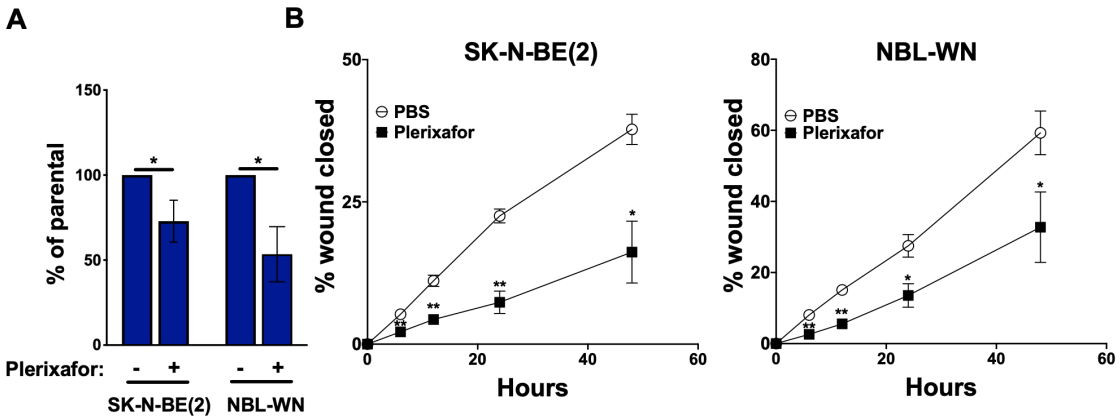

own hypoxic RNA-seq data as well as public RNA-seq data sets. Generally, CXCR4 is a mediator of G Protein Coupled Receptor Kinase (GRK) proteins. I searched our RNA-seq data from SK-N-BE(2) cells for any *GRK* genes that are upregulated in hypoxia and identified one:

Figure 5.9. Measurements of CXCR4 on the surface of SK-N-BE(2) NB cells. Cells stained with anti-CXCR4 antibody (clone 12G5) which competes with plerixafor binding pocket. Cells treated with 10 μg/ml plerixafor (blue) or PBS (pink). A. SK-N-BE(2) NB cells. B. control SUP-T11 lymphocytic cell line.

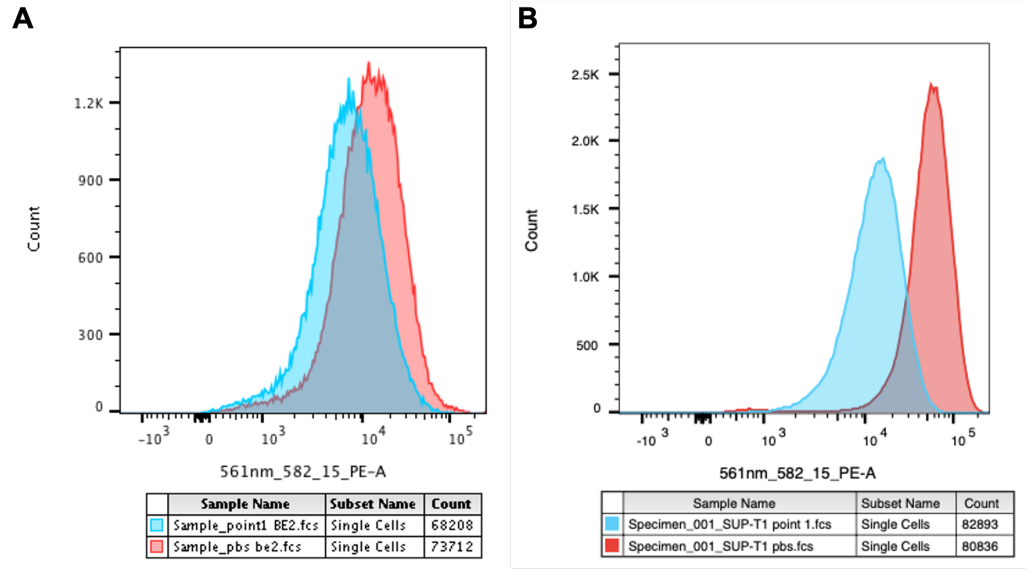

GRK5. *GRK5* expression increases from 6.9 FPKM in normoxia to 13.0 FPKM in hypoxia (Figure 5.10). GRK5 and GRK2 have reported roles in promoting F-actin bundling in neural development and selective phosphorylation of the neurotensin receptor (Chen et al., 2011; Inagaki et al., 2015). Both of these processes indirectly promote cell migration in neural tissue. Given that NBs arise from neural crest tissue, it is possible there is a similar mechanism involving GRK5 and GRK2 in hypoxic NB cell migration: that upregulation of GRK5 in hypoxia is due to downstream signaling of activated CXCR4. However, although, *GRK2* is expressed in SK-N-BE(2) cells, it is not induced in hypoxia (Figure 5.10). I found an additional connection between GRK5 and CXCR4: GRK5 regulates internalization of CXCR4 via phosphorylation of chaperone protein Hip (Barker and Benovic, 2011). I queried our RNA-seq data to determine if the chaperone protein undergoes a change in expression in hypoxia. The

Figure 5.10. Several potential downstream targets of CXCR4 expressed in hypoxic NB cells. RNA-seq expression in FPKM from hypoxic SK-N-BE(2) cells.

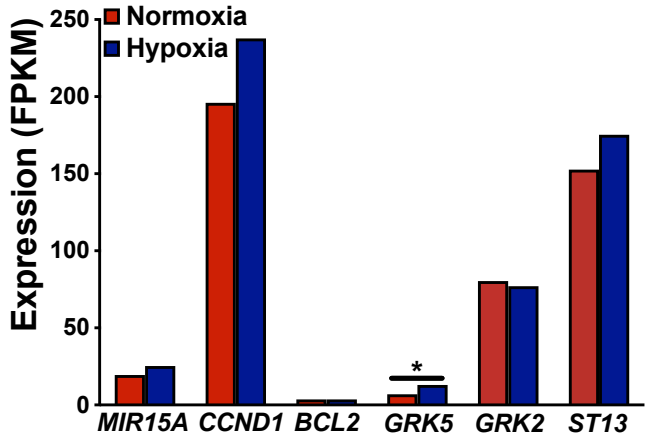

Figure 5.11. Model of proposed CXCR4 downstream targeting in hypoxic NB cells. Solid lines represent experimentally supported interaction. Dashed lines represent hypothesized interaction.

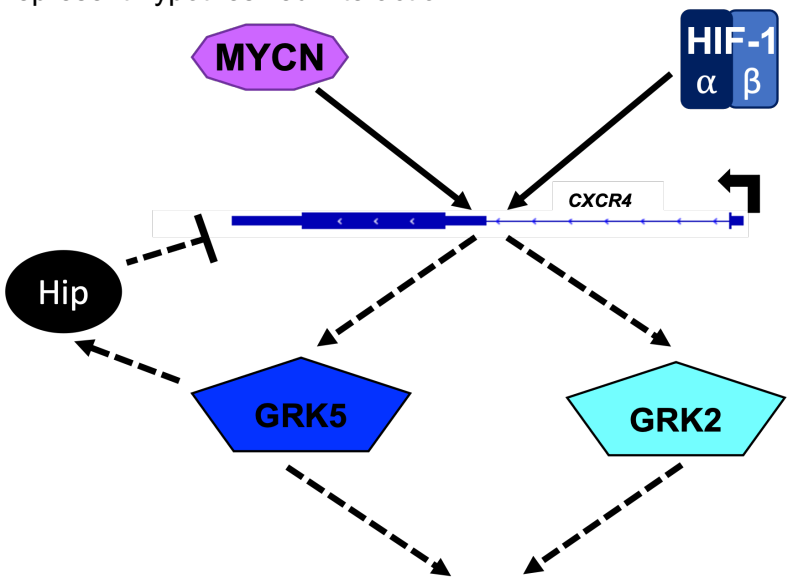

gene that encodes for Hip, *ST13*, is highly expressed in SK-N-BE(2) cells (152.7 FPKM) but does not increase in hypoxia (Figure 5.10). As a whole, I have devised a preliminary model of downstream signaling of CXCR4 in hypoxic SK-N-BE(2) cells (Figure 5.11), where CXCR4 is activated, and subsequently, activates GRK5, which may modulate NB migration or morphology possibly with the assistance of GRK2. GRK5 also may help internalize activated CXCR4 in SK-N-BE(2) cells by phosphorylating chaperone protein Hip (Figure 5.11).

ΔS1/2 *form tumors slower than control SK-N-BE(2) cells*

To determine if any potential changes in 5-hmC enrichment in Δ*S1*/2 cells had an impact on tumorgenicity or tumor growth, I performed tumor xenograft experiments with both clones of Δ*S1*/2 cells and the parental control line. After mice were injected, the parental line had visible tumors within the first three weeks (Figure 5.12). Mice injected with Δ*S1*/2 lines formed tumors slower than the parental line and by the end of the experiment two mice, each injected with a different clone, failed to grow any tumors. Additional experiments are needed that contain NTC replicates as well as NBL-WN cells, however these results show that *TET1* and 5-hmC contribute to NB cells tumorgenicity and overall growth.

Figure 5.12. Incidence curve of mice with tumors greater than 2 cm^3. Mice injected with parental SK-N-BE(2) (red), ΔS1/2.1 SK-N-BE(2) (blue), and ΔS1/2.2 SK-N-BE(2) (purple). Log rank test was used to test for significance **<0.01.

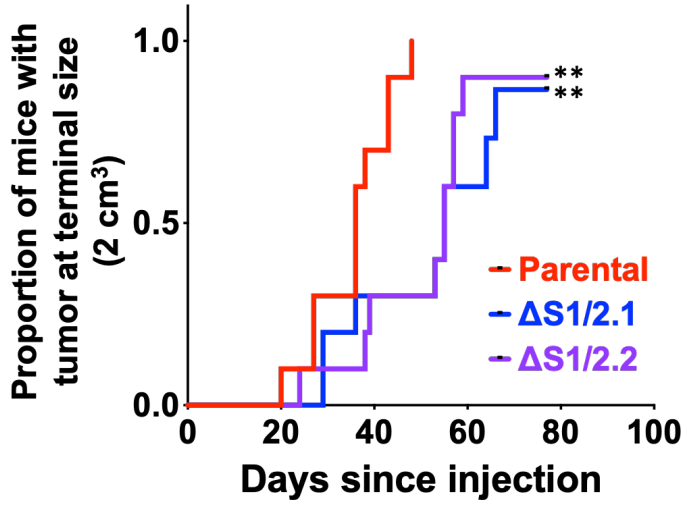

Discussion

In this chapter, I describe how hypoxic 5-hmC is distributed throughout the genome over time and identify 5-hmC target *CXCR4* as a potential driver of tumor cell migration. I have also shown that Δ*S1*/2 cells form tumors slower than the parental tumorigenic *MYCN*-amplified SK-N-BE(2) controls.

I hypothesized that 5-hmC augmented gene expression contributed to the aggressive hypoxic phenotype characteristic of NB. This was supported when the Cohn and Applebaum Laboratories determined 5-hmC profiles from tumor and cell-free DNA can serve as DNA-based biomarkers that are predictive of metastatic burden and prognostic of overall outcome (Applebaum et al., 2020). In this chapter, I performed detailed bioinformatic analyses that determined, in hypoxia, 5-hmC gain is enriched at genes involved in pathways associated with cell migration. Hypoxic *CXCR4* expression, similar to genes like *VEGFA*, appears to be augmented by 5-hmC enrichment in hypoxia, which contributes to *MYCN*-amplified NB migration. Hypoxic upregulation of *CXCR4* has implications both as a biomarker for aggressive disease in *MYCN*-amplified NBs and as a therapeutic target for high risk tumors. *CXCR4* has been identified previously in expression studies of primary NB tumors samples, correlating with metastatic spread and poor outcome (Russell et al., 2004). One study proposes a role for CXCR4 in NB in which CXCR4 promotes cell survival by downregulation of miR-15a/16-1 and upregulation of BCL-2. I proposed a different role for CXCR4 in hypoxia whereby it activates GRK5 and promotes cell migration. Future studies could elucidate more details about the mechanism by which CXCR4 and its downstream targets augment migration in hypoxia in NB, first by identifying those downstream targets. Additionally, future studies of NB tumor growth could determine whether introducing a CXCR4 antagonist or antibody to the NB treatment regimen would serve as a potential method to slow the spread of malignant cells and improve patient outcome.

Finally, I also observed Δ*S1*/2 cells grow slower than parental SK-N-BE(2) cells in tumor xenograft models. These results need to be replicated with an NTC, but they suggest that *TET1* expression is important for overall tumor growth. Future experiments could determine the mechanism by which *TET1* promotes tumor growth in tumorigenic *MYCN*-amplified NB cells.

CHAPTER VI

Discussion

In the previous chapters, I presented results that detailed how MYCN and HIF-1 regulate the *TET1* gene and TET1 protein, and subsequently, how the 5-hmC epigenetic landscape is regulated in NB (Figure 6.1). In addition, I determined 5-hmC was enriched in the gene body of *CXCR4* and CXCR4 protein mediated cell migration in hypoxic NB cells (Figure 6.1). Findings from other recent studies support my observations about *TET1* regulation and 5-hmC

Figure 6.1. Model of *TET1* gene and TET1 protein regulation in normoxia and hypoxia.

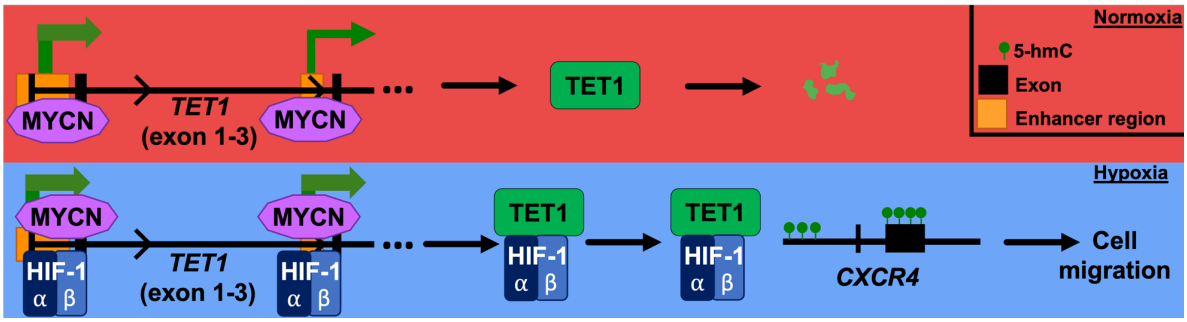

(Applebaum et al., 2019, 2020; Cao et al., 2020; Good et al., 2017; Greer et al., 2021). Collectively, they have emphasized that: (1) alternate *TET1* transcripts are expressed in adult vs embryonic tissues (2) *TET* genes are regulated by HIF-1 via two binding sites in hypoxia in two different biological systems; (3) Study of the 5-hmC profiles in NB tumors has implications for clinical settings and may yield further therapeutic targets in NB (Applebaum et al., 2019, 2020; Cao et al., 2020; Good et al., 2017; Greer et al., 2021).

Implications of the presence of *TET1fl* in NB

In Chapter III, I outlined specific future experiments that could determine the role and significance of TET1s and TET1fl in NB. Here, I will consider broader implications about TET1 isoform switches, or lack thereof, in NB. As previously mentioned, *TET1s* was identified as the

'pathogenic' transcript in cancers (Good et al., 2017). However, it is interesting to note that the cancers surveyed, including breast, uterine, ovarian, and glioblastoma, are all cancers that present in an adult age range. NB is a pediatric cancer and is believed to have embryonic origins (Huang and Weiss, 2013). This is significant because the isoform switch of TET1 protein is occurs during development (Zhang et al., 2016c). *TET1fl* is present in embryonic cells, whereas *TET1s* is expressed in adult tissues (Yosefzon et al., 2017; Zhang et al., 2016c). To help elucidate the mechanism of 'normal' *TET1* transcript switch in neural crest cells, the cell of NB origin, I reviewed a public RNA-seq database from induced pluripotent stem cells (iPSC) that differentiated into neurons (Burke et al., 2020). I searched for expression from all *TET1* exons and all time points from 0 to 77 days. Expression from *TET1* exons 1 and 2 dramatically decreased to near absent expression after 21 days (Figure 6.2A and B). However, expression from exon 3 did not change from 0 to 77 days (Figure 6.2C) (Burke et al., 2020). These results suggest that expression of *TET1fl* decreases to almost nothing over the course of normal neural development. Yet, *TET1fl* is highly expressed in NB cells, *MYCN*-amplified or not. I can only speculate on the origin of this discrepancy in *TET1* expression between NB and normal neural development, but the most likely possibilities are that normal cells turn precancerous before the TET1 protein isoform switch occurs or *TET1fl* is reactivated as part of NB gene expression program.

TET1 is not the only gene subject to alternative splicing in *MYCN*-amplified NB, yet it is one of few to be described (Guo et al., 2011; Zhang et al., 2016b). Two papers have shown that *MYCN*-amplified tumors have distinct alternative splicing patterns that are controlled specifically by MYCN (Guo et al., 2011; Zhang et al., 2016b). However, neither paper addressed the question of what genomic targets were subject to alternative splicing, suggesting there is an entire MYCN-driven alternate transcriptome yet to be described. Additionally, it is completely unknown if expression of these splice variants impacts cell phenotype or, even, if they

Figure 6.2. Expression from the first three *TET1* exons during iPSC neuronal differentiation. A. Expression of *TET1* exon 1 log2(RPKM+1). B. Expression of *TET1* exon 2 log2(RPKM+1). C. Expression of *TET1* exon 3 log2(RPKM+1). Plots were generated by http://stemcell.libd.org/scb/ (Burke et al., 2020).

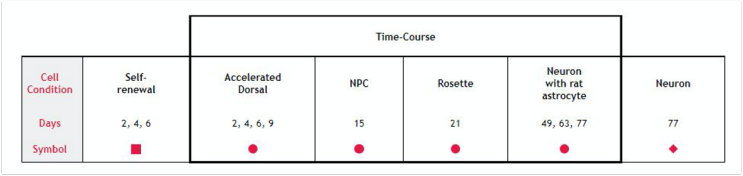

A

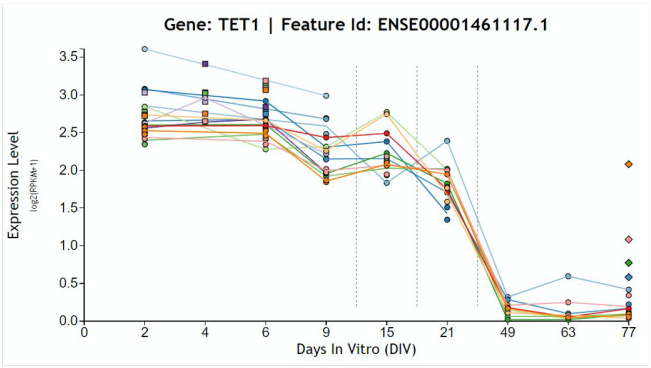

B

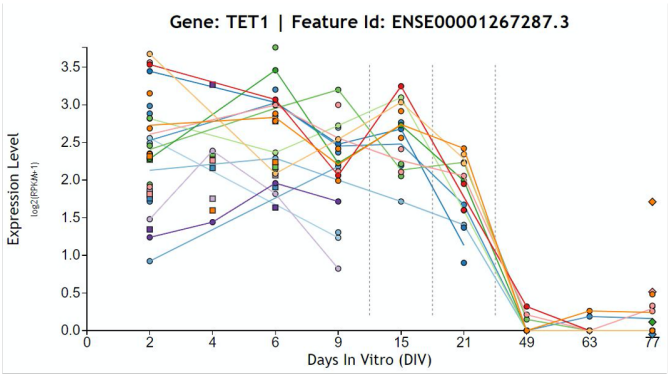

C

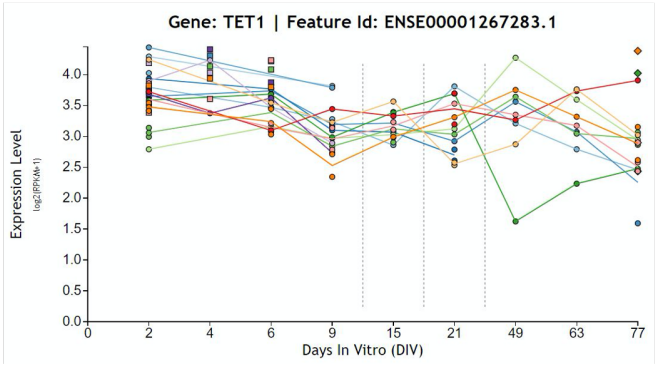

contribute to NB pathology. In conclusion, investigation of splice variants in high risk NB with transcriptomic analysis could identify novel diagnostic biomarkers or even therapeutic targets.

HIF-1 and *TET1* gene interaction

I described TFs and *TET1* gene interactions in both normoxia and hypoxia in MYCN-amplified NB. Recently, the Godley Laboratory identified and published a similar mechanism of HIF-1 regulation of *TET3* in hypoxia during erythropoiesis (Cao et al., 2020). In K562 cells, HIF-1 regulates *TET3* by binding two sites in a predicted enhancer region in the second intron of *TET3* (Figure 6.2). In that system, gene editing was used to delete each and then both sites in *TET3* (Cao et al., 2020). When the control, single, and double-deleted K562 lines were exposed to hypoxia, control lines increased *TET3* expression, as expected (Cao et al., 2020). However, in Δ*S1* and Δ*S2* lines, there was no change in *TET3* expression between normoxia and hypoxia (Cao et al., 2020). Additionally, *TET3* expression was significantly decreased in Δ*S1/2* cells in hypoxia (Cao et al., 2020). Despite being a very dissimilar cell type, this mechanism parallels the one I identified in

Figure 6.3. Model of TF binding of *TET1/3* in NB and erythropoietic systems. Model of TF binding in normoxia (red) and hypoxia (blue) in NB cells and erythroblasts. *TET1* and *TET3* are each regulated through two binding sites in enhancer (orange) regions.

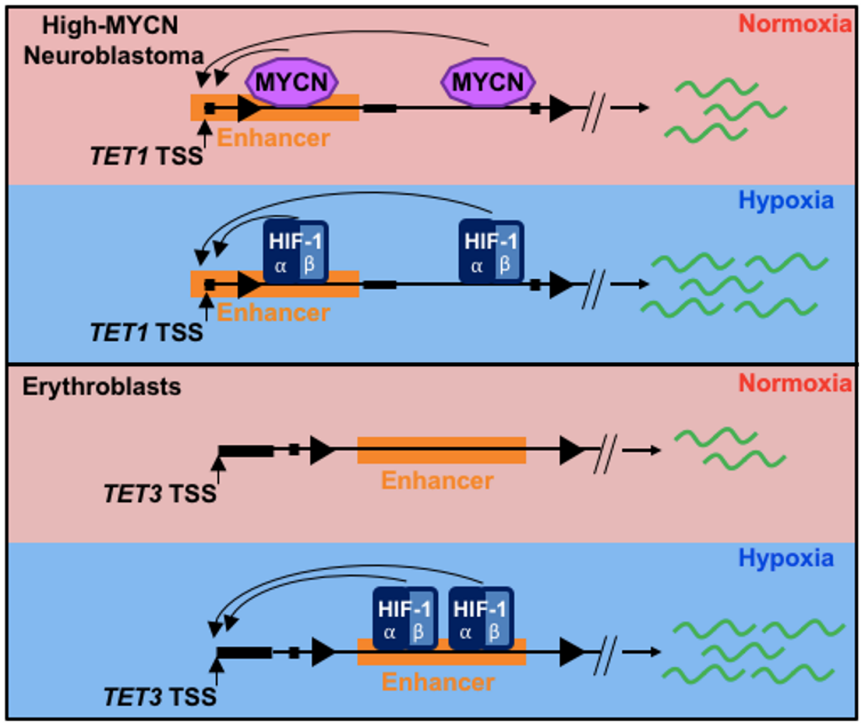

hypoxic NB cells (Figure 6.3). However, although unalike in morphology, both NB tumors and erythrocytes often reside in hypoxic environments: NB because of the lack of organized vasculature in tumors and erythrocytes because the bone marrow is a hypoxic environment. This indicates that there is a necessity that both cell types be primed to respond to fluctuations in oxygen. Future studies of *TET* gene regulation in other biological systems could consider the physiological oxygen level of the microenvironment so these studies can be performed in conditions approximate to physiological ones. Conversely, in the search to identify other biological systems with a similar mechanism of *TET* regulation, researchers could consider cells derived from a source that experiences at least intermittent hypoxia, as these cells are likely to be 'primed' to changes in oxygen level.

Implications for the 5-hmC epigenetic landscape in NB

The results of (Mariani et al., 2014) prompted our collaborators to investigate the 5-hmC epigenetic landscape in NB tumors in a clinical setting. Because the Godley and Cohn Laboratories found 5-hmC deposition was targeted to specific regions (canonical hypoxic response genes), our collaborators studied the 5-hmC profiles of NB tumor DNA (Applebaum et al., 2019, 2020). Additionally, they performed RNA-seq and identified differential gene expression (Applebaum et al., 2019, 2020). Then, they performed hierarchical clustering for both differential 5-hmC profiles and gene expression (Applebaum et al., 2019). Clustering revealed a stark separation of tumors that had been independently classified as low, intermediate, and high risk: 86% of tumors from low risk patients were included in cluster 1, and 89% of high risk tumors were included in cluster 2 (Applebaum et al., 2019). Our colleagues identified 62% of 2,722 genes with significantly differential 5-hmC were also differentially expressed within the two clusters (Applebaum et al., 2019). Among the genes that featured differential 5-hmC profiles, biological pathway analysis of cluster 1 identified oncogenic signatures of activated KRAS signaling and suppression of integral components of the

polycomb repressive complex 1: BMI1 and MEL18 (Applebaum et al., 2019). In cluster 2, biological pathway analysis of 5-hmC profiles found that they were enriched in genes involved in inflammatory response pathways and activation of EZH2 and the PRC2 complex (Applebaum et al., 2020). Ultimately, differential 5-hmC profiles of NB tumors were found to be prognostic of outcome (Applebaum et al., 2020). Our collaborators also performed hierarchical clustering analysis with plasma-derived cell-free DNA collected from blood samples from NB patients (Applebaum et al., 2020). They found increased 5-hmC levels at known oncogenic drivers *MYCN, TERT,* and *ALK* genes (Applebaum et al., 2020). In addition, 5-hmC profiles from cell free DNA were associated with metastatic disease burden, and were even predictive of metastatic disease, indicating analysis of cell-free 5-hmC profiles can be used to detect metastases in patients (Applebaum et al., 2020). Both studies support the work I present here. They corroborate my hypothesis that 5-hmC is a mediator of the aggressive phenotype often observed in NB, particularly the connection I identified between 5-hmC and metastatic spread. Future investigation of the clinical implications of the 5-hmC targets, specifically *CXCR4*, will be discussed later in this chapter.

Future directions

HIF-1 and TET1 protein interaction

Upon discovering that there was abundant TET1 protein in Δ*S1/2* cells that even increased, independent of mRNA, in hypoxia, I hypothesized there must be a mechanism of post-translational regulation of TET1 protein. As previously mentioned in Chapter I, TET1-TF binding has been observed in other biological systems. I hypothesized that there was a binding interaction between HIF-1 and TET1 that would either stabilize it or sequester it from proteasomal degradation. Ultimately, I was able to demonstrate TET1/HIF-1α binding in SK-N-BE(2) cells in hypoxia. However, there are still multiple unanswered questions about this

interaction, the first being: Are TET1 and HIF-1 part of a multiprotein complex? This could be addressed through mass spectrometry after IP of TET1. I hypothesize TET1 is part of a larger protein complex, if only because there are numerous HIF-1 interactors (Semenza, 2017). Unbiased analysis of proteins that CoIP with TET1, in normoxia and hypoxia, would reveal if TET1 is part of a larger protein complex.

The second remaining question is: what domains in HIF-1 and TET1 are critical for their interaction? The second question could be answered with systematic deletion of TET1 binding domains. In earlier studies that identified TET1 TF binding partners, NANOG and EGR1, both studies found that the CXXC domain was unnecessary for TF:TET1 interaction. Indeed, binding occurred between EGR1 and only the TET1 catalytic domain, but was lost when the Cys rich region of the catalytic domain was deleted. It is believed that TET1 is bound by transcription factors through its catalytic domain, whereas the TET1 CXXC domain interacts with DNA (Costa et al., 2013; Sun et al., 2019). Although experiments to identify the NANOG domain that interacts with TET1 were not performed, researchers discovered EGR1 interacts with TET1 through its zinc-finger domain on the C-terminus (Sun et al., 2019). As HIF-1 does not contain a zinc finger domain on either subunit, the question of what domain interacts with TET1 remains open.

Thirdly, does HIF-1 utilize this interaction to recruit TET1 to specific genomic sites, allowing TET1 to modify the gene bodies of canonical HIF-1 targets (Figure 6.4)? Determining if HIF-1 promotes TET1:DNA binding (Figure 6.4A) or if HIF-1 recruits TET1 to specific genomic

sites (Figure 6.4B) will require multiple experiments. I propose performing TET1 ChIP and comparing the peaks to those from the HIF-1 ChIP to create a profile of their binding and where their binding overlaps. Next, I suggest performing HIF-1 and TET1 ChIP in cells that only express TET1 that lacks the HIF-1 binding domain. This way the binding profile of TET1 could be analyzed under conditions where it is incapable of binding HIF-1. Comparing this TET1 binding profile to the original binding profile will determine if TET1 binding is altered when it cannot complex to HIF-1α. In addition, mass spectrometry and hMe-SEAL could determine if the interaction between TET1 and HIF-1α is essential for maintaining the 5-hmC epigenetic landscape in hypoxia.

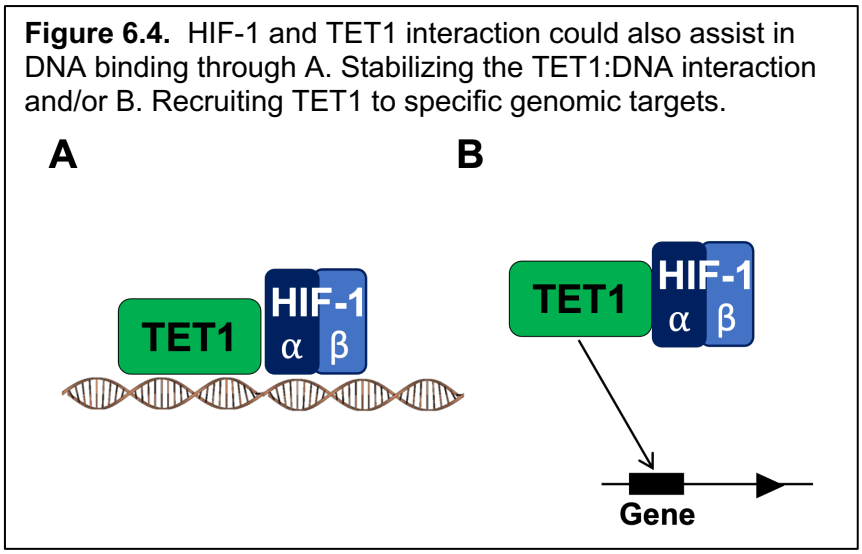

Figure 6.4. HIF-1 and TET1 interaction could also assist in DNA binding through A. Stabilizing the TET1:DNA interaction and/or B. Recruiting TET1 to specific genomic targets.

CXCR4 signaling in neuroblastoma

For several years, it has been known that patients with NB tumors with high CXCR4 protein expression have poor outcome, however the mechanism behind this is not well understood. My work has described a novel mechanism by which *CXCR4* is upregulated in hypoxia via HIF-1 in NB cell lines that express MYCN protein. This has clinical implications because, at the very least, the level of CXCR4 on the surface of a NB tumor cell may serve as an indicator of prognosis or the oxygen level of the tumor microenvironment. Determining the oxygen level of a tumor in a clinical setting may be informative, as hypoxia is known to cause NB cells in culture to dedifferentiate and make them more aggressive. Therefore, there is potential for CXCR4 to serve as a staging biomarker in the diagnosis of NB.

However, it is also possible that CXCR4 could serve as a therapeutic target in patients with NB. Being a receptor on the cell surface, CXCR4 is easily targetable and CXCR4 antagonists are available as currently in use in human medicine. Targeting CXCR4 as part of the NB treatment regimen could slow the spread or reduce the frequency of metastases in NB patients.

Although CXCR4 is an attractive target for researchers developing therapies against NB tumors, it does have its drawbacks. Plerixafor, the drug used in my work, is currently in clinical use as a stem cell mobilizer. Should plerixafor be given to NB patients as a treatment against the primary tumor, it would be an expected side effect that some stem cells would leave the bone marrow. Currently, it is not known if the long-term presence of stem cells in the blood stream has an adverse effect on human health. Future studies of CXCR4 antagonists in NB should test effects on NB cell lines as well as stem cells to identify which antagonists have the most specific effects on NB. Another option would be to test the effectiveness of an anti-CXCR4 antibody against NB cell lines in hypoxia. Alternatively, further investigation into the upstream and downstream pathways leading to and from CXCR4 may yield more targets specific to NB pathogenesis.

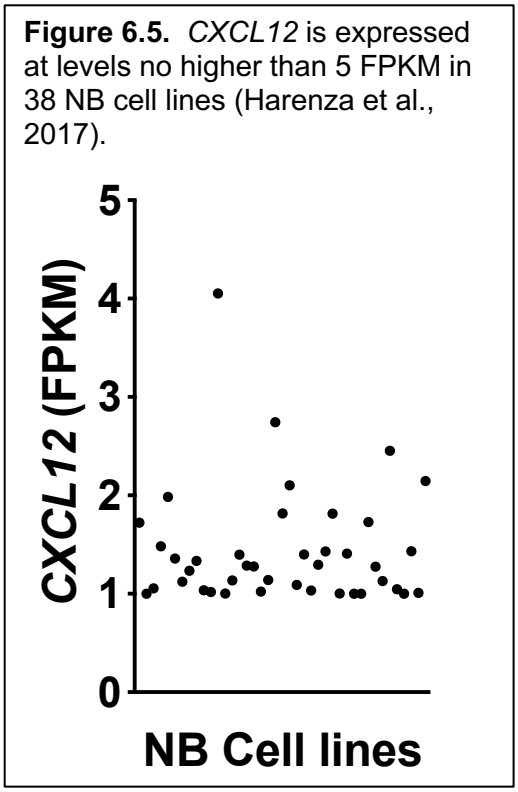

Figure 6.5. *CXCL12* is expressed at levels no higher than 5 FPKM in 38 NB cell lines (Harenza et al., 2017).

The role of surface CXCR4 expression in NB is not understood at all. In other systems, CXCR4 is bound by its canonical ligand SDF-1 and is then internalized and initiates downstream signaling. However, SDF-1 is not highly expressed in NB cell lines, with an FPKM average of about 2 (Figure 6.5). Either NB CXCR4 binds SDF-1 from an outside tissue or the tumor is stimulating CXCR4 from a non-canonical ligand such as

ubiquitin. Future experiments should include testing the effect different CXCR4 ligands have on downstream targets and phenotype in NB.

TET enzyme post-translational modifications (PTMs) in normoxia and hypoxia

TET proteins are subject to a variety of PTMs, many of which are poorly understood functionally. Preliminary research suggests that PTMs play a role in stability, activity, and localization of the TET enzymes. Briefly, I will report on known TET PTMs and what is known about their function. Then I will discuss how TET1 may be post-translationally modified in NB cells and how TET1 PTMs may be altered in response to hypoxia.

Known PTMs of the TET proteins include phosphorylation, O-GlcNAcylation (O-GlcNAc), and ubiquitination (Figure 6.6) (Bauer et al., 2015; Nakagawa et al., 2015; Zhang et al., 2017). A study performed in murine and human systems indicated phosphorylation of the three TET proteins was enriched in the N-terminus (Figure 6.6A) (Bauer et al., 2015). This modification can occur singly or in tandem with another phosphorylation modification (Bauer et al., 2015). O-

Figure 6.6. Approximate distribution of described TET PTMs. A. Representation of a common TET domains featuring modifications that are conserved across all three TET enzymes. The phosphorylation and O-GlcNAcylation rich region is representative of a large cluster of Phosphate and O-GlcNAc marks of variable distribution B. General distribution of modifications specific to TET1 protein. Colors: Acetylation is orange, Ubiquitination is purple, Phosphorylation is blue, O-GlcNAcylation is green.

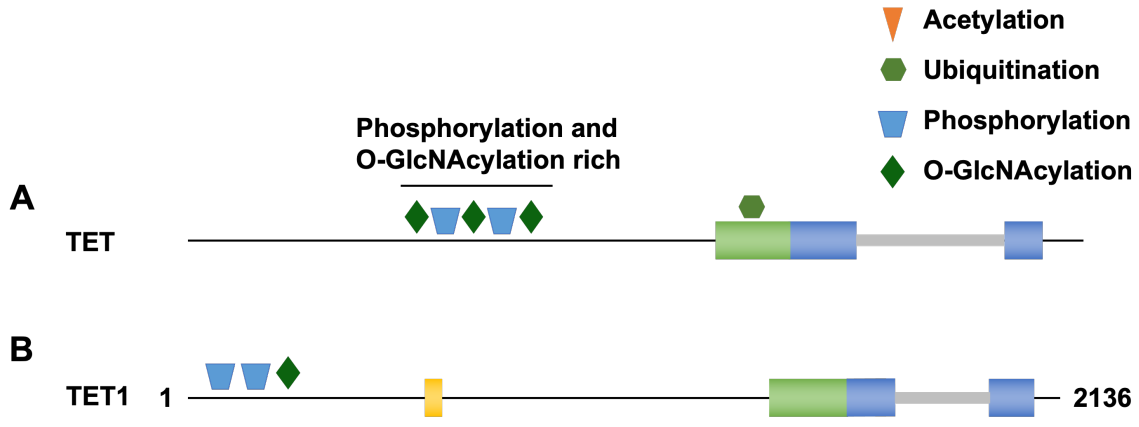

GlcNAc and phosphorylation modifications are thought to be occasionally in competition with each other (Bauer et al., 2015). Specifically, Ser-97 and Ser-374 of TET2 and Ser-362 and Ser-557 of TET3 could be phosphorylated or O-GlcNAcylated. Overall, some TET phosphorylation marks are stable, such as Ser-950 of TET1, but some are lost when *OGT* is highly expressed, like Ser-2016 of TET1.

O-GlcNAc modifications of the TET enzymes are generally concentrated on the N-terminus and the low-complexity insert (Figure 6.A and B). TET1 has fewer O-GlcNAc modifications than TET2 or TET3, with most found in the N-terminus and very few in the C-terminal region (Figure 6.6B). In addition, research has shown O-GlcNAc modifications of TET1 are highly dynamic (Bauer et al., 2015; Shi et al., 2013). There are a myriad of proposed functions of TET O-GlcNAc modifications (Bauer et al., 2015; Hrit et al., 2018; Vella et al., 2013). Several studies have demonstrated that this modification increases Tet1 protein stability and activity (Hrit et al., 2018; Vella et al., 2013). Others have implicated O-GlcNAc groups in mediating binding of TET partners and localization (Bauer et al., 2015).

Monoubiquitination of all three TET proteins occurs on a lysine, mediated by VprBP, in the highly conserved cysteine-rich domain (Figure 6.6A) (Nakagawa et al., 2015). The monoubiquitination occurs on K1589 in TET1, and its loss prevents binding to DNA and therefore results in an overall loss of 5-hmC.

Because there are an extremely large number of reported TET1 PTMs, an unbiased, systematic approach is needed to identify all PTMs on TET1 in normoxia and hypoxia (Bauer et al., 2015; Hrit et al., 2018; Nakagawa et al., 2015; Vella et al., 2013). First, normoxic and hypoxic TET1 protein should be isolated, then mass spectrometry analysis would identify all PTMs present under each condition, then differential PTMs between the two conditions. Then, experiments should be designed to test the function of each PTM.

Although PTM regulation of TET1 function is likely to be complex and nuanced, there is an attractive model of TET2 phosphorylation that also fits our existing data of TET1 in NB

(Jeong et al., 2019). There have been no studies of any TET PTMs under hypoxic conditions, but a study of TET2 phosphorylation described a mechanism that may be relevant for TET1 modifications in hypoxia (Jeong et al., 2019). The study was performed in an erythroid progenitor system and found TET2 was phosphorylated via JAK2, activating it and increasing global 5-hmC levels (Jeong et al., 2019). TET2 was phosphorylated at two tyrosines, Y1939 and Y1964, both located in the catalytic domain of TET2 (Jeong et al., 2019b). When both phospho-marks were present, binding affinity for transcription factor KLF1 increased dramatically (Jeong et al., 2019b). Following the results presented in this study, I hypothesize that, in NB cells, an unknown kinase phosphorylates TET1, similarly in the catalytic domain, that promotes TET1 binding to HIF-1. TET1 is then activated and stabilized and is recruited by HIF-1 to specific sites in the genome. Results from mass spectrometry analysis of TET1 PTMs will determine if this is a possibility.

References

Allis, C.D., and Jenuwein, T. (2016). The molecular hallmarks of epigenetic control. Nature Reviews Genetics *17*, 487–500.

Anders, S., Pyl, P.T., and Huber, W. (2015). HTSeq—a Python framework to work with high-throughput sequencing data. Bioinformatics *31*, 166–169.

Applebaum, M.A., Barr, E.K., Karpus, J., Nie, J., Zhang, Z., Armstrong, A.E., Uppal, S., Sukhanova, M., Zhang, W., Chlenski, A., et al. (2019). 5-Hydroxymethylcytosine Profiles Are Prognostic of Outcome in Neuroblastoma and Reveal Transcriptional Networks That Correlate With Tumor Phenotype. JCO Precis Oncol *3*.

Applebaum, M.A., Barr, E.K., Karpus, J., West-Szymanski, D.C., Oliva, M., Sokol, E.A., Zhang, S., Zhang, Z., Zhang, W., Chlenski, A., et al. (2020). 5-Hydroxymethylcytosine Profiles in Circulating Cell-Free DNA Associate with Disease Burden in Children with Neuroblastoma. Clin Cancer Res *26*, 1309–1317.

Arany, Z., Huang, L.E., Eckner, R., Bhattacharya, S., Jiang, C., Goldberg, M.A., Bunn, H.F., and Livingston, D.M. (1996). An essential role for p300/CBP in the cellular response to hypoxia. PNAS *93*, 12969–12973.

Arita, K., Ariyoshi, M., Tochio, H., Nakamura, Y., and Shirakawa, M. (2008). Recognition of hemi-methylated DNA by the SRA protein UHRF1 by a base-flipping mechanism. Nature *455*, 818–821.

Attiyeh, E.F., London, W.B., Mossé, Y.P., Wang, Q., Winter, C., Khazi, D., McGrady, P.W., Seeger, R.C., Look, A.T., Shimada, H., et al. (2005). Chromosome 1p and 11q deletions and outcome in neuroblastoma. N Engl J Med *353*, 2243–2253.

Avery, O.T., Macleod, C.M., and McCarty, M. (1944). STUDIES ON THE CHEMICAL NATURE OF THE SUBSTANCE INDUCING TRANSFORMATION OF PNEUMOCOCCAL TYPES : INDUCTION OF TRANSFORMATION BY A DESOXYRIBONUCLEIC ACID FRACTION ISOLATED FROM PNEUMOCOCCUS TYPE III. J. Exp. Med. *79*, 137–158.

Barker, B.L., and Benovic, J.L. (2011). G protein-coupled receptor kinase 5 phosphorylation of hip regulates internalization of the chemokine receptor CXCR4. Biochemistry *50*, 6933–6941.

Baubec, T., Ivánek, R., Lienert, F., and Schübeler, D. (2013). Methylation-Dependent and -Independent Genomic Targeting Principles of the MBD Protein Family. Cell *153*, 480–492.

Bauer, C., Göbel, K., Nagaraj, N., Colantuoni, C., Wang, M., Müller, U., Kremmer, E., Rottach, A., and Leonhardt, H. (2015). Phosphorylation of TET Proteins Is Regulated via O-GlcNAcylation by the O-Linked N-Acetylglucosamine Transferase (OGT). J Biol Chem *290*, 4801–4812.

Baylin, S.B., Höppener, J.W., de Bustros, A., Steenbergh, P.H., Lips, C.J., and Nelkin, B.D. (1986). DNA methylation patterns of the calcitonin gene in human lung cancers and lymphomas. Cancer Res. *46*, 2917–2922.

Bell, E., Lunec, J., and Tweddle, D.A. (2007). Cell cycle regulation targets of MYCN identified by gene expression microarrays. Cell Cycle *6*, 1249–1256.

Bellini, A., Bernard, V., Leroy, Q., Frio, T.R., Pierron, G., Combaret, V., Lapouble, E., Clement, N., Rubie, H., Thebaud, E., et al. (2015). Deep Sequencing Reveals Occurrence of Subclonal ALK Mutations in Neuroblastoma at Diagnosis. Clin Cancer Res *21*, 4913–4921.

Bhaskara, V.K., Mohanam, I., Rao, J.S., and Mohanam, S. (2012). Intermittent hypoxia regulates stem-like characteristics and differentiation of neuroblastoma cells. PLoS One *7*, e30905.

Bianchi, M.E., and Mezzapelle, R. (2020). The Chemokine Receptor CXCR4 in Cell Proliferation and Tissue Regeneration. Front Immunol *11*, 2109.

Blaschke, K., Ebata, K.T., Karimi, M.M., Zepeda-Martínez, J.A., Goyal, P., Mahapatra, S., Tam, A., Laird, D.J., Hirst, M., Rao, A., et al. (2013). Vitamin C induces Tet-dependent DNA demethylation and a blastocyst-like state in ES cells. Nature *500*, 222–226.

Bleul, C.C., Farzan, M., Choe, H., Parolin, C., Clark-Lewis, I., Sodroski, J., and Springer, T.A. (1996). The lymphocyte chemoattractant SDF-1 is a ligand for LESTR/fusin and blocks HIV-1 entry. Nature *382*, 829–833.

Booth, M.J., Ost, T.W.B., Beraldi, D., Bell, N.M., Branco, M.R., Reik, W., and Balasubramanian, S. (2013). Oxidative bisulfite sequencing of 5-methylcytosine and 5-hydroxymethylcytosine. Nat Protoc *8*, 1841–1851.

Brodeur, G.M., Seeger, R.C., Schwab, M., Varmus, H.E., and Bishop, J.M. (1984). Amplification of N-myc in untreated human neuroblastomas correlates with advanced disease stage. Science *224*, 1121–1124.

Burke, E.E., Chenoweth, J.G., Shin, J.H., Collado-Torres, L., Kim, S.-K., Micali, N., Wang, Y., Colantuoni, C., Straub, R.E., Hoeppner, D.J., et al. (2020). Dissecting transcriptomic signatures of neuronal differentiation and maturation using iPSCs. Nat Commun *11*, 462.

Camenisch, G., Wenger, R.H., and Gassmann, M. (2002). DNA-Binding Activity of Hypoxia-Inducible Factors (HIFs). In Oxidants and Antioxidants: Ultrastructure and Molecular Biology Protocols, D. Armstrong, ed. (Totowa, NJ: Humana Press), pp. 117–129.

Cao, J.Z., Hains, A.E., and Godley, L.A. (2019). Regulation of 5-Hydroxymethylcytosine Distribution by the TET Enzymes. In The DNA, RNA, and Histone Methylomes, S. Jurga, and J. Barciszewski, eds. (Cham: Springer International Publishing), pp. 229–263.

Cao, J.Z., Liu, H., Wickrema, A., and Godley, L.A. (2020). HIF-1 directly induces TET3 expression to enhance 5-hmC density and induce erythroid gene expression in hypoxia. Blood Adv *4*, 3053–3062.

Carreau, A., Hafny-Rahbi, B.E., Matejuk, A., Grillon, C., and Kieda, C. (2011). Why is the partial oxygen pressure of human tissues a crucial parameter? Small molecules and hypoxia. J Cell Mol Med *15*, 1239–1253.

Cartron, P.-F., Nadaradjane, A., Lepape, F., Lalier, L., Gardie, B., and Vallette, F.M. (2013). Identification of TET1 Partners That Control Its DNA-Demethylating Function. Genes Cancer *4*, 235–241.

Chandru, A., Bate, N., Vuister, G.W., and Cowley, S.M. (2018). Sin3A recruits Tet1 to the PAH1 domain via a highly conserved Sin3-Interaction Domain. Sci Rep *8*, 14689.

Chatterjee, S., Azad, B.B., and Nimmagadda, S. (2014). The Intricate Role of CXCR4 in Cancer. Adv Cancer Res *124*, 31–82.

Chen, B.-F., and Chan, W.-Y. (2014). The de novo DNA methyltransferase DNMT3A in development and cancer. Epigenetics *9*, 669–677.

Chen, J., Guo, L., Zhang, L., Wu, H., Yang, J., Liu, H., Wang, X., Hu, X., Gu, T., Zhou, Z., et al. (2013). Vitamin C modulates TET1 function during somatic cell reprogramming. Nat Genet *45*, 1504–1509.

Chen, L., Lin, Y.-L., Peng, G., and Li, F. (2012). Structural basis for multifunctional roles of mammalian aminopeptidase N. Proc Natl Acad Sci U S A *109*, 17966–17971.

Chen, S., Zhang, M., Xing, L., Wang, Y., Xiao, Y., and Wu, Y. (2015). HIF-1α Contributes to Proliferation and Invasiveness of Neuroblastoma Cells via SHH Signaling. PLoS One *10*.

Chen, Y., Wang, F., Long, H., Chen, Y., Wu, Z., and Ma, L. (2011). GRK5 promotes F-actin bundling and targets bundles to membrane structures to control neuronal morphogenesis. J Cell Biol *194*, 905–920.

Cheng, Y., He, C., Wang, M., Ma, X., Mo, F., Yang, S., Han, J., and Wei, X. (2019). Targeting epigenetic regulators for cancer therapy: mechanisms and advances in clinical trials. Signal Transduction and Targeted Therapy *4*, 1–39.

Chlenski, A., Park, C., Dobratic, M., Salwen, H.R., Budke, B., Park, J.-H., Miller, R., Applebaum, M.A., Wilkinson, E., Nakamura, Y., et al. (2019). Maternal Embryonic Leucine Zipper Kinase (MELK), a Potential Therapeutic Target for Neuroblastoma. Mol Cancer Ther *18*, 507–516.

Chung, T.-L., Brena, R.M., Kolle, G., Grimmond, S.M., Berman, B.P., Laird, P.W., Pera, M.F., and Wolvetang, E.J. (2010). Vitamin C promotes widespread yet specific DNA demethylation of the epigenome in human embryonic stem cells. Stem Cells *28*, 1848–1855.

Cohen-Karni, D., Xu, D., Apone, L., Fomenkov, A., Sun, Z., Davis, P.J., Morey Kinney, S.R., Yamada-Mabuchi, M., Xu, S., Davis, T., et al. (2011). The MspJI family of modification-dependent restriction endonucleases for epigenetic studies. Proc Natl Acad Sci U S A *108*, 11040–11045.

Cohn, S.L., Salwen, H., Quasney, M.W., Ikegaki, N., Cowan, J.M., Herst, C.V., Kennett, R.H., Rosen, S.T., DiGiuseppe, J.A., and Brodeur, G.M. (1990). Prolonged N-myc protein half-life in a neuroblastoma cell line lacking N-myc amplification. Oncogene *5*, 1821–1827.

Concordet, J.-P., and Haeussler, M. (2018). CRISPOR: intuitive guide selection for CRISPR/Cas9 genome editing experiments and screens. Nucleic Acids Research *46*, W242–W245.

Costa, Y., Ding, J., Theunissen, T.W., Faiola, F., Hore, T.A., Shliaha, P.V., Fidalgo, M., Saunders, A., Lawrence, M., Dietmann, S., et al. (2013). Nanog-dependent function of Tet1 and Tet2 in establishment of pluripotency. Nature *495*, 370–374.

Dang, L., White, D.W., Gross, S., Bennett, B.D., Bittinger, M.A., Driggers, E.M., Fantin, V.R., Jang, H.G., Jin, S., Keenan, M.C., et al. (2009). Cancer-associated IDH1 mutations produce 2-hydroxyglutarate. Nature *462*, 739–744.

Decock, A., Ongenaert, M., Vandesompele, J., and Speleman, F. (2011). Neuroblastoma epigenetics: from candidate gene approaches to genome-wide screenings. Epigenetics *6*, 962–970.

Delloye-Bourgeois, C., and Castellani, V. (2019). Hijacking of Embryonic Programs by Neural Crest-Derived Neuroblastoma: From Physiological Migration to Metastatic Dissemination. Frontiers in Molecular Neuroscience *12*, 52.

Deplus, R., Delatte, B., Schwinn, M.K., Defrance, M., Méndez, J., Murphy, N., Dawson, M.A., Volkmar, M., Putmans, P., Calonne, E., et al. (2013). TET2 and TET3 regulate GlcNAcylation and H3K4 methylation through OGT and SET1/COMPASS. EMBO J *32*, 645–655.

Domanska, U.M., Kruizinga, R.C., Nagengast, W.B., Timmer-Bosscha, H., Huls, G., de Vries, E.G.E., and Walenkamp, A.M.E. (2013). A review on CXCR4/CXCL12 axis in oncology: no place to hide. Eur J Cancer *49*, 219–230.

Dungwa, J.V., Uparkar, U., May, M.T., and Ramani, P. (2012). Angiogenin up-regulation correlates with adverse clinicopathological and biological factors, increased microvascular density and poor patient outcome in neuroblastomas. Histopathology *60*, 911–923.

Durbin, A.D., Zimmerman, M.W., Dharia, N.V., Abraham, B.J., Iniguez, A.B., Weichert-Leahey, N., He, S., Krill-Burger, J.M., Root, D.E., Vazquez, F., et al. (2018). Selective gene dependencies in MYCN-amplified neuroblastoma include the core transcriptional regulatory circuitry. Nat. Genet. *50*, 1240–1246.

Edsjö, A., Holmquist, L., and Påhlman, S. (2007). Neuroblastoma as an experimental model for neuronal differentiation and hypoxia-induced tumor cell dedifferentiation. Seminars in Cancer Biology *17*, 248–256.

Feinberg, A.P., and Tycko, B. (2004). The history of cancer epigenetics. Nat. Rev. Cancer *4*, 143–153.

Feinberg, A.P., and Vogelstein, B. (1983). Hypomethylation distinguishes genes of some human cancers from their normal counterparts. Nature *301*, 89–92.

Fernandez, A.F., Bayón, G.F., Sierra, M.I., Urdinguio, R.G., Toraño, E.G., García, M.G., Carella, A., López, V., Santamarina, P., Pérez, R.F., et al. (2018). Loss of 5hmC identifies a new type of aberrant DNA hypermethylation in glioma. Hum Mol Genet *27*, 3046–3059.

Fernandis, A.Z., Cherla, R.P., Chernock, R.D., and Ganju, R.K. (2002). CXCR4/CCR5 down-modulation and chemotaxis are regulated by the proteasome pathway. J Biol Chem *277*, 18111–18117.

Ficz, G., Branco, M.R., Seisenberger, S., Santos, F., Krueger, F., Hore, T.A., Marques, C.J., Andrews, S., and Reik, W. (2011). Dynamic regulation of 5-hydroxymethylcytosine in mouse ES cells and during differentiation. Nature *473*, 398–402.

Field, S.F., Beraldi, D., Bachman, M., Stewart, S.K., Beck, S., and Balasubramanian, S. (2015). Accurate Measurement of 5-Methylcytosine and 5-Hydroxymethylcytosine in Human Cerebellum DNA by Oxidative Bisulfite on an Array (OxBS-Array). PLoS One *10*.

Figueroa, M.E., Abdel-Wahab, O., Lu, C., Ward, P.S., Patel, J., Shih, A., Li, Y., Bhagwat, N., Vasanthakumar, A., Fernandez, H.F., et al. (2010). Leukemic IDH1 and IDH2 mutations result in a hypermethylation phenotype, disrupt TET2 function, and impair hematopoietic differentiation. Cancer Cell *18*, 553–567.

Fotsis, T., Breit, S., Lutz, W., Rössler, J., Hatzi, E., Schwab, M., and Schweigerer, L. (1999). Down-regulation of endothelial cell growth inhibitors by enhanced MYCN oncogene expression in human neuroblastoma cells. Eur J Biochem *263*, 757–764.

Frauer, C., Hoffmann, T., Bultmann, S., Casa, V., Cardoso, M.C., Antes, I., and Leonhardt, H. (2011). Recognition of 5-hydroxymethylcytosine by the Uhrf1 SRA domain. PLoS ONE *6*, e21306.

Gaidzik, V.I., Paschka, P., Späth, D., Habdank, M., Köhne, C.-H., Germing, U., von Lilienfeld-Toal, M., Held, G., Horst, H.-A., Haase, D., et al. (2012). TET2 mutations in acute myeloid leukemia (AML): results from a comprehensive genetic and clinical analysis of the AML study group. J Clin Oncol *30*, 1350–1357.

Gama-Sosa, M.A., Slagel, V.A., Trewyn, R.W., Oxenhandler, R., Kuo, K.C., Gehrke, C.W., and Ehrlich, M. (1983). The 5-methylcytosine content of DNA from human tumors. Nucleic Acids Res. *11*, 6883–6894.

Gao, T., He, B., Liu, S., Zhu, H., Tan, K., and Qian, J. (2016). EnhancerAtlas: a resource for enhancer annotation and analysis in 105 human cell/tissue types. Bioinformatics *32*, 3543–3551.

Gartlgruber, M., Sharma, A.K., Quintero, A., Dreidax, D., Jansky, S., Park, Y.-G., Kreth, S., Meder, J., Doncevic, D., Saary, P., et al. (2021). Super enhancers define regulatory subtypes and cell identity in neuroblastoma. Nature Cancer *2*, 114–128.

George, R.E., London, W.B., Cohn, S.L., Maris, J.M., Kretschmar, C., Diller, L., Brodeur, G.M., Castleberry, R.P., and Look, A.T. (2005). Hyperdiploidy plus nonamplified MYCN confers a favorable prognosis in children 12 to 18 months old with disseminated neuroblastoma: a Pediatric Oncology Group study. J Clin Oncol *23*, 6466–6473.

Globisch, D., Münzel, M., Müller, M., Michalakis, S., Wagner, M., Koch, S., Brückl, T., Biel, M., and Carell, T. (2010). Tissue distribution of 5-hydroxymethylcytosine and search for active demethylation intermediates. PLoS ONE *5*, e15367.

Good, C.R., Madzo, J., Patel, B., Maegawa, S., Engel, N., Jelinek, J., and Issa, J.-P.J. (2017). A novel isoform of TET1 that lacks a CXXC domain is overexpressed in cancer. Nucleic Acids Res. *45*, 8269–8281.

Gordan, J.D., Thompson, C.B., and Simon, M.C. (2007). HIF and c-Myc: sibling rivals for control of cancer cell metabolism and proliferation. Cancer Cell *12*, 108–113.

Greer, C.B., Wright, J., Weiss, J.D., Lazarenko, R.M., Moran, S.P., Zhu, J., Chronister, K.S., Jin, A.Y., Kennedy, A.J., Sweatt, J.D., et al. (2021). Tet1 Isoforms Differentially Regulate Gene Expression, Synaptic Transmission, and Memory in the Mammalian Brain. J. Neurosci. *41*, 578–593.

van Groningen, T., Koster, J., Valentijn, L.J., Zwijnenburg, D.A., Akogul, N., Hasselt, N.E., Broekmans, M., Haneveld, F., Nowakowska, N.E., Bras, J., et al. (2017). Neuroblastoma is composed of two super-enhancer-associated differentiation states. Nature Genetics *49*, 1261–1266.

Guo, F., Wang, Y., Liu, J., Mok, S.C., Xue, F., and Zhang, W. (2016). CXCL12/CXCR4: a symbiotic bridge linking cancer cells and their stromal neighbors in oncogenic communication networks. Oncogene *35*, 816–826.

Guo, X., Chen, Q.-R., Song, Y.K., Wei, J.S., and Khan, J. (2011). Exon array analysis reveals neuroblastoma tumors have distinct alternative splicing patterns according to stage and MYCN amplification status. BMC Med Genomics *4*, 35.

Hahn, M.A., Qiu, R., Wu, X., Li, A.X., Zhang, H., Wang, J., Jui, J., Jin, S.-G., Jiang, Y., Pfeifer, G.P., et al. (2013). Dynamics of 5-Hydroxymethylcytosine and Chromatin Marks in Mammalian Neurogenesis. Cell Reports *3*, 291–300.

Harenza, J.L., Diamond, M.A., Adams, R.N., Song, M.M., Davidson, H.L., Hart, L.S., Dent, M.H., Fortina, P., Reynolds, C.P., and Maris, J.M. (2017). Transcriptomic profiling of 39 commonly-used neuroblastoma cell lines. Scientific Data *4*, 170033.

Hatzi, E., Breit, S., Zoephel, A., Ashman, K., Tontsch, U., Ahorn, H., Murphy, C., Schweigerer, L., and Fotsis, T. (2000). MYCN oncogene and angiogenesis: down-regulation of endothelial growth inhibitors in human neuroblastoma cells. Purification, structural, and functional characterization. Adv Exp Med Biol *476*, 239–248.

He, Y.-F., Li, B.-Z., Li, Z., Liu, P., Wang, Y., Tang, Q., Ding, J., Jia, Y., Chen, Z., Li, L., et al. (2011). Tet-mediated formation of 5-carboxylcytosine and its excision by TDG in mammalian DNA. Science *333*, 1303–1307.

Heinz, S., Benner, C., Spann, N., Bertolino, E., Lin, Y.C., Laslo, P., Cheng, J.X., Murre, C., Singh, H., and Glass, C.K. (2010). Simple combinations of lineage-determining transcription factors prime cis-regulatory elements required for macrophage and B cell identities. Mol Cell *38*, 576–589.

Holliday, R., and Pugh, J.E. (1975). DNA modification mechanisms and gene activity during development. Science *187*, 226–232.

Hornbeck, P.V., Zhang, B., Murray, B., Kornhauser, J.M., Latham, V., and Skrzypek, E. (2015). PhosphoSitePlus, 2014: mutations, PTMs and recalibrations. Nucleic Acids Res *43*, D512–D520.

Hotchkiss, R.D. (1948). The quantitative separation of purines, pyrimidines, and nucleosides by paper chromatography. J. Biol. Chem. *175*, 315–332.

Hrit, J., Goodrich, L., Li, C., Wang, B.-A., Nie, J., Cui, X., Martin, E.A., Simental, E., Fernandez, J., Liu, M.Y., et al. (2018). OGT binds a conserved C-terminal domain of TET1 to regulate TET1 activity and function in development. Elife *7*.

Hu, L., Li, Z., Cheng, J., Rao, Q., Gong, W., Liu, M., Shi, Y.G., Zhu, J., Wang, P., and Xu, Y. (2013). Crystal Structure of TET2-DNA Complex: Insight into TET-Mediated 5mC Oxidation. Cell *155*, 1545–1555.

Hu, L., Lu, J., Cheng, J., Rao, Q., Li, Z., Hou, H., Lou, Z., Zhang, L., Li, W., Gong, W., et al. (2015). Structural insight into substrate preference for TET-mediated oxidation. Nature *527*, 118–122.

Huang, M., and Weiss, W.A. (2013). Neuroblastoma and MYCN. Cold Spring Harb Perspect Med *3*, a014415.

Huang, L.E., Gu, J., Schau, M., and Bunn, H.F. (1998). Regulation of hypoxia-inducible factor 1alpha is mediated by an O2-dependent degradation domain via the ubiquitin-proteasome pathway. Proc. Natl. Acad. Sci. U.S.A. *95*, 7987–7992.

Huertas-Castaño, C., Gómez-Muñoz, M.A., Pardal, R., and Vega, F.M. (2019). Hypoxia in the Initiation and Progression of Neuroblastoma Tumours. Int J Mol Sci *21*.

Iliopoulos, O., Levy, A.P., Jiang, C., Kaelin, W.G., and Goldberg, M.A. (1996). Negative regulation of hypoxia-inducible genes by the von Hippel-Lindau protein. Proc Natl Acad Sci U S A *93*, 10595–10599.

Inagaki, S., Ghirlando, R., Vishnivetskiy, S.A., Homan, K.T., White, J.F., Tesmer, J.J.G., Gurevich, V.V., and Grisshammer, R. (2015). G Protein-Coupled Receptor Kinase 2 (GRK2) and 5 (GRK5) Exhibit Selective Phosphorylation of the Neurotensin Receptor in Vitro. Biochemistry *54*, 4320–4329.

Ito, S., D'Alessio, A.C., Taranova, O.V., Hong, K., Sowers, L.C., and Zhang, Y. (2010). Role of Tet proteins in 5mC to 5hmC conversion, ES cell self-renewal, and ICM specification. Nature *466*, 1129–1133.

Ito, S., Shen, L., Dai, Q., Wu, S.C., Collins, L.B., Swenberg, J.A., He, C., and Zhang, Y. (2011). Tet proteins can convert 5-methylcytosine to 5-formylcytosine and 5-carboxylcytosine. Science *333*, 1300–1303.

Iurlaro, M., Ficz, G., Oxley, D., Raiber, E.-A., Bachman, M., Booth, M.J., Andrews, S., Balasubramanian, S., and Reik, W. (2013). A screen for hydroxymethylcytosine and formylcytosine binding proteins suggests functions in transcription and chromatin regulation. Genome Biol *14*, R119.

Ivan, M., Kondo, K., Yang, H., Kim, W., Valiando, J., Ohh, M., Salic, A., Asara, J.M., Lane, W.S., and Kaelin, W.G. (2001). HIFalpha targeted for VHL-mediated destruction by proline hydroxylation: implications for O2 sensing. Science *292*, 464–468.

Jaakkola, P., Mole, D.R., Tian, Y.M., Wilson, M.I., Gielbert, J., Gaskell, S.J., von Kriegsheim, A., Hebestreit, H.F., Mukherji, M., Schofield, C.J., et al. (2001). Targeting of HIF-alpha to the von Hippel-Lindau ubiquitylation complex by O2-regulated prolyl hydroxylation. Science *292*, 468–472.

Jeong, J.J., Gu, X., Nie, J., Sundaravel, S., Liu, H., Kuo, W.-L., Bhagat, T.D., Pradhan, K., Cao, J., Nischal, S., et al. (2019). Cytokine-Regulated Phosphorylation and Activation of TET2 by JAK2 in Hematopoiesis. Cancer Discov *9*, 778–795.

Jjingo, D., Conley, A.B., Yi, S.V., Lunyak, V.V., and Jordan, I.K. (2012). On the presence and role of human gene-body DNA methylation. Oncotarget *3*, 462–474.

Jögi, A., Vallon-Christersson, J., Holmquist, L., Axelson, H., Borg, A., and Påhlman, S. (2004). Human neuroblastoma cells exposed to hypoxia: induction of genes associated with growth, survival, and aggressive behavior. Exp Cell Res *295*, 469–487.

Jones, P.A. (2012). Functions of DNA methylation: islands, start sites, gene bodies and beyond. Nat. Rev. Genet. *13*, 484–492.

Justus, C.R., Leffler, N., Ruiz-Echevarria, M., and Yang, L.V. (2014). In vitro Cell Migration and Invasion Assays. J Vis Exp.

Kafer, G.R., Li, X., Horii, T., Suetake, I., Tajima, S., Hatada, I., and Carlton, P.M. (2016). 5-Hydroxymethylcytosine Marks Sites of DNA Damage and Promotes Genome Stability. Cell Reports *14*, 1283–1292.

Kang, J., Rychahou, P.G., Ishola, T.A., Mourot, J.M., Evers, B.M., and Chung, D.H. (2008). N-myc is a novel regulator of PI3K-mediated VEGF expression in neuroblastoma. Oncogene *27*, 3999–4007.

Kim, D., Pertea, G., Trapnell, C., Pimentel, H., Kelley, R., and Salzberg, S.L. (2013). TopHat2: accurate alignment of transcriptomes in the presence of insertions, deletions and gene fusions. Genome Biology *14*, R36.

Klein, S., Abraham, M., Bulvik, B., Dery, E., Weiss, I.D., Barashi, N., Abramovitch, R., Wald, H., Harel, Y., Olam, D., et al. (2018). CXCR4 Promotes Neuroblastoma Growth and Therapeutic Resistance through miR-15a/16-1-Mediated ERK and BCL2/Cyclin D1 Pathways. Cancer Res. *78*, 1471–1483.

Ko, M., Huang, Y., Jankowska, A.M., Pape, U.J., Tahiliani, M., Bandukwala, H.S., An, J., Lamperti, E.D., Koh, K.P., Ganetzky, R., et al. (2010). Impaired hydroxylation of 5-methylcytosine in myeloid cancers with mutant TET2. Nature *468*, 839–843.

Kohl, N.E., Kanda, N., Schreck, R.R., Bruns, G., Latt, S.A., Gilbert, F., and Alt, F.W. (1983). Transposition and amplification of oncogene-related sequences in human neuroblastomas. Cell *35*, 359–367.

Kriaucionis, S., and Heintz, N. (2009). The nuclear DNA base, 5-hydroxymethylcytosine is present in brain and enriched in Purkinje neurons. Science *324*, 929–930.

Kuiper, C., and Vissers, M.C.M. (2014). Ascorbate as a co-factor for fe- and 2-oxoglutarate dependent dioxygenases: physiological activity in tumor growth and progression. Front Oncol *4*, 359.

Laukka, T., Mariani, C.J., Ihantola, T., Cao, J.Z., Hokkanen, J., Kaelin, W.G., Godley, L.A., and Koivunen, P. (2016). Fumarate and Succinate Regulate Expression of Hypoxia-inducible Genes via TET Enzymes. J. Biol. Chem. *291*, 4256–4265.

Lee, H.J., Hore, T.A., and Reik, W. (2014). Reprogramming the Methylome: Erasing Memory and Creating Diversity. Cell Stem Cell *14*, 710–719.

Li, C. (2013). DNA Demethylation Pathways: Recent Insights. Genet Epigenet *5*, 43–49.

Li, H., and Durbin, R. (2009). Fast and accurate short read alignment with Burrows-Wheeler transform. Bioinformatics *25*, 1754–1760.

Lin, I.-H., Chen, Y.-F., and Hsu, M.-T. (2017). Correlated 5-Hydroxymethylcytosine (5hmC) and Gene Expression Profiles Underpin Gene and Organ-Specific Epigenetic Regulation in Adult Mouse Brain and Liver. PLOS ONE *12*, e0170779.

Lio, C.-W., Zhang, J., González-Avalos, E., Hogan, P.G., Chang, X., and Rao, A. Tet2 and Tet3 cooperate with B-lineage transcription factors to regulate DNA modification and chromatin accessibility. ELife *5*, e18290.

Liutkevičiūtė, Z., Kriukienė, E., Ličytė, J., Rudytė, M., Urbanavičiūtė, G., and Klimašauskas, S. (2014). Direct decarboxylation of 5-carboxylcytosine by DNA C5-methyltransferases. J Am Chem Soc *136*, 5884–5887.

London, W.B., Castleberry, R.P., Matthay, K.K., Look, A.T., Seeger, R.C., Shimada, H., Thorner, P., Brodeur, G., Maris, J.M., Reynolds, C.P., et al. (2005). Evidence for an age cutoff greater than 365 days for neuroblastoma risk group stratification in the Children's Oncology Group. J Clin Oncol *23*, 6459–6465.

Losman, J.-A., and Kaelin, W.G. (2013). What a difference a hydroxyl makes: mutant IDH, (R)-2-hydroxyglutarate, and cancer. Genes Dev *27*, 836–852.

Louis, C.U., and Shohet, J.M. (2015). Neuroblastoma: molecular pathogenesis and therapy. Annu. Rev. Med. *66*, 49–63.

Lutz, W., Stöhr, M., Schürmann, J., Wenzel, A., Löhr, A., and Schwab, M. (1996). Conditional expression of N-myc in human neuroblastoma cells increases expression of alpha-prothymosin and ornithine decarboxylase and accelerates progression into S-phase early after mitogenic stimulation of quiescent cells. Oncogene *13*, 803–812.

Madzo, J., Liu, H., Rodriguez, A., Vasanthakumar, A., Sundaravel, S., Caces, D.B.D., Looney, T.J., Zhang, L., Lepore, J.B., Macrae, T., et al. (2014). Hydroxymethylation at Gene Regulatory Regions Directs Stem/Early Progenitor Cell Commitment during Erythropoiesis. Cell Rep *6*, 231–244.

Mahon, P.C., Hirota, K., and Semenza, G.L. (2001). FIH-1: a novel protein that interacts with HIF-1alpha and VHL to mediate repression of HIF-1 transcriptional activity. Genes Dev. *15*, 2675–2686.

Maiti, A., and Drohat, A.C. (2011). Thymine DNA glycosylase can rapidly excise 5-formylcytosine and 5-carboxylcytosine: potential implications for active demethylation of CpG sites. J. Biol. Chem. *286*, 35334–35338.

Maleki Vareki, S. (2018). High and low mutational burden tumors versus immunologically hot and cold tumors and response to immune checkpoint inhibitors. Journal for ImmunoTherapy of Cancer *6*, 157.

Mariani, C.J., Vasanthakumar, A., Madzo, J., Yesilkanal, A., Bhagat, T., Yu, Y., Bhattacharyya, S., Wenger, R.H., Cohn, S.L., Nanduri, J., et al. (2014). TET1-mediated hydroxymethylation facilitates hypoxic gene induction in neuroblastoma. Cell Rep *7*, 1343–1352.

Maris, J.M., Hogarty, M.D., Bagatell, R., and Cohn, S.L. (2007). Neuroblastoma. Lancet *369*, 2106–2120.

Mayer, W., Niveleau, A., Walter, J., Fundele, R., and Haaf, T. (2000). Demethylation of the zygotic paternal genome. Nature *403*, 501–502.

Meier, R., Mühlethaler-Mottet, A., Flahaut, M., Coulon, A., Fusco, C., Louache, F., Auderset, K., Bourloud, K.B., Daudigeos, E., Ruegg, C., et al. (2007). The Chemokine Receptor CXCR4 Strongly Promotes Neuroblastoma Primary Tumour and Metastatic Growth, but not Invasion. PLoS One *2*, e1016.

Mellen, M., Ayata, P., Dewell, S., Kriaucionis, S., and Heintz, N. (2012). MeCP2 binds to 5hmc enriched within active genes and accessible chromatin in the nervous system. Cell *151*, 1417–1430.

Minor, E.A., Court, B.L., Young, J.I., and Wang, G. (2013). Ascorbate induces ten-eleven translocation (Tet) methylcytosine dioxygenase-mediated generation of 5-hydroxymethylcytosine. J Biol Chem *288*, 13669–13674.

Moffat, J., Grueneberg, D.A., Yang, X., Kim, S.Y., Kloepfer, A.M., Hinkle, G., Piqani, B., Eisenhaure, T.M., Luo, B., Grenier, J.K., et al. (2006). A Lentiviral RNAi Library for Human and Mouse Genes Applied to an Arrayed Viral High-Content Screen. Cell *124*, 1283–1298.

Molenaar, J.J., Koster, J., Zwijnenburg, D.A., van Sluis, P., Valentijn, L.J., van der Ploeg, I., Hamdi, M., van Nes, J., Westerman, B.A., van Arkel, J., et al. (2012a). Sequencing of neuroblastoma identifies chromothripsis and defects in neuritogenesis genes. Nature *483*, 589–593.

Molenaar, J.J., Koster, J., Zwijnenburg, D.A., van Sluis, P., Valentijn, L.J., van der Ploeg, I., Hamdi, M., van Nes, J., Westerman, B.A., van Arkel, J., et al. (2012b). Sequencing of neuroblastoma identifies chromothripsis and defects in neuritogenesis genes. Nature *483*, 589–593.

Monclair, T., Brodeur, G.M., Ambros, P.F., Brisse, H.J., Cecchetto, G., Holmes, K., Kaneko, M., London, W.B., Matthay, K.K., Nuchtern, J.G., et al. (2009). The International Neuroblastoma Risk Group (INRG) Staging System: An INRG Task Force Report. J Clin Oncol *27*, 298–303.

Moreno, L., Guo, D., Irwin, M.S., Berthold, F., Hogarty, M., Kamijo, T., Morgenstern, D., Pasqualini, C., Ash, S., Potschger, U., et al. (2020). A nomogram of clinical and biologic factors to predict survival in children newly diagnosed with high-risk neuroblastoma: An International Neuroblastoma Risk Group project. Pediatr Blood Cancer e28794.

Muth, D., Ghazaryan, S., Eckerle, I., Beckett, E., Pöhler, C., Batzler, J., Beisel, C., Gogolin, S., Fischer, M., Henrich, K.-O., et al. (2010). Transcriptional repression of SKP2 is impaired in MYCN-amplified neuroblastoma. Cancer Res *70*, 3791–3802.

Nakagawa, T., Lv, L., Nakagawa, M., Yu, Y., Yu, C., D'Alessio, A.C., Nakayama, K., Fan, H.-Y., Chen, X., and Xiong, Y. (2015). CRL4VprBP E3 ligase promotes monoubiquitylation and chromatin binding of TET dioxygenases. Mol Cell *57*, 247–260.

Nestor, C.E., and Meehan, R.R. (2014). Hydroxymethylated DNA immunoprecipitation (hmeDIP). Methods Mol Biol *1094*, 259–267.

Nie, Y., Waite, J., Brewer, F., Sunshine, M.-J., Littman, D.R., and Zou, Y.-R. (2004). The Role of CXCR4 in Maintaining Peripheral B Cell Compartments and Humoral Immunity. J Exp Med *200*, 1145–1156.

Oberlin, E., Amara, A., Bachelerie, F., Bessia, C., Virelizier, J.L., Arenzana-Seisdedos, F., Schwartz, O., Heard, J.M., Clark-Lewis, I., Legler, D.F., et al. (1996). The CXC chemokine SDF-1 is the ligand for LESTR/fusin and prevents infection by T-cell-line-adapted HIV-1. Nature *382*, 833–835.

Ochiai, H., Takenobu, H., Nakagawa, A., Yamaguchi, Y., Kimura, M., Ohira, M., Okimoto, Y., Fujimura, Y., Koseki, H., Kohno, Y., et al. (2010). Bmi1 is a MYCN target gene that regulates tumorigenesis through repression of KIF1Bbeta and TSLC1 in neuroblastoma. Oncogene *29*, 2681–2690.

Okano, M., Bell, D.W., Haber, D.A., and Li, E. (1999). DNA methyltransferases Dnmt3a and Dnmt3b are essential for de novo methylation and mammalian development. Cell *99*, 247–257.

Opel, D., Poremba, C., Simon, T., Debatin, K.-M., and Fulda, S. (2007). Activation of Akt predicts poor outcome in neuroblastoma. Cancer Res *67*, 735–745.

Otte, J., Dyberg, C., Pepich, A., and Johnsen, J.I. (2021). MYCN Function in Neuroblastoma Development. Frontiers in Oncology *10*, 3210.

Ozer, E., Altungoz, O., Unlu, M., Aygun, N., Tumer, S., and Olgun, N. (2007). Association of MYCN amplification and 1p deletion in neuroblastomas with high tumor vascularity. Appl Immunohistochem Mol Morphol *15*, 181–186.

Park, J.R., Kreissman, S.G., London, W.B., Naranjo, A., Cohn, S.L., Hogarty, M.D., Tenney, S.C., Haas-Kogan, D., Shaw, P.J., Kraveka, J.M., et al. (2019). Effect of Tandem Autologous Stem Cell Transplant vs Single Transplant on Event-Free Survival in Patients With High-Risk Neuroblastoma. JAMA *322*, 746–755.

Patel, J.P., Gönen, M., Figueroa, M.E., Fernandez, H., Sun, Z., Racevskis, J., Van Vlierberghe, P., Dolgalev, I., Thomas, S., Aminova, O., et al. (2012). Prognostic relevance of integrated genetic profiling in acute myeloid leukemia. N Engl J Med *366*, 1079–1089.

Pfeiffer, M., Hartmann, T.N., Leick, M., Catusse, J., Schmitt-Graeff, A., and Burger, M. (2009). Alternative implication of CXCR4 in JAK2/STAT3 activation in small cell lung cancer. Br J Cancer *100*, 1949–1956.

Pidugu, L.S., Flowers, J.W., Coey, C.T., Pozharski, E., Greenberg, M.M., and Drohat, A.C. (2016). Structural Basis for Excision of 5-Formylcytosine by Thymine DNA Glycosylase. Biochemistry *55*, 6205–6208.

Pinto, N., Mayfield, J.R., Raca, G., Applebaum, M.A., Chlenski, A., Sukhanova, M., Bagatell, R., Irwin, M.S., Little, A., Rawwas, J., et al. (2016). Segmental Chromosomal Aberrations in Localized Neuroblastoma Can be Detected in Formalin-Fixed Paraffin-Embedded Tissue Samples and Are Associated With Recurrence. Pediatr Blood Cancer *63*, 1019–1023.

Plantaz, D., Mohapatra, G., Matthay, K.K., Pellarin, M., Seeger, R.C., and Feuerstein, B.G. (1997). Gain of chromosome 17 is the most frequent abnormality detected in neuroblastoma by comparative genomic hybridization. Am J Pathol *150*, 81–89.

Pollard, P.J., Brière, J.J., Alam, N.A., Barwell, J., Barclay, E., Wortham, N.C., Hunt, T., Mitchell, M., Olpin, S., Moat, S.J., et al. (2005). Accumulation of Krebs cycle intermediates and over-expression of HIF1alpha in tumours which result from germline FH and SDH mutations. Hum Mol Genet *14*, 2231–2239.

Pugh, C.W., O'Rourke, J.F., Nagao, M., Gleadle, J.M., and Ratcliffe, P.J. (1997). Activation of hypoxia-inducible factor-1; definition of regulatory domains within the alpha subunit. J. Biol. Chem. *272*, 11205–11214.

Pugh, T.J., Morozova, O., Attiyeh, E.F., Asgharzadeh, S., Wei, J.S., Auclair, D., Carter, S.L., Cibulskis, K., Hanna, M., Kiezun, A., et al. (2013). The genetic landscape of high-risk neuroblastoma. Nat Genet *45*, 279–284.

Quinlan, A.R., and Hall, I.M. (2010). BEDTools: a flexible suite of utilities for comparing genomic features. Bioinformatics *26*, 841–842.

Rankin, E., and Giaccia, A. (2008). The role of hypoxia-inducible factors in tumorigenesis. Cell Death Differ *15*, 678–685.

Riggs, A.D. (1975). X inactivation, differentiation, and DNA methylation. Cytogenet. Cell Genet. *14*, 9–25.

Robertson, A.B., Dahl, J.A., Ougland, R., and Klungland, A. (2012). Pull-down of 5-hydroxymethylcytosine DNA using JBP1-coated magnetic beads. Nat Protoc *7*, 340–350.

Robinson, J.T., Thorvaldsdóttir, H., Winckler, W., Guttman, M., Lander, E.S., Getz, G., and Mesirov, J.P. (2011). Integrative genomics viewer. Nature Biotechnology *29*, 24–26.

Russell, H.V., Hicks, J., Okcu, M.F., and Nuchtern, J.G. (2004). CXCR4 expression in neuroblastoma primary tumors is associated with clinical presentation of bone and bone marrow metastases. J Pediatr Surg *39*, 1506–1511.

Sanjana, N.E., Shalem, O., and Zhang, F. (2014). Improved vectors and genome-wide libraries for CRISPR screening. Nat Methods *11*, 783–784.

Sanmartín, E., Yáñez, Y., Fornés-Ferrer, V., Zugaza, J.L., Cañete, A., Castel, V., and de Mora, J.F. (2017). TIAM1 variants improve clinical outcome in neuroblastoma. Oncotarget *8*, 45286–45297.

Schmidt, M.L., Lal, A., Seeger, R.C., Maris, J.M., Shimada, H., O'Leary, M., Gerbing, R.B., and Matthay, K.K. (2005). Favorable prognosis for patients 12 to 18 months of age with stage 4 nonamplified MYCN neuroblastoma: a Children's Cancer Group Study. J Clin Oncol *23*, 6474–6480.

Schulte, J.H., Marschall, T., Martin, M., Rosenstiel, P., Mestdagh, P., Schlierf, S., Thor, T., Vandesompele, J., Eggert, A., Schreiber, S., et al. (2010). Deep sequencing reveals differential expression of microRNAs in favorable versus unfavorable neuroblastoma. Nucleic Acids Res *38*, 5919–5928.

Schwab, M., Alitalo, K., Klempnauer, K.H., Varmus, H.E., Bishop, J.M., Gilbert, F., Brodeur, G., Goldstein, M., and Trent, J. (1983). Amplified DNA with limited homology to myc cellular oncogene is shared by human neuroblastoma cell lines and a neuroblastoma tumour. Nature *305*, 245–248.

Seeger, R.C., Brodeur, G.M., Sather, H., Dalton, A., Siegel, S.E., Wong, K.Y., and Hammond, D. (1985). Association of multiple copies of the N-myc oncogene with rapid progression of neuroblastomas. N. Engl. J. Med. *313*, 1111–1116.

Seiler, M., Peng, S., Agrawal, A.A., Palacino, J., Teng, T., Zhu, P., Smith, P.G., Cancer Genome Atlas Research Network, Buonamici, S., and Yu, L. (2018). Somatic Mutational Landscape of Splicing Factor Genes and Their Functional Consequences across 33 Cancer Types. Cell Rep *23*, 282-296.e4.

Semenza, G.L. (2017). A compendium of proteins that interact with HIF-1α. Exp Cell Res *356*, 128–135.

Shang, Y., Hu, X., DiRenzo, J., Lazar, M.A., and Brown, M. (2000). Cofactor Dynamics and Sufficiency in Estrogen Receptor–Regulated Transcription. Cell *103*, 843–852.

Sharif, J., Muto, M., Takebayashi, S., Suetake, I., Iwamatsu, A., Endo, T.A., Shinga, J., Mizutani-Koseki, Y., Toyoda, T., Okamura, K., et al. (2007). The SRA protein Np95 mediates epigenetic inheritance by recruiting Dnmt1 to methylated DNA. Nature *450*, 908–912.

Shi, F.-T., Kim, H., Lu, W., He, Q., Liu, D., Goodell, M.A., Wan, M., and Songyang, Z. (2013). Ten-Eleven Translocation 1 (Tet1) Is Regulated by O-Linked N-Acetylglucosamine Transferase (Ogt) for Target Gene Repression in Mouse Embryonic Stem Cells. J Biol Chem *288*, 20776–20784.

Slack, A., Chen, Z., Tonelli, R., Pule, M., Hunt, L., Pession, A., and Shohet, J.M. (2005). The p53 regulatory gene MDM2 is a direct transcriptional target of MYCN in neuroblastoma. Proc Natl Acad Sci U S A *102*, 731–736.

Slyvka, A., Mierzejewska, K., and Bochtler, M. (2017). Nei-like 1 (NEIL1) excises 5-carboxylcytosine directly and stimulates TDG-mediated 5-formyl and 5-carboxylcytosine excision. Scientific Reports *7*, 9001.

Sokol, E., and Desai, A.V. (2019). The Evolution of Risk Classification for Neuroblastoma. Children (Basel) *6*, 27.

Song, C.-X., Szulwach, K.E., Fu, Y., Dai, Q., Yi, C., Li, X., Li, Y., Chen, C.-H., Zhang, W., Jian, X., et al. (2011). Selective chemical labeling reveals the genome-wide distribution of 5-hydroxymethylcytosine. Nature Biotechnology *29*, 68–72.

Song, L., James, S.R., Kazim, L., and Karpf, A.R. (2005). Specific method for the determination of genomic DNA methylation by liquid chromatography-electrospray ionization tandem mass spectrometry. Anal Chem *77*, 504–510.

Song, L., Ara, T., Wu, H.-W., Woo, C.-W., Reynolds, C.P., Seeger, R.C., DeClerck, Y.A., Thiele, C.J., Sposto, R., and Metelitsa, L.S. (2007). Oncogene MYCN regulates localization of NKT cells to the site of disease in neuroblastoma. J Clin Invest *117*, 2702–2712.

Souvorov, A., Kapustin, Y., Kiryutin, B., Chetvernin, V., Tatusova, T., and Lipman, D. (2010). Gnomon – NCBI eukaryotic gene prediction.

Spruijt, C.G., Gnerlich, F., Smits, A.H., Pfaffeneder, T., Jansen, P.W.T.C., Bauer, C., Münzel, M., Wagner, M., Müller, M., Khan, F., et al. (2013). Dynamic readers for 5-(hydroxy)methylcytosine and its oxidized derivatives. Cell *152*, 1146–1159.

Sullivan, C.H., and Grainger, R.M. (1987). Delta-crystallin genes become hypomethylated in postmitotic lens cells during chicken development. Proc. Natl. Acad. Sci. U.S.A. *84*, 329–333.

Sun, Z., Xu, X., He, J., Murray, A., Sun, M., Wei, X., Wang, X., McCoig, E., Xie, E., Jiang, X., et al. (2019). EGR1 recruits TET1 to shape the brain methylome during development and upon neuronal activity. Nat Commun *10*, 3892.

Szulwach, K.E., Li, X., Li, Y., Song, C.-X., Han, J.W., Kim, S., Namburi, S., Hermetz, K., Kim, J.J., Rudd, M.K., et al. (2011). Integrating 5-Hydroxymethylcytosine into the Epigenomic Landscape of Human Embryonic Stem Cells. PLOS Genetics *7*, e1002154.

Tahiliani, M., Koh, K.P., Shen, Y., Pastor, W.A., Bandukwala, H., Brudno, Y., Agarwal, S., Iyer, L.M., Liu, D.R., Aravind, L., et al. (2009). Conversion of 5-Methylcytosine to 5-Hydroxymethylcytosine in Mammalian DNA by MLL Partner TET1. Science *324*, 930–935.

Talks, K.L., Turley, H., Gatter, K.C., Maxwell, P.H., Pugh, C.W., Ratcliffe, P.J., and Harris, A.L. (2000). The expression and distribution of the hypoxia-inducible factors HIF-1alpha and HIF-2alpha in normal human tissues, cancers, and tumor-associated macrophages. Am. J. Pathol. *157*, 411–421.

R Core Team (2014). R: A language and environment for statistical computing. R Foundation for Statistical Computing, Vienna, Austria. URL http://www.R-project.org/

Thienpont, B., Steinbacher, J., Zhao, H., D'Anna, F., Kuchnio, A., Ploumakis, A., Ghesquière, B., Dyck, L.V., Boeckx, B., Schoonjans, L., et al. (2016). Tumour hypoxia causes DNA hypermethylation by reducing TET activity. Nature *537*, 63–68.

Thomas, P.D., Campbell, M.J., Kejariwal, A., Mi, H., Karlak, B., Daverman, R., Diemer, K., Muruganujan, A., and Narechania, A. (2003). PANTHER: A Library of Protein Families and Subfamilies Indexed by Function. Genome Res. *13*, 2129–2141.

Thomas, S.N., Liao, Z., Clark, D., Chen, Y., Samadani, R., Mao, L., Ann, D.K., Baulch, J.E., Shapiro, P., and Yang, A.J. (2013). Exosomal Proteome Profiling: A Potential Multi-Marker Cellular Phenotyping Tool to Characterize Hypoxia-Induced Radiation Resistance in Breast Cancer. Proteomes *1*, 87–108.

Trapnell, C., Roberts, A., Goff, L., Pertea, G., Kim, D., Kelley, D.R., Pimentel, H., Salzberg, S.L., Rinn, J.L., and Pachter, L. (2012). Differential gene and transcript expression analysis of RNA-seq experiments with TopHat and Cufflinks. Nature Protocols *7*, 562–578.

Turcan, S., Rohle, D., Goenka, A., Walsh, L.A., Fang, F., Yilmaz, E., Campos, C., Fabius, A.W.M., Lu, C., Ward, P.S., et al. (2012). IDH1 mutation is sufficient to establish the glioma hypermethylator phenotype. Nature *483*, 479–483.

Tweddle, D.A., Malcolm, A.J., Cole, M., Pearson, A.D., and Lunec, J. (2001). p53 cellular localization and function in neuroblastoma: evidence for defective G(1) arrest despite WAF1 induction in MYCN-amplified cells. Am J Pathol *158*, 2067–2077.

Upton, K., Modi, A., Patel, K., Kendsersky, N.M., Conkrite, K.L., Sussman, R.T., Way, G.P., Adams, R.N., Sacks, G.I., Fortina, P., et al. (2020). Epigenomic profiling of neuroblastoma cell lines. Sci Data *7*.

Valinluck, V., and Sowers, L.C. (2007). Endogenous cytosine damage products alter the site selectivity of human DNA maintenance methyltransferase DNMT1. Cancer Res. *67*, 946–950.

Valsesia-Wittmann, S., Magdeleine, M., Dupasquier, S., Garin, E., Jallas, A.-C., Combaret, V., Krause, A., Leissner, P., and Puisieux, A. (2004). Oncogenic cooperation between H-Twist and N-Myc overrides failsafe programs in cancer cells. Cancer Cell *6*, 625–630.

Van Arendonk, K.J., and Chung, D.H. (2019). Neuroblastoma: Tumor Biology and Its Implications for Staging and Treatment. Children (Basel) *6*.

Varley, K.E., Gertz, J., Bowling, K.M., Parker, S.L., Reddy, T.E., Pauli-Behn, F., Cross, M.K., Williams, B.A., Stamatoyannopoulos, J.A., Crawford, G.E., et al. (2013). Dynamic DNA methylation across diverse human cell lines and tissues. Genome Res. *23*, 555–567.

Vasanthakumar, A., and Godley, L.A. (2015). 5-hydroxymethylcytosine in cancer: significance in diagnosis and therapy. Cancer Genetics *208*, 167–177.

Vaupel, P., Höckel, M., and Mayer, A. (2007). Detection and characterization of tumor hypoxia using pO2 histography. Antioxid. Redox Signal. *9*, 1221–1235.

Vella, P., Scelfo, A., Jammula, S., Chiacchiera, F., Williams, K., Cuomo, A., Roberto, A., Christensen, J., Bonaldi, T., Helin, K., et al. (2013). Tet Proteins Connect the O-Linked N-acetylglucosamine Transferase Ogt to Chromatin in Embryonic Stem Cells. Molecular Cell *49*, 645–656.

Wang, G.L., and Semenza, G.L. (1995). Purification and characterization of hypoxia-inducible factor 1. J. Biol. Chem. *270*, 1230–1237.

Wang, Y., and Zhang, Y. (2014). Regulation of TET Protein Stability by Calpains. Cell Rep *6*, 278–284.

Wang, H., Guan, S., Quimby, A., Cohen-Karni, D., Pradhan, S., Wilson, G., Roberts, R.J., Zhu, Z., and Zheng, Y. (2011). Comparative characterization of the PvuRts1I family of restriction enzymes and their application in mapping genomic 5-hydroxymethylcytosine. Nucleic Acids Res *39*, 9294–9305.

Wen, L., Li, X., Yan, L., Tan, Y., Li, R., Zhao, Y., Wang, Y., Xie, J., Zhang, Y., Song, C., et al. (2014). Whole-genome analysis of 5-hydroxymethylcytosine and 5-methylcytosine at base resolution in the human brain. Genome Biol *15*, R49.

Westermann, F., Muth, D., Benner, A., Bauer, T., Henrich, K.-O., Oberthuer, A., Brors, B., Beissbarth, T., Vandesompele, J., Pattyn, F., et al. (2008). Distinct transcriptional MYCN/c-MYC activities are associated with spontaneous regression or malignant progression in neuroblastomas. Genome Biology *9*, R150.

Whyte, W.A., Orlando, D.A., Hnisz, D., Abraham, B.J., Lin, C.Y., Kagey, M.H., Rahl, P.B., Lee, T.I., and Young, R.A. (2013). Master Transcription Factors and Mediator Establish Super-Enhancers at Key Cell Identity Genes. Cell *153*, 307–319.

Williams, K., Christensen, J., Pedersen, M.T., Johansen, J.V., Cloos, P.A.C., Rappsilber, J., and Helin, K. (2011). TET1 and hydroxymethylcytosine in transcription and DNA methylation fidelity. Nature *473*, 343–348.

Xu, C., Zhao, H., Chen, H., and Yao, Q. (2015). CXCR4 in breast cancer: oncogenic role and therapeutic targeting. Drug Des Devel Ther *9*, 4953–4964.

Xu, W., Yang, H., Liu, Y., Yang, Y., Wang, P., Kim, S.-H., Ito, S., Yang, C., Wang, P., Xiao, M.-T., et al. (2011). Oncometabolite 2-Hydroxyglutarate Is a Competitive Inhibitor of α-Ketoglutarate-Dependent Dioxygenases. Cancer Cell *19*, 17–30.

Xue, B., Wu, W., Huang, K., Xie, T., Xu, X., Zhang, H., Qi, C., Ge, J., and Yu, Y. (2013). Stromal cell-derived factor-1 (SDF-1) enhances cells invasion by αvβ6 integrin-mediated signaling in ovarian cancer. Mol Cell Biochem *380*, 177–184.

Yamaguchi, S., Hong, K., Liu, R., Shen, L., Inoue, A., Diep, D., Zhang, K., and Zhang, Y. (2012). Tet1 controls meiosis by regulating meiotic gene expression. Nature *492*, 443–447.

Yildirim, O., Li, R., Hung, J.-H., Chen, P.B., Dong, X., Ee, L., Weng, Z., Rando, O.J., and Fazzio, T.G. (2011). Mbd3/NURD complex regulates expression of 5-hydroxymethylcytosine marked genes in embryonic stem cells. Cell *147*, 1498–1510.

Yin, R., Mao, S.-Q., Zhao, B., Chong, Z., Yang, Y., Zhao, C., Zhang, D., Huang, H., Gao, J., Li, Z., et al. (2013). Ascorbic acid enhances Tet-mediated 5-methylcytosine oxidation and promotes DNA demethylation in mammals. J Am Chem Soc *135*, 10396–10403.

Yosefzon, Y., David, C., Tsukerman, A., Pnueli, L., Qiao, S., Boehm, U., and Melamed, P. (2017). An epigenetic switch repressing Tet1 in gonadotropes activates the reproductive axis. PNAS *114*, 10131–10136.

Yu, M., Hon, G.C., Szulwach, K.E., Song, C.-X., Zhang, L., Kim, A., Li, X., Dai, Q., Shen, Y., Park, B., et al. (2012). Base-resolution analysis of 5-hydroxymethylcytosine in the mammalian genome. Cell *149*, 1368–1380.

Zeid, R., Lawlor, M.A., Poon, E., Reyes, J.M., Fulciniti, M., Lopez, M.A., Scott, T.G., Nabet, B., Erb, M.A., Winter, G.E., et al. (2018). Enhancer invasion shapes MYCN-dependent transcriptional amplification in neuroblastoma. Nature Genetics *50*, 515–523.

Zhang, F., Pomerantz, J.H., Sen, G., Palermo, A.T., and Blau, H.M. (2007). Active tissue-specific DNA demethylation conferred by somatic cell nuclei in stable heterokaryons. Proc. Natl. Acad. Sci. U.S.A. *104*, 4395–4400.

Zhang, L., Hua, Q., Tang, K., Shi, C., Xie, X., and Zhang, R. (2016a). CXCR4 activation promotes differentiation of human embryonic stem cells to neural stem cells. Neuroscience *337*, 88–97.

Zhang, S., Wei, J.S., Li, S.Q., Badgett, T.C., Song, Y.K., Agarwal, S., Coarfa, C., Tolman, C., Hurd, L., Liao, H., et al. (2016b). MYCN controls an alternative RNA splicing program in high-risk metastatic neuroblastoma. Cancer Lett *371*, 214–224.

Zhang, W., Xia, W., Wang, Q., Towers, A.J., Chen, J., Gao, R., Zhang, Y., Yen, C.-A., Lee, A.Y., Li, Y., et al. (2016c). Isoform Switch of TET1 Regulates DNA Demethylation and Mouse Development. Mol. Cell *64*, 1062–1073.

Zhang, Y., Liu, T., Meyer, C.A., Eeckhoute, J., Johnson, D.S., Bernstein, B.E., Nusbaum, C., Myers, R.M., Brown, M., Li, W., et al. (2008). Model-based Analysis of ChIP-Seq (MACS). Genome Biology *9*, R137.

Zhang, Y.W., Wang, Z., Xie, W., Cai, Y., Xia, L., Easwaran, H., Luo, J., Yen, R.-W.C., Li, Y., and Baylin, S.B. (2017). Acetylation Enhances TET2 Function in Protecting against Abnormal DNA Methylation during Oxidative Stress. Mol. Cell *65*, 323–335.

Zhu, F., Zhu, Q., Ye, D., Zhang, Q., Yang, Y., Guo, X., Liu, Z., Jiapaer, Z., Wan, X., Wang, G., et al. (2018). Sin3a–Tet1 interaction activates gene transcription and is required for embryonic stem cell pluripotency. Nucleic Acids Res *46*, 6026–6040.